Dissertation

submitted to the

Combined Faculty of Natural Sciences and Mathematics

of the Ruperto Carola University Heidelberg, Germany

for the degree of

Doctor of Natural Sciences

Presented by

M.Sc. Anna Cazzola

born in: Lecco

Oral examination: 10/07/2019

Identification and characterization of aneuploidy-selective compounds in acute myeloid leukemia

Referees: PD Dr. Karin Müller-Decker

Prof. Dr. Alwin Krämer

Table of contents

Summary

Aneuploidy is a rare condition in untransformed cells and one of the hallmarks of cancer. It often coexists with chromosomal instability and correlates with intra-tumor heterogeneity and poor clinical outcome. Several studies performed in various organisms engineered to harbor chromosome abnormalities have revealed that aneuploidy confers common phenotypes such as intracellular pathway deregulation and increased energy and metabolic requests, all eventually impairing cellular fitness. Even if the majority of aneuploid cells are less proliferatively active than normal diploid cells, favorable karyotypic variants and selection pressure can confer a growth advantage to chromosomally unstable cells, due to their improved adaptability, possibly promoting tumorigenesis.

As a rare event in normal tissues, aneuploidy constitutes an attractive potential therapeutic target for cancer treatment. Indeed, some studies have started to investigate this opportunity, mainly in cell line models, leading to the identification of some compounds that specifically target aneuploidy.

Acute myeloid leukemia (AML) patients with aneuploid karyotypes respond poorly to conventional chemotherapy. Thus, the identification of aneuploidy-specific antiproliferative compounds that could be used for the treatment of this subset of AML patients constitutes an intriguing strategy.

Here we show that 8-azagunanine is a potential aneuploidy-selective antiproliferative compound in AML. 8-Azaguanine causes endoplasmic reticulum stress, possibly exacerbating proteotoxic stress as one of the predominant features of aneuploid cells, and specifically enhances the death of cells with abnormal karyotypes.

Moreover, we demonstrate in AML cells that p53 deficiency enables the propagation of extensive karyotypic heterogeneity and chromosome abnormalities including structural aneuploidy (gains or losses of sub-chromosomal regions) and structural rearrangements (alterations of chromosome structure), which are conversely prevented in p53-proficient cells. Numerical aneuploidy, on the other hand, does not inevitably trigger p53 activation. These results suggest that p53 provides maintenance of genomic stability especially with regard to structural chromosome abnormalities.

Zusammenfassung

Aneuploidie tritt selten in untransformierten Zellen auf und stellt ein Kennzeichen von Krebs dar. Sie tritt häufig in Verbindung mit chromosomaler Instabilität auf und korreliert mit Intra-Tumor-Heterogenität und infauster Prognose. Mehrere Studien an verschiedenen Modellorganismen mit Chromosomenanomalien haben gezeigt, dass Aneuploidie eine Deregulierung der intrazellulären Signalwege und eine erhöhte Energie- und Stoffwechselanforderung verursacht, was schließlich die zelluläre Fitness beeinträchtigt. Obwohl der Großteil aneuploider Zellen eine eingeschränkte Proliferation aufweist, können günstige karyotypische Varianten und Selektionsdruck einen Wachstumsvorteil für die chromosomal instabilen Zellen bedeuten, welcher die Tumorgenese unterstützen kann.

Da Aneuploidie nur selten in normalem Gewebe nachzuweisen ist, repräsentiert sie ein attraktives therapeutisches Ziel für die Entwicklung von Krebstherapien. Aus diesem Grund wurden aneuploide Zelllinien bereits in Studien für die Entwicklung aneuploidie-selektiver Wirkstoffe verwendet.

Patienten mit akuter myeloischer Leukämie (AML), die einen aneuploiden Karyotyp aufweisen, sprechen schlecht auf eine konventionelle Chemotherapie an. Daher stellt die Identifizierung aneuploidie-selektiver antiproliferativer Wirkstoffe eine attraktive Strategie zur Behandlung dieser AML Patienten dar.

In dieser Arbeit konnten wir zeigen, dass 8-Azagunanin eine aneuploidie-selektive Wirkung in der akuten myeloischen Leukämie besitzt. 8-Azaguanin ruft eine Stressreaktion im endoplasmatischen Retikulum hervor, die möglicherweise proteotoxischen Stress, ein Hauptmerkmal von aneuploiden Zellen, verstärkt und somit in Zellen mit abnormalem Karyotyp häufiger zu Zelltod führt.

Darüber hinaus konnten wir in AML Zellen zeigen, dass das Fehlen von p53 die Weitergabe umfangreicher karyotypischer Heterogenität und Chromosomenanomalien, einschließlich struktureller Aneuploidie (Gewinn oder Verlust subchromosomaler Regionen) und Umlagerungen (Veränderungen der Chromosomenstruktur) ermöglicht, die im Vergleich dazu in p53-kompetenten Zellen verhindert werden. Hingegen löst eine numerische Aneuploidie die Aktivierung von p53 nicht zwangsläufig aus. Diese Ergebnisse legen nahe, dass p53 die Aufrechterhaltung der genomischen Stabilität, insbesondere im Hinblick auf strukturelle Chromosomenanomalien, gewährleistet.

Acknowledgments

My acknowledgements to all the people who contributed to my PhD project and supported me during my time as a PhD student.

I would like to thank my supervisor Prof. Dr. Alwin Krämer for offering me the opportunity to work on this project and for the helpful discussions, valuable advice and suggestions during the course of my research.

I would also like to thank the members of my thesis advisory committee PD Dr. Karin Müller-Decker and Prof. Dr. Stefan Duensing for their helpful advice and suggestions.

Thanks to Prof. Dr. Anna Jauch, Brigitte Schoell, Prof. Dr. Benedikt Brors, Mohamoud Abdelrahman for our cooperation.

I am grateful to Ilka and Christin and to all the members of the lab: Amira, Andrey, Anja, Baowen, Bianca, Claudia, Elena, Gabor, Gianmatteo, Jana, Jing, Marc, Marco, Marion, Michael, Tilmann, Tobias and Viani for help, suggestions and the enjoyable work atmosphere.

1 Introduction

1.1 Aneuploidy

The term aneuploidy was coined in 1922 by Gunnar Täckholm[1] and refers to a condition in which the number of chromosomes within a cell differs from the whole multiple of the haploid number for a certain species. Indeed, the term aneuploidy derives from the Greek *an* meaning not, *eu* meaning good and *ploos* meaning fold: "*not the right fold*". Aneuploidy can be caused by gains and losses of entire chromosomes (numerical or whole chromosome aneuploidy) and by gains and losses of parts of chromosomes (structural or segmental aneuploidy). Aneuploidy differs from polyploidy, defined by the acquisition of entire sets of chromosomes (Fig. 1).

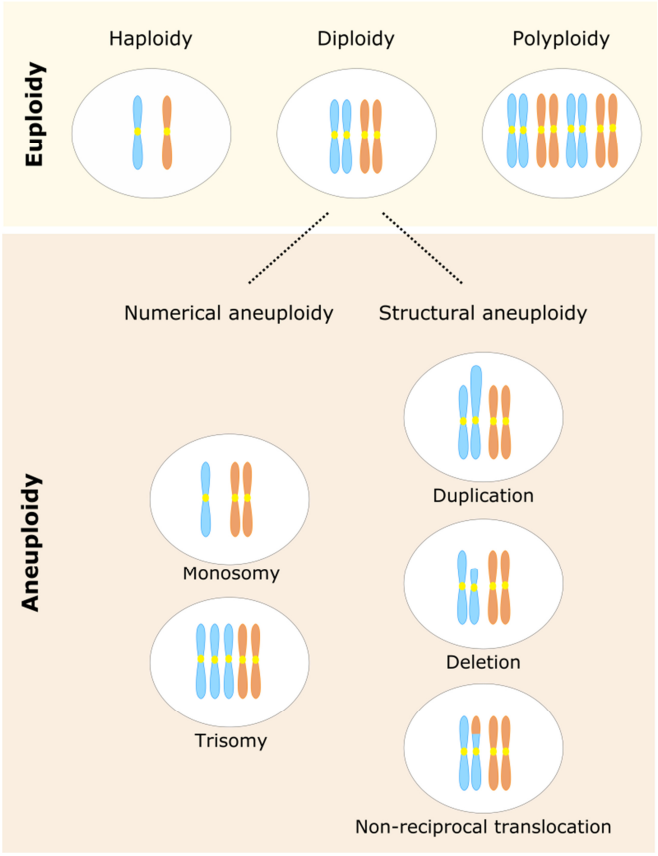

Figure 1 | Euploid, polyploid and aneuploid karyotypes

Euploidy refers to the normal genomic state of a species. Depending on the species, euploidy can describe a haploid, diploid or polyploid karyotype. On the other hand, aneuploidy is an aberrant genomic state that describes a range of karyotype abnormalities including chromosome losses and gains as well as duplications, deletions or unbalanced translocations of sub-chromosomal regions.

1.1.1 Aneuploidy in normal tissues

Aneuploidy is a rare event in untransformed tissues. When aneuploidy is caused by errors which occur during germ cell formation, usually during meiosis, it is termed constitutional aneuploidy. Somatic aneuploidy (mosaicism), by contrast, results from a post-zygotic event as a consequence of mitotic errors. While constitutional aneuploidy affects all the cells of a multicellular organism, in mosaicism only some cells harbor an aberrant karyotype.

The consequences of aneuploidy are typically detrimental in many living beings from yeast to plants and mammals. Thus, the preservation of a correct chromosome set is indispensable for the development and survival of an organism. In humans, constitutive autosomal chromosome gains are normally incompatible with survival until adulthood, with the exception of Down syndrome (47, XY, +21) where the presence of an extra chromosome 21 results in a complex pathologic phenotype. Individuals with Edward (47, XY, +18) and Patau (47, XY, +13) syndromes die shortly after birth. All autosomal losses cause embryonic lethality. Sex chromosome aneuploidies, such as Turner (45, X) and Klinefelter (47, XXY) syndromes, also show developmental defects even if they have less adverse consequences than autosomal aneuploidy probably due to less genetic contribution of X and Y chromosomes.

Mosaic aneuploidy can be benign; some normal cells such as neuronal progenitors, neurons and hepatocytes have been described to show a certain level of aneuploidy[2,3,4,5,6]. Nevertheless, more recent findings contradict these results arguing that the aneuploidy level in brain and liver is not different from that in skin and involves fewer than 5% of cells[7]. Mosaicism can also cause abnormal phenotypes. A rare disorder termed mosaic variegated aneuploidy (MVA) syndrome manifests with growth retardation, microcephaly and cancer at young age[8]. Among others, mutations in the *BUB1B* gene, required for correct chromosome segregation, have a causal role in MVA development[9]. Mosaicism can affect both somatic and germ line cells. When gametes are involved, some of them are normal while others carry chromosome aberrations which eventually are inherited by the offspring.

Mosaicism frequency increases with age and this phenomenon seems also to be associated with neurodegenerative diseases[10] and with cancer development[3,11,12,13].

Given the adverse effects of aneuploidy, it is not unexpected that perturbed chromosome segregation fidelity is a rare event in untransformed cells. Indeed, the rate of chromosomal segregation errors in these cells is only approximately 0.025% per chromosome, with an estimate of global chromosomal missegregation of one chromosome every 100 cell divisions[14].

1.1.2 Aneuploidy in cancer

Whereas aneuploidy occurs rarely in normal tissues, it is a common characteristic of both solid and hematological malignancies. About 85% of all human cancers harbor an aneuploid karyotype[15]. Many cancer cells, besides harboring aneuploidy, are characterized by high rates of chromosome missegregation, namely chromosomal instability (CIN), which leads to extensive genome heterogeneity within tumor tissues[16]. Aneuploidy is furthermore associated with poor prognosis[17] indicating that chromosome missegragation contributes to cancer progression and increasing genetic diversity among cancer cells which can acquire novel phenotypes such as drug resistance.

Whether aneuploidy and CIN contribute to tumor initiation and progression or constitute a mere epiphenomenon of cell transformation is still an open issue.

The possible role of aneuploidy in cancer progression was already foreseen in 1890 by David von Hansemann who identified multipolar divisions in epithelial tumor cells[18]. Moreover, the observations made at the beginning of the twentieth century by the German biologist Theodor Boveri, who was studying aneuploid cells generated in sea urchin embryos undergoing multipolar divisions, led to the hypothesis that tumors could develop from normal cells that have become aneuploid after aberrant mitosis[19].

The discovery of oncogenes and tumor-suppressor genes made scientists conceive the idea that specific mutations in these genes might be responsible for cancer development and that aneuploidy could be just a consequence of neoplastic transformation[20]. At the same time, however, mounting evidence that aneuploidy could trigger tumorigenesis gained new support. For example, trisomy of chromosome 8, which is harbored by approximately 15% of individuals with AML besides other blood cells malignancies, seems to promote blood tumor development[21]. Indeed, trisomy 8 causes the presence of an extra copy of *MYC*, an oncogene that could drive hematopoietic stem cell malignant transformation.

Moreover, recent work again supports a role of reduced mitotic fidelity and aneuploidy in early steps of tumorigenesis[22,23]. Transient *Mad2* overexpression in transgenic mice leads to CIN, which may take place before cell transformation and tumor formation in a wide spectrum of tissues. Additionally, MAD2 has been described to be upregulated in a subset of human cancer types[22]. Furthermore, aneuploidy caused by increased rates of numerical chromosome missegregation in *Cenp-E*$^{+/-}$ mice promotes tumorigenesis, giving rise to splenic lymphomas and lung adenomas, without evidence of additional defects. However, the same animals were less likely to develop spontaneous liver tumors and tumors provoked by exposure to a carcinogen, thus leading to the conclusion that CIN can act

both as tumor promoter and tumor suppressor[23]. This double-sided nature of CIN might be explained by the observation that low missegregation rates can be tolerated and become tumor-promoting, whereas cells with high rates of missegregation cannot survive, resulting in tumor suppression[24].

1.1.3 Pathways leading to aneuploidy

The maintenance of a euploid karyotype after each cell division is the result of a perfect interaction among the components of the chromosome segregation machinery. However, errors which give rise to daughter cells that have gained or lost genetic material can occur. Mechanisms described as major contributors to aneuploidy include defects of the spindle assembly checkpoint (SAC), erroneous microtubules-kinetochore interactions, chromatid cohesion defects and supernumerary centrosomes.

1.1.3.1 Impaired Spindle Assembly Checkpoint

The SAC prohibits anaphase onset in absence of stable microtubule-kinetochore attachments and kinetochore tension. SAC proteins are recruited to the outer surface of unattached kinetochores inhibiting the activation of the E3 ubiquitin ligase CDC20-APC, or anaphase promoting complex (APC/C), and the subsequent degradation of securin and cyclin B1. Once the checkpoint requests are satisfied, APC/C mediates the ubiquitination of securin and cyclin B1, whose degradation leads to the activation of separase. Separase activity induces cohesin cleavage and the ensuing sister-chromatid separation, cyclin-dependent kinase 1 (CDK1) inactivation and mitotic exit. Mutations or reduced concentrations of these proteins may impair checkpoint functionality. Cells might enter anaphase with unattached or misaligned chromosomes causing missegregation of sister-chromatids into the same daughter cell. The majority of studies that describe a correlation between weakened SAC activity and high incidence of aneuploidy and tumorigenesis have been performed in mouse models. Mice heterozygous for SAC-related genes show high levels of aneuploidy in comparison to wild-type controls[25,26,27]. However, in human cancer, mutations in SAC genes are rare[28]. Consistently, the majority of primary cancer cells have been described to have an intact SAC[29,30].

1.1.3.2 Erroneous microtubule-kinetochore interactions

During mitosis progression the establishment of correct interactions between microtubules and kinetochores is fundamental. Microtubules bind and release kinetochores several times until sister kinetochores have bound to opposite spindle poles. Correct microtubule-kinetochore configuration is called amphitelic attachment (Fig. 2A) and only when all kinetochores are connected to microtubules in an amphitelic orientation cells can proceed into anaphase. However, erroneous orientation frequently occurs in early mitosis and must be corrected in order to have accurate chromosome

segregation into daughter cells. The SAC is able to detect some types of erroneous microtubule-kinetochore attachments such as monotelic and syntelic ones, whereas merotelic attachments are not sensed by the checkpoint.

Monotelic attachments (Fig. 2B) result from the capture of microtubules by just one of the sister-kinetochores and lead to the movement of both sister-chromatids to one pole. In cells with an active SAC, it is unlikely that aneuploid daughter cells arise by this type of attachment error as the presence of one unattached kinetochore is already sensed by the mitotic checkpoint[31].

Syntelic attachments (Fig. 2C) occur when microtubules from one spindle pole bind to both sister-kinetochores of a chromosome, leading to activation of the SAC and prevention of anaphase entry as well[32].

Merotelic attachments (Fig. 2D), conversely, occur when microtubules generated from both spindle poles bind to the same kinetochore. In this case, sufficient tension necessary to inactivate the SAC is established and cells can proceed into anaphase without any mitotic delay[33]. For this reason, chromosomes bound to both spindle poles are either segregated to the pole from which the thicker microtubules bundle nucleates or maintained at the metaphase plate after anaphase onset, constituting lagging chromosomes. Merotelic orientations thus have the potential to drive cell transformation and carcinogenesis even in cells with an active SAC[34,35].

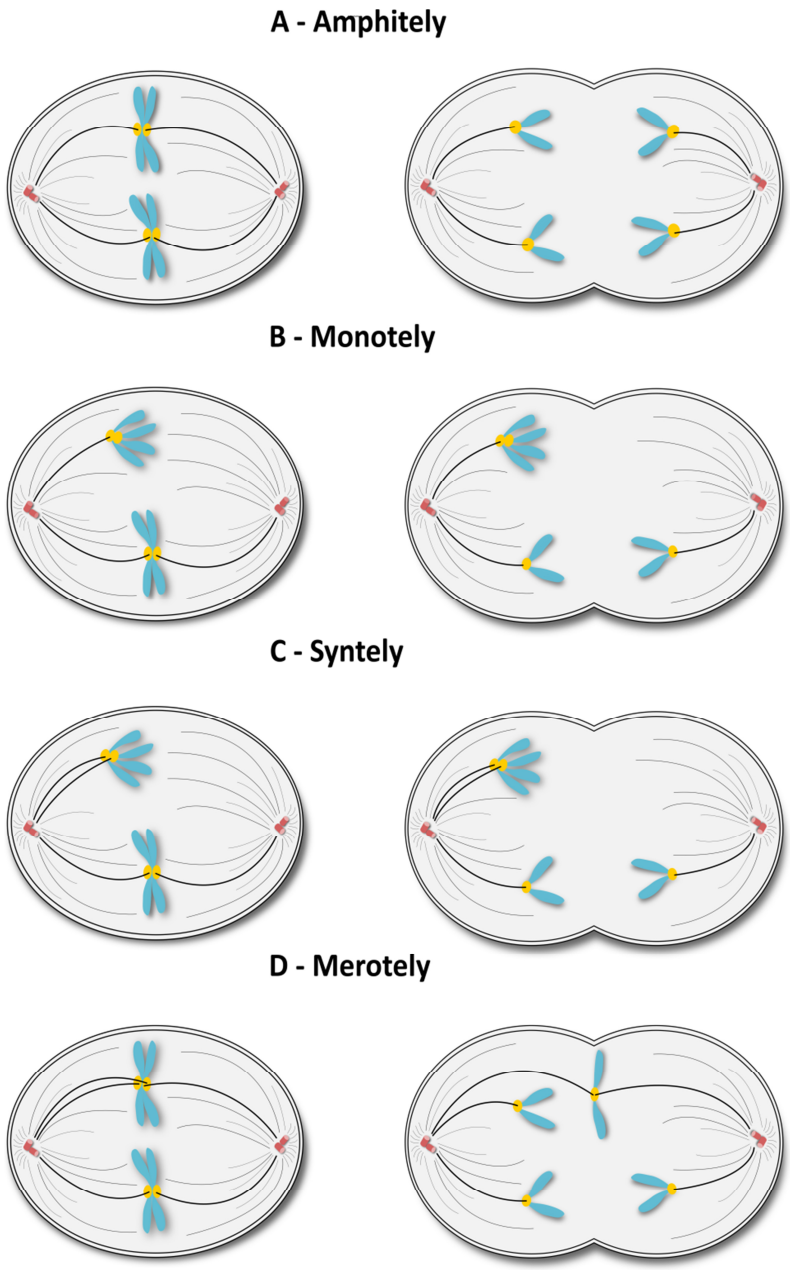

Figure 2 | Microtubule-kinetochore attachments

Amphitely describes the correct state of microtubule-kinetochore attachment. Monotely, syntely and merotely represent erroneous microtubule-kinetochore connections.

1.1.3.3 Chromatid cohesion defects

More recent analyses suggest that chromatid cohesion defects might be involved in aneuploidy and cancer progression. These errors lead to a premature separation of sister-chromatids and to the subsequent failure of an equal segregation of chromosomes into daughter cells. Mutations in many

genes encoding for cohesion complex subunits have been frequently found in various human tumor types[36,37,38]. Nevertheless, many of the patients described to harbor mutations in those genes have normal karyotypes, suggesting that other mechanisms of action of these proteins might be involved in the transformation process [39,40,38].

1.1.3.4 Supernumerary centrosomes

Mechanistically, the presence of supernumerary centrosomes is believed to be the main cause of chromosome missegregation[41]. Indeed, centrosome aberrations are recurrent in the majority of cancers, both solid and hematological[42,43,44,45], and correlate with karyotype abnormalities and poor prognosis. Supernumerary centrosomes can arise from centriole overduplication, *de novo* centriole synthesis, mitotic slippage, aborted cell division and cell fusion[46]. Chromosome missegregation can result from a transient multipolar spindle in which merotelic attachments occur before supernumerary centrosomes cluster into a bipolar spindle[47] (Fig. 3). More recently, an additional mechanism has been described: mitoses which immediately follow centriole overduplication are bipolar, with a centriole rosette at one or both spindle poles (Fig. 3). Mitotic rosettes at the two poles of a mitotic spindle frequently harbor an unbalanced centriole number which correlates with the number of nucleated microtubules. Consequently, the spindle pole with the rosette containing more centrioles captures more chromosomes, increasing the probability to establish merotelic attachment defects and causing lagging chromosomes[48].

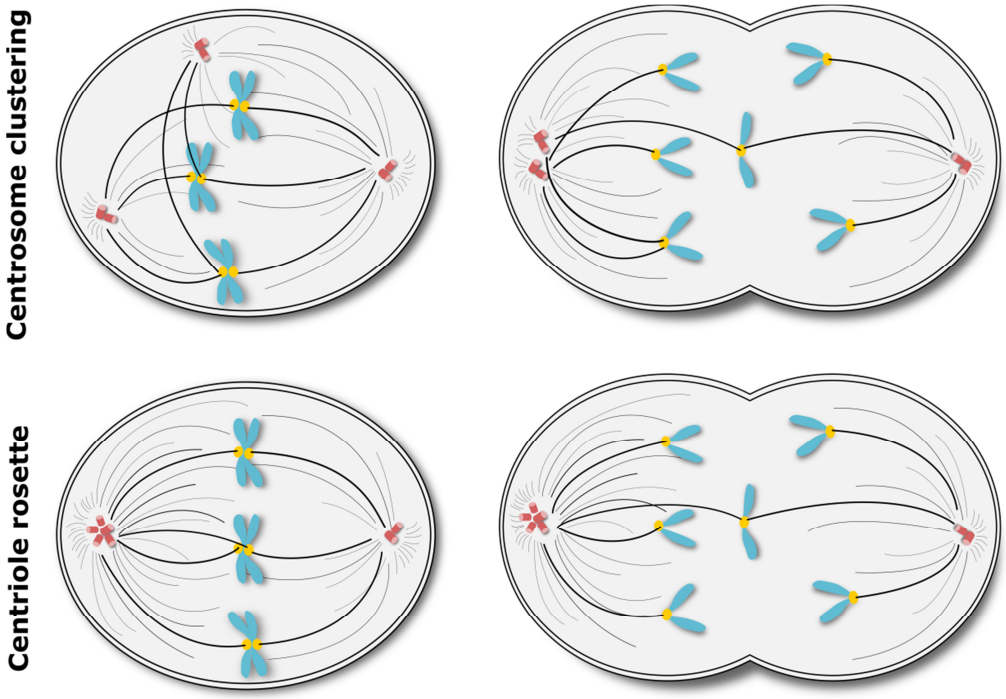

Figure 3 | Centrosome clustering and centriole rosettes

Both types of centrosome aberrations cause erroneous merotelic microtubule-kinetochore attachments.

1.1.4 Consequences of aneuploidy

Several studies performed on aneuploid yeast, mammalian cell lines, flies and plants have revealed that all of these organisms display shared phenotypes which can be attributed to aneuploidy, such as pathway deregulation (DNA and RNA metabolism; endoplasmic reticulum, Golgi apparatus and lysosome function; membrane and mitochondrial metabolism), hampered proliferation and increased energy and metabolic requests.

1.1.4.1 Inhibition of cell proliferation

Typically, aneuploidy comes with a fitness cost. Aneuploid cells generally grow slow and are prone to replication stress, ensuing DNA damage and gene mutations. Cultured skin fibroblasts from patients with Down syndrome have a significantly longer doubling time relative to cells of healthy donors with the same age[49]. Aneuploid yeast strains show G_1-phase delay and even those which do not exhibit a proliferative impairment have a lower growth capacity than wild-type strains[50]. Furthermore, G_1 delay has been described in human engineerized trisomic cells as well[51]. An altered proliferative capacity has also been detected in trisomic mouse embryonic fibroblasts (MEFs) and correlates with the size of the additional chromosome[52]. Together, these observations indicate that impaired proliferation is a common finding in aneuploid cells.

1.1.4.2 Transcriptional responses and effects on the proteome

Chromosome number alterations markedly influence the physiology of organisms. The mechanisms responsible for the detrimental effects of aneuploidy are still not completely unraveled, but it has been shown that aneuploidy causes changes at both transcriptional [50,52,51,53,54] and protein levels[51,55,56].

In both yeast and humans, it has been demonstrated that the expression of the majority of genes which are present at additional chromosome copies is proportionately increased[50,52,51,54]. Although in most of the cases the amount of proteins scales with gene copy number, some proteins which are encoded by genes present on extra chromosomes are buffered to diploid levels. Among these proteins maintained at stoichiometric levels, several reports list protein complex subunits[50,51,55,57] and protein kinases[51].

Conversely, a peculiar feature named “aneuploidy-associated protein signature (APS)” has been described in disomic versus wild-type yeast. It implies the upregulation of proteins associated with

cellular response to oxidative stress without an increase of the corresponding transcripts, possibly due to protein stabilization[55].

Interestingly, studies in budding yeast indicate that the altered phenotypes associated with chromosome aberrations are due to the relative amount of supernumerary genes. Indeed, phenotype abnormalities derived from the acquisition of a single chromosome are more emphasized in haploid than diploid yeast[50].

In addition to the increased mRNA abundance derived from the presence of supernumerary chromosomes, the expression of other genes is often altered in aneuploid cells as well. This occurs as a consequence of the overexpression of regulatory proteins which influence expression of genes present on other chromosomes and/or as a consequence of the activation of specific responses to aneuploidy[50,53,58]. Derived phenotypes are thus the result of concurrent changes in the transcript amount of many genes, which would have only little impact on cellular function individually. The response to the aneuploid state occurs independently of the identity of the extra chromosome and seems to be conserved, involving similar pathways in different organisms, from plants to mice and humans[58]. It mainly implies the upregulation of pathways related to cellular stress and membrane metabolism as well as the downregulation of pathways connected to nucleic acid metabolism and cell proliferation[51,53].

1.1.4.3 Proteotoxic stress

Proteotoxic stress is one of the most prominent features of aneuploid cells. It results from the accumulation of unfolded or misfolded proteins due to altered and overwhelmed regulatory mechanisms which preserve protein homeostasis. In normal cells chaperone-mediated protein folding, as well as proteasome and autophagy activation, ensure that only an appropriate amount of proteins and their active forms are maintained. Many subunits of protein complexes are unstable until they bind to their partners and for this reason they interact with chaperones in order to maintain their solubility. If no partner is found, they are degraded by proteases. In aneuploid cells protein stoichiometries are impaired and this affects the quality control machinery. Enhanced protein production, which occurs in karyotypically aberrant cells, induces saturation of the protein folding pathways, which in turn leads to protein misfolding and degradation. It has been proposed that subsequent chronic proteotoxic stress may inhibit the activity of additional factors fundamental for the cellular response to this pathological state, resulting in a vicious cycle.

The molecular chaperone heat shock protein 90 (HSP90), whose client proteins are mostly kinases and signal transduction proteins, has been shown to have diminished activity and folding capacity in aneuploid yeast strains[59]. In line with these findings, aneuploid versions of human immortalized retinal pigment epithelial (RPE-1) cells and tumorigenic human colon cancer (HCT116) cells have

consistently lower amounts of HSP90 transcripts and protein levels than their diploid cognates, probably due to defective activation of heat shock factor 1 (HSF1)[60]. Both aneuploid yeast strains and human cell lines are also more sensitive to chaperone inhibitors geldanamycin and 17-AAG, in comparison to euploid cells[50,60]. By contrast, trisomic MEFs harbor increased heat shock protein 72 (HSP72) levels. Despite this difference they are still sensitive to the HSP90 inhibitor 17-AAG, suggesting that defective HSP90 protein folding activity represents a conserved consequence of aneuploidy [61].

Aneuploidy also compromises protein degradation pathways. Aneuploid yeast strains exhibit hampered proliferation after treatment with the proteasome inhibitor MG132 at concentrations which do not affect euploid cells as well as after treatment with drugs which interfere with protein synthesis[50]. Moreover, inactivating mutation of the proteasome-associated deubiquitinating enzyme *UBP6* gene reverses the negative effect of aneuploidy on protein composition and cellular fitness[57,55]. Conversely, proteasome-mediated degradation of proteins and autophagy seem to be increased in mammalian cells with an abnormal karyotype. Indeed, trisomic MEFs do not show the same sensitivity to proteasome inhibitors as yeast and exhibit an increased lipidated form of the autophagy marker light chain 3 (LC3)[61]. Similarly, LC3 foci are also increased in aneuploid human cell lines in which p62/sequestosome-1 (SQSTM1)-mediated autophagy takes place[51]. Further studies proposed the idea that, due the overloaded chaperone capacity and compromised proteasome activity, misfolded proteins form aggregates which become included into autophagosomes. Subsequent lysosomal saturation triggers lysosome stress response. Indeed, TFEB, a regulator of genes involved in autophagy, is overexpressed in aneuploid cells in order to generate additional autophagosome and lysosome activity[62]. Thus, increased lysosomal burden contributes to the reduction of cellular fitness and to augmented sensitivity of trisomic MEFs to the lysosome inhibitor chloroquine[61].

1.1.4.4 Genomic instability

It is becoming evident that the presence of an altered karyotype has a detrimental effect on genome stability. It has been shown that budding yeast strains with abnormal karyotypes display increased rates of chromosome missegregation, mitotic recombination and DNA damage. Aneuploid strains are also more sensitive to genotoxic agents[63]. Similarly, human cell lines with extra copies of a single chromosome exhibit DNA damage as shown by increased 53BP1 foci in G_1 cells. Furthermore, these cells are more sensitive to agents inducing replication stress such as aphidicolin[64].

Genomic rearrangements occur frequently due to lagging chromosome breakage during cytokinesis leading to chromosomal deletions and translocations[65]. Chromosomes which lag behind during anaphase, even if segregated properly, are frequently not incorporated with the other chromosomes into the newly forming nucleus, but form separate micronuclei instead. Micronuclei can persist for

several cell division cycles. DNA replication within micronuclei is often defective and mitotic entry can occur before micronuclear DNA replication has been concluded[66]. As a consequence, chromosomes entrapped in micronuclei frequently become fragmented in a process called chromothripsis[67], which designates a one-time catastrophic event during which chromosomes or chromosome arms are shattered into fragments. When these fragments are subsequently stitched together by DNA repair mechanisms, intrachromosomal rearrangements including deletions, duplications, inversions and translocations occur. These rearranged chromosomes can join the main nucleus in subsequent mitoses generating both numerical and structural chromosomal instability. Chromothripsis has been described in many types of malignancies and is found in about 2-3% of cancers[67].

1.1.5 Cellular tolerance to aneuploidy

Although the detrimental effects of aneuploidy and CIN are well described, karyotype imbalances may confer proliferative advantages and promote tumorigenesis. Under certain circumstances aneuploidy can have a tumor suppressor role, but once aneuploid cells overcome certain limitations, aneuploidy itself becomes beneficial for cancer development.

Chromosome missegregation may be accompanied by DNA damage, structural aberrations and subsequent genomic instability, which can be the driver of tumor evolution. Loss of tumor suppressor genes and gain of oncogenes lead to impairment of signaling pathways that normally restrict aneuploid cell proliferation, thus allowing cells to tolerate the adverse effects of aneuploidy and tumor evolution. For example, TP53 (also known as p53) activation is known to be triggered by errors in chromosome segregation[65,68,69], even if the aspects of chromosome missegregation that cause p53 activation are still not clarified and multiple mechanisms might be responsible[70]. *TP53*, at the same time, is one of the most frequently mutated genes in human cancers, arguing that mutations of genes that suppress the antiproliferative effects of aneuploidy and CIN are important factors in carcinogenesis.

Aneuploidy generates phenotypic diversity that might induce a selective advantage for tumor evolution in a changing environment. Even if the majority of aneuploid cells is less proliferatively active than normal diploid cells, favorable karyotypic variants and selection pressure can confer a growth advantage to chromosomally unstable cells due to their improved adaptability[71,72].

It seems that in certain cases aneuploid cells, in order to survive, become polyploid. The gain or loss of a single chromosome seems to have a greater impact on haploid compared to diploid and tetraploid cells and thus the acquisition of an additional chromosome set may attenuate the

consequences of aneuploidy, balancing gene dosage alterations[73].

Additionally, compensatory events such as the degradation of certain proteins (e.g. the members of protein complexes[50,51]) might be important for the re-establishment of stoichiometric balance and aneuploidy tolerance.

1.1.6 Aneuploidy as a therapeutic target

Since aneuploidy is a hallmark of cancer associated with poor prognosis and a rare event in normal tissues, it constitutes an attractive potential therapeutic target. Some studies have started to investigate this opportunity. With the idea to interfere with pathways compromised in aneuploid cells, Tang *et al.* identified compounds (AICAR, 17-AAG and chloroquine) that show specificity against triploid MEFs[61]. They seem to exaggerate the basal stress associated with chromosome copy number changes. Interestingly, AICAR and 17-AAG impair the growth of colon cancer cell lines with CIN. The combination of the two drugs is even more effective with regard to inhibition of cell viability[61]. 17-AAG shows selective efficacy also against trisomic and tetrasomic HCT116 cells and trisomic human immortalized RPE-1 cells[60]. More recently, an additional drug screening reported that several agents which stimulate the activation of the AMP-activated protein kinase (AMPK), such as resveratrol, piceatannol, salicylates, AICAR, and A-769662, selectively eliminate tetraploid cells in diverse cancer cell lines as well as *in vivo*[74]. Tetraploid cells are transitionally found in pre-malignant lesions and early stages of multiple tumor cell types before they develop aneuploid karyotypes by chromosomal loss in mitosis [75,76]. Additionally, 8-azaguanine and DPBQ have been shown to be more effective against high-ploidy RPE-1 and breast epithelial MCF10A cells compared to their diploid counterparts[77].

1.2 Acute myeloid leukemia

Acute myeloid leukemia (AML) is a clonal malignancy of hematopoietic progenitor cells characterized by arrest of differentiation, uncontrolled proliferation and the consequential presence of atypical immature myeloid cells, called blasts, in bone marrow, peripheral blood and other tissues. Early signs and symptoms, which are mainly attributable to progressive bone marrow insufficiency, are paleness, weakness, shortness of breath and tachycardia (due to anemia), easy bruising or haemorrhages (due to thrombocytopenia) and susceptibility to infections (due to granulocytopenia). Symptoms and signs caused by the infiltration of liver, spleen, lymph nodes, skin and central nervous system can also occur.

1.2.1 Epidemiology

AML is the most common acute leukemia in adults. It has a higher prevalence in elderly people, with a median age at diagnosis of 68 years[78]. The incidence of new cases seems to be rising over the years, probably due to the increasing age of the population and to previous exposition to toxic agents or chemotherapy. AML can occur after progression of other hematological diseases or as a consequence of prior cytotoxic therapy, but it arises *de novo* in most of the cases[79,80]. An older age at diagnosis is associated with worse prognosis. The disease is currently cured in 35-40% of patients younger than 60 and only in 5-15% of older patients[81]. With intensive induction therapy complete remission is reached in 60-80% of young patients and 40-60% of elderly patients[82]; however, in most individuals the disease relapses within 3 years after diagnosis[81].

1.2.2 AML classifications

In the 1970s AML was initially classified according to the French-American-British (FAB) classification system considering morphologic features of blasts[83]. AML was divided in 8 classes, M0-M7, on the basis of the hematopoietic lineage and differentiation status of the neoplasm. Starting from 2002 the World Health Organization (WHO) classification has almost completely replaced the FAB classification. It assigns a strong importance to cytogenetic and molecular genetic features besides the morphologic and immunophenotypic evaluation[84,85].

1.2.3 Diagnosis

Procedures currently used to diagnose AML include complete blood count and differential leukocyte count, morphologic studies of bone marrow specimens and blood smear, immunophenotyping of cell surface and cytoplasmic markers, cytogenetics and molecular genetic studies.

Morphology and immunophenotypic features are used to assess the blast lineage and to evaluate the level of maturation of the neoplastic cells. According to WHO guidelines, AML is diagnosed by the presence of >20% of blasts among total cells in either bone marrow (BM) or peripheral blood (PB) after the analysis of at least 200 leukocytes in PB and 500 nucleated cells in BM[86]. Cytogenetic studies together with the screening for selected mutations constitute mandatory diagnostic procedures because certain abnormalities are strongly correlated with long-term prognosis and allow for specific treatment.

1.2.4 Prognostic factors

Thanks to the progress made in the next-generation-sequencing field, the molecular heterogeneity of AML has been highlighted and genetic abnormalities have gained increasing interest not only as diagnostic markers, but also as prognostic factors. Indeed, according to the European LeukemiaNet (ELN) recommendations, AML is classified into three prognostic risk groups which take into account both karyotype abnormalities and genetic mutations: favourable, intermediate and adverse (Tab. 1)[82].

Risk Group	Abnormalities
Favourable	t(8;21)(q22;q22.1); *RUNX1-RUNX1T1* inv(16)(p13.1q22) or t(16;16)(p13.1;q22); *CBFB-MYH11* Mutated *NPM1* without *FLT3-ITD* or with *FLT3-ITD^{low}* Biallelic mutated *CEBPA*
Intermediate	Mutated *NPM1* and *FLT3-ITD^{high}* Wild-type *NPM1* without *FLT3-ITD* or with *FLT3-ITD^{low}* (without adverse-risk genetic lesions) t(9;11)(p21.3;q23.3); *MLLT3-KMT2A* Cytogenetic abnormalities not classified as favorable or adverse
Adverse	t(6;9)(p23;q34.1); *DEK-NUP214* t(v;11q23.3); *KMT2A* rearranged t(9;22)(q34.1;q11.2); *BCR-ABL1* inv(3)(q21.3q26.2) or t(3;3)(q21.3;q26.2); *GATA2,MECOM(EVI1)* -5 or del(5q); -7; -17/abn(17p) Complex karyotype, monosomal karyotype Wild-type *NPM1* and *FLT3-ITD^{high}* Mutated *RUNX1* Mutated *ASXL1* Mutated *TP53*

Table 1 | AML risk groups and respective abnormalities according to ELN recommendations

t: translocation; inv: inversion; del: deletion; abn: abnormal.

Recurrent mutations in leukemia-associated genes such as *FLT3, NPM1, C-KIT, N-RAS, CEBPA, WT1, ASXL1, DNMT3A, MLL, TET2, IDH1* and *IDH2* have been identified. Nevertheless, more than 25% of AML patients carry no mutations in those genes[87]. *NPM1, FLT3* and *CEBPA* mutation screening has been introduced into routine clinical practice[88]. Indeed, *CEBPA* biallelic mutations and mutated *NPM1*, in presence of wild-type *FLT3-ITD*, are considered favorable prognostic risk factors independently of other coexisting abnormalities[89,90], whereas patients with mutations in both *NPM1* and *FL3-ITD* genes are classified into the intermediate risk group. By contrast, *FLT3-ITD* mutations in the absence of *NPM1* mutations confer an adverse risk[82]. Thus, the prognostic impact of one factor can be strongly dependent on the presence or absence of other abnormalities.

1.2.5 Complex karyotype

An abnormal karyotype is found in approximately 60% of patients with AML[91]. Among all chromosome aberrations t(8;21)(q22;q22.1), inv(16)(p13.1q22) or t(16;16)(p13.1;q22) and t(15;17) are considered markers of good prognosis, independently of the presence of additional abnormalities. t(6;9)(p23;q34.1), t(v;11q23.3), t(9;22)(q34.1;q11.2), inv(3)(q21.3q26.2) or t(3;3)(q21.3;q26.2), monosomy 5 or del(5q), as well as monosomy 7 and 17 or abn(17p) are instead included in the adverse risk group together with complex and monosomal karyotypes[92]. According to the ELN criteria a complex karyotype is defined by the presence of three or more chromosome aberrations, in the absence of recurrent translocations or inversions including t(8;21), inv(16) or t(16;16), t(15;17), t(9;11), t(6;9), t(v;11q23.3), t(9;22), inv(3) or t(3;3)[82]. Aberrations such as derivative chromosomes, marker chromosomes, ring chromosomes and double minutes should also be taken into account[93,94,95]. In AML cells chromosomal losses are more frequent than chromosomal gains[96]. Approximately 10-14% of all AML patients and 23% of elderly patients harbor a complex karyotype and their prognosis is dismal despite intensive treatment[97,98].

1.3 Aim of the project

The aim of this study is to identify compounds which show selective activity against aneuploid AML cells and to further investigate the mechanisms leading to this specific effect.

The general treatment approach for AML has been maintained similar for the last 40 years[99]. Indeed, conventional therapy for most patients consists in the combination of the nucleoside analog cytarabine and the anthracycline daunorubicin. Since patients with aneuploid karyotypes respond poorly to conventional chemotherapy there is a high clinical need for the development of new compounds and new therapeutic approaches. The advances made in the identification of recurrent cytogenetic aberrations and mutations in AML suggest development of specific therapies for different AML subgroups[100]. The introduction of drugs with selective efficacy against aneuploid karyotypes appears as a reasonable and competitive approach in patients affected by complex karyotype AML. Indeed the effectiveness of the use of compounds specifically targeting aneuploidy has already been proven in other models.

For this purpose, first, compounds including drugs already described as selectively active against aneuploid cells and some other anti-cancer drugs were tested on AML primary samples.

Subsequently an isogenic AML cell line model was generated to evaluate the specific efficacy of the identified aneuploidy-selective antiproliferative compounds and the mechanisms involved in their action.

Since p53 might limit the propagation of aneuploidy and p53 loss is frequently found in complex karyotype AML, we also introduced a *TP53* knock-out into the AML EEB cell line. We aimed at expanding the number of clones that constitute the model by the development of new different karyotypic aberrations and testing the compounds of interest in a p53-deficient setting as well. Furthermore, we investigated whether p53 deficiency is sufficient to cause aneuploidy and CIN in AML cells and whether p53-deficient and p53-proficient AML cells tolerate segregation errors to a different extent.

2 Material

2.1 Material for cell biology methods

2.1.1 Patient material

34 bone marrow aspirates or peripheral blood samples from patients with acute myeloid leukemia, characterized by the presence of at least 80% of blasts, were provided by the Department of Internal Medicine V, University Hospital Heidelberg and by the Department of Medicine Clinic and Polyclinic I, University of Dresden. Cells were cultured in Mononuclear Cell Medium (MCM) supplemented with 0.5 µg/ml gentamicin and 2.5 µg/ml amphotericin B.

2.1.2 Cell lines

Name	Origin	Characteristics	Culture conditions
EEB	Homo sapiens, AML	EEB cell line was provided by the RIKEN BRC through the National Bio-Resource Project of the MEXT, Japan	StemSpan SFEM, 15% FBS
1C1 - 46, XY		Derived from single cell seeding of EEB cell line	
1C6 - 46, X, -Y		Derived from single cell seeding of EEB cell line	
5C3 - 90, XX, -Y, -Y		Derived from single cell seeding of EEB cell line	
MC3 - 47, XY, +12		Derived from single cell seeding of EEB cell line after treatment with CENP-E and MPS1 inhibitors	
MC7 - 47, X, -Y, +7, +21		Derived from single cell seeding of EEB cell line after treatment with CENP-E and MPS1 inhibitors	
MC27 - 47, XY, +22		Derived from single cell seeding of EEB cell line after treatment with CENP-E and MPS1 inhibitors	
10-1		Derived from 1C1 – 46, XY cell line after p53 knock-out	
9-5		Derived from 1C1 – 46, XY cell line after p53 knock-out	
8-1		Derived from 1C1 – 46, XY cell line after p53 knock-out	

Table 2 | Cell lines

2.1.3 Media and supplements for cell culture

Name	Company, Catalogue number
Mononuclear Cell Medium (MCM)	PromoCell, Cat. No. C-28030
StemSpan SFEM	STEMCELL Technologies, Cat. No 09650
Fetal Bovine Serum (FBS)	Clontech, Cat. No. 631106
Gentamicin	Sigma-Aldrich, Cat. No. G1272-10ML
Amphotericin B	Biochrom, Cat. No. A 2612

Table 3 | Media and supplements for cell culture

2.1.4 Buffers and solutions for mononuclear cells extraction

Name	Ingredients, Company, Catalogue number
Biocoll separating solution	Biochrom AG, Merk Millipore, Cat. No. L6115
1x Dulbecco's Phosphate Buffered Saline (D-PBS)	Life Technologies, Cat. No. 14200067
Erythrocyte lysis buffer	NH_4Cl 1.5M, $KHCO_3$ 0.10M, EDTA 1mM, pH 7.3

Table 4 | Buffers and solutions for mononuclear cells extraction

2.1.5 Compounds

Name	Company, Catalogue number
AICAR	Cayman Chemical, Cat. No. Cay10010241-50
Cytarabine	Cayman Chemical, Cat. No. Cay16069-500
Daunorubicin	Cayman Chemical, Cat. No. Cay14159-5
Metformin	Cayman Chemical, Cat. No. Cay13118-1
Vincristine	Cayman Chemical, Cat. No. Cay11764-5
Acetylsalycilic acid	Sigma-Aldrich, Cat. No. A5376-100G
Chloroquine	Sigma-Aldrich, Cat. No. C6628-25G
Cisplatin	Sigma-Aldrich, Cat. No. P4394-25MG
Resveratrol	Sigma-Aldrich, R5010-100MG
8-Azaguanine	Santa Cruz, Cat. No. sc-207194
Paclitaxel	AdipoGen, Cat. No. AG-CN2-0045-M005
17-AAG	Selleckchem, Cat. No. S1141
Crenolanib	Selleckchem, Cat. No. S2730
Centrinone	MedChemexpress Co., Ltd., Cat. No. HY-18682

Table 5 | Compounds tested

2.1.6 Reagents for fixation and cell staining

Name	Ingredients, Company, Catalogue number
Acetone	Sigma-Aldrich, Cat. No. 179973-2.5L
Methanol	Sigma-Aldrich, Cat. No. 32213-2.5L
Parafolmaldehyde	Applichem, Cat. No. A3813,1000
Acetic acid glacial	Fisher Scientific, Cat. No. 10171460
Triton X-100	Sigma-Aldrich, Cat. No. 114K0182
Blocking solution	10% goat serum in 1x PBS
Goat serum	Life Technologies, Cat. No. 16210064
Fluoromount-G™	eBioscience, Cat. No. 00-4958-02
Vectashield antifade mounting medium	Vector Laboratories, Cat. No. H-1000

Table 6 | Reagents for fixation and cell staining

2.1.7 Primary antibodies for immunofluorescence staining or Western blotting

Name	Clone	Species	Dilution	Company, Catalogue number
γH2AX	JBW301	Mouse (m)	1:1000	Merck Milllipore, Cat. No. 05-636
Actin	C4	Mouse (m)	1:5000	Santa Cruz Biotechnology, Cat. No. sc-47778 HRP
Caspase-2	11B4	Rat (m)	5 µg/ml	Merck Milllipore, Cat. No. MAB3507
Caspase-3	3G2	Mouse (m)	1:1000	Cell Signalling, Cat. No. 9668
Cleaved Caspase-3 Asp175	5A1E	Rabbit (m)	1:1000	Cell Signalling, Cat. No. 9664
Caspase-8 p18	2B12.1	Mouse (m)	2 µg/ml	Merck Milllipore, Cat. No. MAB10754
Caspase-9	C9	Mouse (m)	1:1000	Cell Signalling, Cat. No. 9508
CHOP	L63F7	Mouse (m)	1:1000	Cell Signalling, Cat. No. 2895
GAPDH	411	Mouse (m)	1:2000	Santa Cruz Biotechnology, Cat. No. sc-47724
HGPRT	EPR5299	Rabbit (m)	1:5000	Abcam. Cat. No. ab109021
MCM7	142.1	Mouse (m)	1:2000	Santa Cruz Biotechnology, Cat. No. sc-9966
PARP	46D11	Rabbit (m)	1:1000	Cell Signalling, Cat. No. 9532
p44/45 MAPK (Erk1/2)		Rabbit (p)	1:1000	Cell Signalling, Cat. No. 9102
Phospho-p44/42 MAPK (Erk1/2) (Thr202/Tyr204)	D13.14.4E	Rabbit (m)	1:1000	Cell Signalling, Cat. No. 4370
Phospho-SAPK/JNK (Thr183/Tyr185)	98F2	Rabbit (m)	1:1000	Cell Signalling, Cat. No. 4671

p53	Bp53.11	Mouse (m)	1:5000	Progen, Cat. No.61039
p21	DCS60	Mouse (m)	1:2000	Cell Signalling, Cat. No. 2946

Table 7 | Primary antibodies

(m) monoclonal; (p) polyclonal

2.1.8 Secondary antibodies for immunofluorescence staining or Western blotting

Name	Fluorochrome	Species	Dilution	Company, Catalogue number
Mouse IgG	Alexa Fluor 488	Goat (p)	1:1000	Life Technologies, Cat. No. A11029
Mouse IgG	Alexa Fluor 568	Goat (p)	1:1000	Life Technologies, Cat. No. A11031
Rabbit IgG	Alexa Fluor 488	Goat (p)	1:1000	Life Technologies, Cat. No. A11034
Rabbit IgG	Alexa Fluor 568	Goat (p)	1:1000	Life Technologies, Cat. No. A11036
IgG anti-mouse IgG (H+L)-HRPO		Goat (p)	1:10000	Jackson immuno research, Cat. No. 115-035-003
IgG anti-rabbit IgG (H+L)-HRPO		Goat (p)	1:10000	Jackson immuno research, Cat. No. 111-035-003
IgG anti-rat IgG (H+L)-HRPO		Goat (p)	1:10000	Jackson immuno research, Cat. No. 112-035-003

Table 8 | Secondary antibodies

(p) polyclonal

2.1.9 Cell stains

Name	Dilution	Company, Catalogue number
Hoechst 33342, trihydrochloride, trihydrate	Stock: 10 mg/ml, 1:1000	Life Technologies, Cat. No. H1399
Propidium Iodide	Stock: 1 mg/ml, 1:100	Life Technologies, Cat. No. P3566

Table 9 | Cell stains

2.1.10 Small molecules and inhibitors

Name	Treatment conditions	Company, Catalogue number
Thymidine	2 mM, for 24 h	Sigma-Aldrich, Cat. No. T1895-5G
NMS-P715	480 nM, for 24 h	Merck Millipore, Cat. No. 475949-5MG
GSK923295	50 nM, for 24 h	Selleckchem, Cat. No. S7090
U0126	1 µM, 2.5 µM, for 48h	Promega, Cat. No. V1121

Table 10 | Small molecules and inhibitors

2.1.11 Reagents for cell viability testing and caspase activity analysis

Name	Company, Catalogue number
TC10 Trypan Blue Dye 0,4%	Bio-Rad Laboratories GmbH, Cat. No. 145-0013
CellTiter-Glo® 2.0 Assay	Promega, Cat. No. G9242
WST-1	Roche, Cat. No. 11644807001
Caspase-Glo® 3/7 Assay	Promega, Cat. No. G8091

Table 11 | Reagents for cell viability testing and caspase activity analysis

2.1.12 Reagents and solutions for metaphase preparation

Name	Ingredients, Company, Catalogue number
Colcemid	Biochrom, Cat. No. L 6221
Hypotonic solution	0.075 M KCl

Table 12 | Reagents and solutions for metaphase preparation

2.1.13 Kits

Name	Company, Catalogue number
Annexin V Apoptosis Detection Kit 1	Becton Dickinson, Cat. No. 556547
Neon™ Transfection System 10 µL Kit (Buffer R, Electrolytic Buffer E)	Invitrogen, Cat. No. MPK1096

Table 13 | Kits for cell biology methods

2.2 Material for protein biochemistry methods

2.2.1 Reagents and material for cell lysis and Western blotting

Name	Ingredients, Company, Catalogue number
Protein lysis buffer, RIPA	50 mM Tris/HCl pH 7.4, 1% NP-40, 0.25% Sodium deoxycholate, 1 mM NaCl, 1 mM EDTA, 1 tablet per 50ml Complete Protease inhibitor, 5 tablets per 50 ml Phospho-Stop
cOmplete™ tablets EASYpack	Roche, Cat. No. 05892970001
PhosStop™ EASYpack	Roche, Cat. No. 04906837001
Quick Start™ Bradford 1x Dye Reagent	Bio-Rad Laboratories, Cat. No. 500-0205
6x SDS sample loading buffer	7 ml 1M Tris-Cl/0.4% SDS pH 6.8, 3 ml Glycerol, 1 g SDS, 0.93 g DTT, 0.01% bromophenol blue
Precision Plus Protein™ Dual Color Standards	Bio-Rad Laboratories, Cat. No. 161-0394
Acrylamide/Bis-Acrylamide	30% Acrylamide, 0.15% Bis-Acrylamide
Solution B	3 M Tris-Base, 0.4% SDS, pH 8.8
Solution C	0.75 M Tris-Base, 0.4% SDS, pH 6.8
Rotiphorese® Gel 30 (37,5:1)	Roth, Cat. No. 3029.1
Separating gel	Acrylamide/Bis-Acrylamide, Solution B, ddH_2O (volumes were adjusted according to gel percentage)
Stacking gel	Rotiphorese® Gel 30 (37,5:1), Solution C, ddH_2O (volumes were adjusted according to gel percentage)
Electrode buffer	0.6% Tris-Base, 2.87% Glycine, 0.1% SDS
APS	10% APS in ddH_2O
TEMED	Serva Electrophoresis, Cat. No. 35925.01
Trans-Blot® Turbo™ RTA Transfer Kit, PVDF	Bio-Rad Laboratories, Cat. No. 1704272
Skim Milk Powder	Gerbu, Cat. No. 1602.025
BSA	Applichem, Cat. No. A1391,0250
1x TBS-T	10 mM Tris, 150mM NaCl, 0.1% Tween 20
Clarity™ Western Blotting ECL Substrate	Bio-Rad Laboratories, Cat. No. 170-5061

Table 14 | Reagents and materials for cell lysis and Western blotting

2.3 Material for molecular biology methods

2.3.1 Media for bacteria transformation

Name	Ingredients
SOB Medium	2% Trypton, 0.5% Yeast extract, 0.05% NaCl, 2.5 mM KCl, 10 mM $MgCl_2$, pH 7.0
SOC Medium	SOB medium, 20 mM Glucose
LB medium	1% Trypton, 0.5% Yeast extract, 1% NaCl pH 7.2
LB agar	LB medium, 1.5% Agar

Table 15 | Media for bacteria transformation

2.3.2 Buffers and loading dyes for DNA and RNA electrophoresis

Name	Ingredients, Company, Catalogue number
6x DNA loading dye	100 mM Tris/HCl pH 7.5, 100 mM Tris/HCl pH 7.5, 200 mM EDTA, 0.01% Bromophenol, 0.01% Blue Xylencyanol, 30% Glycerol
10x TAE buffer	400 mM Tris/HCl pH 8.0, 10 mM EDTA, 200 mM Acetic acid
LowRanger DNA Ladder	Norgen Biotek, Cat. No. 11500
RNA Sample Loading buffer	Sigma-Aldrich, Cat. No. R4268-1VL
10x MOPS buffer	200 mM MOPS, 50 mM Sodium acetate, 10 mM EDTA, pH 6.6

Table 16 | Buffers and loading dyes for DNA and RNA electrophoresis

2.3.3 Primers for PCR and sequencing

Name	Sequence	Manufacturer
p53-long isoforms-Fwd	5´- CTGGTCCTCTGACTGCTCTTTTC - 3´	Eurofins MWG Operon
p53-long isoforms-Rev	5´- TAGAGACGAGGTTTCATCATGTTACC - 3´	
p53-all isoforms-Fwd	5´- CTAGCTCGCTAGTGGGTTGCA - 3´	
p53-all isoforms-Rev	5´- AGTGCTGGGATTACAGGCATGAG - 3´	
p53-all isoforms-Fwd	5´- TGTAGACGCCAACTCTCTCTAGC - 3´	
p53-all isoforms-Rev	5´- GGATTACAGGCATGAGCCACTG - 3´	
hU6-Fwd	5'-GAGGGCCTATTTCCCATGATT-3'	

Table 17 | Primers for PCR and sequencing

2.3.4 Plasmid used for transfection

Name	Company, Catalogue number
pSpCas9(BB)-2A-Puro (PX459) V2.0	Addgene, Cat. No. 62988

Table 18 | Plasmid used for transfection

2.3.5 Enzymes and reagents

Name	Company, Catalogue number
BbsI HF	New England Biolabs, Cat. No. R3539S
CutSmart® Buffer	New England Biolabs, Cat. No. B7204S
Shrimp Alkaline Phosphatase	Thermo Fisher Scientific, Cat. No. 783901000UN
T4 Polynucleotide Kinase	New England Biolabs, Cat. No. B0201S
T4 Polynucleotide Kinase Reaction Buffer	New England Biolabs, Cat. No. B0201S
NxGen T4 DNA Ligase	Lucigen, Cat. No. 30241-1-LU
10x T4 ligase buffer	Lucigen, Cat. No. 30241-1-LU
RNase A	Analytik Jena, Cat. No. A3832,0500
CloneAmp™ HiFi PCR Premix	Clontech, Cat. No. 639298
Phusion® High-Fidelity DNA Polymerase	New England Biolabs, Cat. No. M0530S

Table 19 | Enzymes and reagents

2.3.6 sgRNA

Target	Exon targeted	Sequence	Manufacturer
p53-all isoforms 1	3	5´- GCAGTCACAGCACATGACGGAGG -3´	Eurofins MWG Operon
p53-all isoforms 2	3	5´- CGCTATCTGAGCAGCGCTCATGG - 3´	
p53-long isoforms 1	4	5´- GGCAGCTACGGTTTCCGTCTGGG - 3´	
p53-long isoforms 2	4	5´- CCCCGGACGATATTGAACAATGG - 3´	

Table 20 | sgRNA

2.3.7 Antibiotic for transfected cell selection

Name	Company, Catalogue number
Puromycin	Addgene, Cat. No. 62988

Table 21 | Antibiotic for transfected cell selection

2.3.8 Kits

Name	Company, Catalogue number
QIAmp DNA Mini Kit	Qiagen, Cat. No. 51304
RNeasy Mini Kit	Qiagen, Cat. No. 217004
RNase-Free DNase Set	Qiagen, Cat. No. 79254
QIAprep Spin Miniprep Kit	Qiagen, Cat. No. 27106

Plasmid Maxi Kit	Qiagen, Cat. No. 12163
High Pure PCR Product Purification Kit	Roche, Cat. No. 11732676001
Guide-it™ sgRNA In Vitro Transcription Kit	Takara, Cat. No. 632635
Guide-it™ Complete sgRNA Screening System	Takara, Cat. No. 632636
Qubit RNA BR Assay Kits	Invitrogen, Cat. No. Q10210

Table 22 | Kits for molecular biology methods

2.4 Laboratory equipment

2.4.1 General lab devices

Name	Company
Accuri C6 flow cytometer	Becton Dickinson
Agarose detection system	Intas
Agarose gel casting system	BioRad Laboratories
Centrifuge 5408R	Eppendorf
Centrifuge 5417R	Eppendorf
Centrifuge Megafuge 1.0R	Heraeus
Centrifuge Sorvall RC6Plus	Thermo Fisher Scientific
ChemiDoc™ Touch Imaging System	Bio-Rad Laboratories
Electrophoresis chamber	BioRad Laboratories
Fine scale, LA120S	Sartorius
Heat stirrer, MR Hei-Standard	Heidolph
Incubator for bacteria	Memmert
Incubator for cell culture, C200 Labotec	BeLoTec
Flex Cycler^2	Analytik Jena
pH-Meter SevenMulti	Mettler Toledo
Biophotometer	Eppendorf
Polyacrilamyde gel casting system	BioRad Laboratories
Consort EV power supply unit	Sigma-Aldrich
Qubit fluorometer	Invitrogen
Shaker for bacteria, SM-30 Control	Edmund Bühler
Shaker for Western blot membranes, ST5	CAT
Shandon Cytospin III	Thermo electron corporation
Spark microplate reader	TECAN
Spectrophotometer NanoDrop 2000	PeqLab Biotechnologie Erlangen
Sterile hood, Hera safe KS	Thermo electron corporation
TC20™ automated cell counter	Cell Bio-Rad Laboratories
Thermomixer comfort	Eppendorf
Trans-Blot® Turbo™ System	Bio-Rad Laboratories
UV Table	Konra Benda
Vortex Genie2	Scientific industries
Waterbath Thermomix ME	B.Braun

Table 23 | General lab devices

2.4.2 Devices used for cell transfection

Name	Company
Neon™ Transfection System	Invitrogen
Neon™ Transfection System Pipette	Invitrogen
Neon™ Transfection System Pipette Station	Invitrogen

Table 24 | Devices for cell transfection

2.4.3 Microscopes

Name	Company
Cell observer.Z1 equipped with AxioCam MRm	Carl Zeiss
Fluorescence microscope Axioskop equipped with AxioCam MRm	Carl Zeiss
DMIL	Leica

Table 25 | Microscopes

2.5 Software

Name	Company
BD Accuri™ C6	Becton Dickinson
ZEN lite 2011	Carl Zeiss
ImageJ	Wayne Rasband
Image Lab™	Bio-Rad Laboratories
Microsoft Office 2010	Microsoft Corporation
GraphPad Prism version 7	GraphPad Software
Ingenuity® Pathway Analysis IPA®	QIAGEN

Table 26 | Software

2.6 Reagents

Molecular biology grade or purest available reagents were obtained from the following companies: Applichem, Arcos Organics, Carl Roth, Fisher Scientific, Fluka Chemicals, Gerbu, Merck Millipore, Serva Electrophoresis, Sigma-Aldrich.

2.7 Consumables

Consumables from the following companies were employed: GE Healthcare, Starlab, Sarstedt, Eppendorf and Whatman.

2.8 Solution preparation

All solutions were prepared with double distilled water or Milli-Q® water. Solutions were sterilized by autoclaving them for 20 min at 121°C or by filtration through 0.22 µm filters. Solutions were stored at room temperature unless otherwise stated.

3 Methods

3.1 Cell biology methods

3.1.1 Mononuclear cell isolation

Bone marrow mononuclear cells (BMNCs) and peripheral blood mononuclear cells (PBMCs) were isolated by density gradient centrifugation. 20 ml of bone marrow aspirates or peripheral blood were layered on 15 ml of Biocoll separating solution. The solution was spun down at 425 rcf in a swinging-bucket rotor for 15 minutes without brake. After centrifugation the mononuclear cells were isolated from the interphase between Biocoll and serum. Cells were washed in 1x D-PBS and red blood cells were lysed for 10 minutes in the dark in 1x erythrocyte lysis buffer/Milli-Q® water when needed. In order to inactivate the lysis buffer cells where washed in 1x D-PBS.

3.1.2 Cell culture

Cells were maintained at 37°C in a humidified 5% CO_2 environment. Primary cells were cultured in Mononuclear Cell Medium (MCM) supplemented with 0.5 µg/ml gentamicin and 2.5 µg/ml amphotericin B. EEB cell line and EEB-aneuploid clones were cultured with StemSpan SFEM medium supplemented with 15% FBS.

3.1.3 Cryopreservation of cells

Cells were resuspended in FBS with 10% DMSO at a concentration of 5-8*10^6 cells/ml and transferred to cryovials. Cryovials were stored at -80°C overnight and then moved to liquid nitrogen for long-term storage.

3.1.4 Aneuploid cell enrichment

To enrich for aneuploid cells, EEB cells were synchronized at G1/S phase transition by thymidine treatment (2 mM) for 24 hours. After thymidine washout the cells were treated with 50 nM CENP-E inhibitor (GSK923295) and 480 nM MPS1 inhibitor (NMS-P715) for 24 hours and single seeded in 96-well plates.

3.1.5 Single cell cloning by limited dilution of suspension cells

Single cells were seeded in 96-well plates. 1.25*10^5 cells were diluted in 500 µl of medium, 50 µl were added to 950 µl of medium, 10 µl were transferred in 20 ml and 200µl were plated in each well.

3.1.6 Cell growth curves

Cell growth was evaluated by trypan blue exclusion with TC10 Trypan Blue Dye 0.4%. Cells were counted at 24 hours intervals with TC20™ automated cell counter.

3.1.7 Drug-response curves

$1*10^4$ primary cells per well with 25 µl medium were seeded at day zero in 384-well plates. Cells were treated after 24 hours with the addition of the drug in 25 µl medium. All experiments were carried out in triplicate. Cell viability was measured after 72 hours of treatment with an ATP-based detection system, the CellTiter-Glo® 2.0 Assay, according to manufacturer´s instructions. Luminescence was measured with Spark microplate reader.

$2*10^5$ cells per well were seeded in 96-well plates with 100 µl of medium to which the compounds were added. All experiments were carried out in triplicate. Cell viability was measured after 48 hours of treatment, following the addition of the WST-1 reagent, according to manufacturer´s instructions. Absorbance was measured with Spark microplate reader.

3.1.8 Cell cycle analysis

$1*10^6$ cells were collected and resuspended in 250 µl 1x PBS. Cells were fixed with dropwise addition of 700 µl of ice-cold 100% methanol and stored at 4°C for at least 1 hour. Samples were centrifuged at 350 rcf, washed with 10 ml 1x PBS and stained with 200 µl of working solution (propidium iodide (stock 1 mg/ml, 1:100) with the addition of RNase A (stock 10 mg/ml, 1:40)) for at least 30 minutes in the dark. Cells were acquired with Accuri C6 flow cytometer and cell cycle was analyzed with BD Accuri C6 software.

3.1.9 Caspase activity assay

Cells were seeded at day zero in 384-well plates and treated with the compound of interest after 24 hours. All experiments were carried out in triplicate. Caspase activity was measured with a luminescent assay, the Caspase-Glo® 3/7 Assay according to manufacturer´s instructions. Luminescence was measured with Spark microplate reader.

3.1.10 Apoptosis assay

Apoptotic cells were detected with the FITC Annexin V Apoptosis Detection Kit 1 according to manufacturer´s instructions. Samples were analyzed with Accuri C6 flow cytometer.

3.1.11 Immunofluorescence staining

$4*10^5$ cells were cytospun on slides and fixed with either ice-cold methanol/acetone (1:1) for 7 minutes or 4% PFA for 10 minutes according to the antibodies used. Cells were permeabilized with 0.2% tryton for 5 minutes, washed once with 1x PBS, blocked in 10% goat serum in 1x PBS for 30 minutes and incubated with primary antibodies for 1 hour. Following the primary antibody incubation, the cells were washed three times for 5 minutes in 1x PBS and incubated for 30 minutes with appropriate species-specific secondary antibodies. DNA was counterstained with Hoechst 33342 diluted 1:1000 in 1x PBS for 5 minutes. The slides where washed three times with 1x PBS and once with double distilled water. Coverslips were mounted in Vectashield antifade mounting medium and were analyzed by fluorescence microscopy on a Zeiss Cell Observer.Z1 system equipped with an AxioCam MRm camera, or an Axioskop equipped with an AxioCam MRm camera. For image analysis the software ZEN lite 2011 was used.

3.1.12 Metaphase spreads

Confluent cells were treated with 10 µg/ml colcemid for 1 hour at 37°C followed by centrifugation at 280 rcf for 10 minutes. Hypotonic treatment of the samples with pre-warmed to 37°C 0.075 M KCl was performed and samples were incubated for 10 minutes at 37°C. Cells were fixed by dropwise addition of ice-cold methanol/glacial acetic acid (3:1) and centrifuged for 10 minutes at 280 rcf. Three additional steps of fixation followed. Cells were dropped on glass slides from a height of about 30 cm; slides were dried at 56°C, stained with Hoechst 33342 and mounted in Fluoromount-G™ or prepared for whole chromosome multiplex fluorescence in situ hybridization (M-FISH). Control of mitotic index (1-2 mitoses/field) was performed at bright field microscope (20X objective). Samples were stored at -20°C.

3.1.13 Multiplex fluorescence in situ hybridization and karyotyping

M-FISH and karyotyping were performed by Brigitte Schoell and Prof. Dr. Anna Jauch, Institute of Human Genetics, University Hospital Heidelberg.

3.1.14 Evaluation of surface markers

The evaluation of surface markers by flow cytometry was performed at the Department of Internal Medicine V, University Hospital Heidelberg.

3.1.15 Transfection with plasmids

For transfection of plasmids the Neon™ Transfection System was used. One day prior to electroporation the cells were transferred into a flask with fresh medium. 24-well plates were

prepared by filling the wells with 500 µl of medium and kept in a humidified 37°C/5% CO_2 incubator. 2.5*10^5 cells per well were used; they were washed with 1x PBS and resuspended in 10 µl Buffer R. 1 µl plasmid DNA was transferred to a 1.5 ml microcentrifuge tube, cells were added to it and gently mixed. A Neon™ Transfection Tube was filled with 3 ml Electrolytic Buffer E into the Neon™ Pipette station. The DNA/cells mixture was aspirated with the Neon™ Pipette with a 10 µl Neon™ Tip. The Neon™ Pipette was inserted into the Neon™ Transfection Tube placed in the Neon™ Pipette Station. Cells were electroporated with 1200 mV or 1350 mV, pulse width 35, pulse 1 and finally transferred to a well.

3.1.16 Selection of transfected cells

Transfected cells were selected 72 hours after electroporation. Cells were treated with 2 µM puromycin for 7 days. Puromycin was added freshly every 2 days.

3.2 Protein biochemistry methods

3.2.1 Cell lysates and determination of protein concentration

Cells where collected and washed with ice-cold 1x PBS. RIPA buffer was added to the cell pellet and samples were incubated on ice for 30 minutes with frequent vortexing. Samples were centrifuged for 10 minutes at 18000 rcf at 4°C and the supernatant was transferred into precooled tubes.

To determine the protein concentration of the lysates the Bradford assay was used. 1 ml dye reagent for the Quick Start™ Bradford Protein Assay and 1 µL of the protein lysate were mixed and incubated for 5 minutes. Absorbance at 595 nm was measured by spectrophotometry. To create a calibration curve BSA standard was used. Cell lysates were mixed with 1x SDS protein loading buffer and boiled for 5 minutes at 95 °C. Samples were directly used or stored at -80°C.

3.2.2 Gel electrophoresis

The electrophoretic separation of proteins was performed under denaturing conditions. Gels with 6-15% acrylamide gels, depending on the size of the proteins to be detected, were prepared following Thomas and Kornberg protocol[101]. 20-50 µg of proteins were loaded for each well. The separation was performed at 90 V for 2 hours.

3.2.3 Western blot analysis and immunodetection

Separated proteins were transferred to an Immun-Blot® PVDF membrane by semi-dry transfer method using Trans-Blot® Turbo™ System. The membrane was activated in 100% ethanol for one minute and sandwiched with the gel between Trans-Blot® Turbo™ Midi Size Transfer Stacks, soaked in 1x transfer buffer (5x Trans-Blot® Turbo™ 100 ml, ethanol 200 ml, ddH_2O 700 ml). Protein transfer was performed for 10 minutes for the transfer of high molecular weight proteins according to the manufacturer's instructions. The proteins were then detected by immunodetection.

For the detection of proteins by means of immunodetection the membrane was blocked for one hour with 5% of either milk powder or BSA in 1x TBS-T at room temperature and then incubated with the primary antibody overnight at 4°C with gentle shaking. After three 5-minute washes with 1x TBS-T, the membrane was incubated with the secondary antibody for 1 hour at room temperature and then again washed three times for 5 minutes each with 1x TBS-T. Both primary and secondary antibodies were diluted in either 5% milk powder or 5% BSA in 1x TBS-T. Detection was done by incubating the membrane for 5 minutes with Clarity™ Western Blotting ECL Substrate followed by chemoluminescence signal detection with ChemiDoc™ Touch Imaging System following manufacturer's instructions. Image analysis was performed with the Image Lab software.

3.3 Molecular biology methods

3.3.1 DNA extraction

DNA extraction was performed using QIAmp DNA Mini Kit following manufacturer's specifications. DNA concentration and purity was measured at 260nm/280nm with a NanoDrop 2000 Spectrophotometer.

3.3.2 RNA extraction

Total RNA extraction was performed using RNeasy Mini Kit following manufacturer's specifications. RNA was subjected to DNAse I treatment. RNA concentration and purity were measured with a Qubit fluorometer.

3.3.3 Polymerase chain reaction (PCR)

To amplify regions of interest of genomic DNA, a polymerase chain reaction (PCR) was performed using either Phusion® High-Fidelity DNA Polymerase or CloneAmp™ HiFi PCR Premix, following manufacturer´s protocol.

3.3.4 Agarose gel electrophoresis

For analysis and quality control purposes, size separation of DNA and RNA fragments by agarose gel electrophoresis was performed.

For DNA samples, 1% agarose gels were prepared and supplemented with 0.1 µL/mL ethidium-bromide. Samples were mixed with 6x loading dye and were run in an electrophoresis chamber filled with 1x TAE buffer for 40 minutes at 110 V.

Isolated RNA samples were mixed 1:1 with RNA Sample Loading buffer, added to 8 µl of nuclease-free water and cooked at 65°C for 10 minutes. Samples were run in an electrophoresis chamber with 1x MOPS buffer for 1 hour at 80 V.

Both DNA and RNA separated bands were visualized by UV light in a gel documentation system.

3.3.5 RNA sequencing

50 µl of 40 ng/µl RNA of each sample with RIN values >8 were prepared and sent for processing to the Core Facility Genomics and Proteomics, DKFZ. Each sample was sent in biological triplicate. Libraries were made with TruSeq Stranded mRNA Prep Kit (Illumina). 100bp paired-end sequencing was carried out on an Illumina HiSeq 4000 sequencing system. The resulting reads were analyzed by Mahmoud Abdelrahman, Division of Applied Bioinformatics, DKFZ. Data were also analyzed through

the use of QIAGEN's Ingenuity® Pathway Analysis (IPA®, QIAGEN Redwood City, www.qiagen.com/ingenuity) in order to evaluate most significant canonical pathways across the dataset and predict upstream regulators that could account for the possible gene expression differences. The z-scores determine whether a pathway or an upstream transcriptional regulator is predicted to be significantly activated (z>0) or inhibited (z<0). p values were calculated using Fisher's exact test.

3.3.6 sgRNA design

Four sgRNA targeting the human *TP53* were designed using the CRISPOR tool which predicts, among many scores, the specificity score and the off-target count. sgRNA were chosen among those with the highest specificity score and the lowest off-target count.

3.3.7 sgRNA testing

The guide RNAs used for the CRISPR/Cas9 genome editing were tested with the Guide-it™ sgRNA In Vitro Transcription and Screening Systems according to the manufacturer's instructions.

3.3.8 Plasmid digestion

2-3 µg of plasmids were digested with proper restriction enzymes according to manufacturer´s instructions. Dephosphorylation with 2 µl Shrimp Alkaline Phosphatase (SAP) for 30 minutes followed. 5 µl of the digested plasmids were loaded on an agarose gel to assess the digestion of the vectors. Digested plasmids were purified with High Pure PCR Product Purification Kit according to manufacturer´s instructions.

3.3.9 Annealing and phosphorylation of oligonucleotides

For each sgRNA 100 nM of the top strand and 100 nM of the bottom strand of oligonucleotides were annealed in a thermocycler: the lid temperature was set at 99°C, samples were incubated for 5 minutes at 95°C, and then the temperature was gradually reduced by 0.1°C/second up to 25°C and maintained at 25°C for 5 more minutes.

The annealed oligos were phosphorylated for 30 minutes at 37°C (16 µl annealed oligos, 2 µl 10x T4 Polynucleotide Kinase Reaction Buffer (PNK buffer), 1 µl T4 Polynucleotide Kinase, 1 µl ATP 10 mM). The reaction was inactivated at 65°C for 15 minutes.

3.3.10 Ligation

8 µl of vector, 8 µl of annealed and phosphorylated oligos, 2 µl ligase buffer, 0.5 µl 10 mM ATP and 1 µl ligase were incubated at room temperature for 30 minutes. The ligation process was inactivated

incubating the samples at 70°C for 15 minutes. The ligated product was diluted 1:5 in nuclease-free water.

3.3.11 Heat shock transformation of bacteria

To amplify DNA constructs, the replication system of *E. Coli* was exploited. Transformation of competent *E. Coli* DH5α strain F^- ϕ80*lac*ZΔM15 Δ(*lac*ZYA-*arg*F)U169 *rec*A1 *end*A1 *hsd*R17(rK^-, mK^+) *pho*A *sup*E44 *thi*-1 *gyr*A96 *rel*A1 λ^- bacteria was accomplished by heat shock transformation. Frozen aliquots of *E. Coli* DH5α strain were thawed on ice and 100 µL of competent bacteria were added to 5 µL of plasmid DNA. The mixture was then incubated on ice for 30 minutes. Heat shock transformation was performed for 45 seconds at 42°C, quickly followed by 2 minutes incubation on ice. Transformed bacteria were then transferred to 900 µL of SOB medium freshly supplemented with 20 mM glucose (SOC medium), without antibiotics, and incubated for 1 hour at 37°C under shaking. Bacteria were pelleted by centrifugation for 5 minutes at 350 rcf, resuspended in about 100 µL of SOC medium and plated at different dilutions on LB-agar supplemented with an appropriate selection antibiotic. Bacteria colonies grew overnight in a 37°C incubator.

3.3.12 Isolation of plasmid DNA

Transformed bacteria colonies were isolated and transferred to liquid cultures in LB-medium. Bacteria were selected under appropriate antibiotics. To obtain small amounts of plasmid, 3 ml of liquid culture were incubated overnight at 37°C under shaking. Plasmid DNA was purified from small liquid culture using QIAprep Spin Miniprep Kit according to manufacturer's instruction.
For larger amounts of DNA, following this first step, the purified plasmid was retransformed. 10 ml of liquid culture were finally incubated for about 4-5 hours at 37°C under shaking and then transferred to 100 ml of liquid culture and incubated overnight at 37°C under shaking. Plasmid DNA was purified from larger cultures with the QIAGEN Plasmid Maxi Kit. Concentration of the obtained DNA was determined using a NanoDrop 2000 spectrophotometer at 260nm/280nm.

3.3.13 PCR product and plasmid DNA sequencing

Samples were sent to GATC for Sanger sequencing. PCR products and plasmids were diluted in 20 µl to a concentration of 10-50 ng/µl and 30-100 ng/µl, respectively. Primers were diluted in 20 µl at a concentration of 100 pmol/µl.

3.4 Statistical analysis

Data were analyzed in Prism 7 (GraphPad Software, La Jolla, California, USA, www.graphpad.com).

4 Results

4.1 Identification of compounds that inhibit the proliferation of aneuploid AML cells

4.1.1 Drug screening in AML patient samples

14 compounds (Tab. 27) were screened in AML patient samples with both normal and complex karyotypes, thereby comparing euploid versus aneuploid karyotype AML cell response. Standard anticancer drugs and compounds with proposed selective efficacy against aneuploid cells identified in non-hematopoietic cell types were included in the screen[61,74,77]. In detail, 8-azaguanine, 17-AAG, AICAR, ASA, chloroquine, metformin and resveratrol were tested. Conventional chemotherapeutic drugs cytarabine and daunorubicin, which are used in daily practice for AML treatment, were also included in the analysis. Agents interfering with the mitotic spindle such as taxol and vincristine and the alkylating agent cisplatin were tested as well. Since PLK4 drives centrosome replication, which is responsible for the set-up of the normal bipolar mitotic spindle apparatus and the correct distribution of chromosomes into the two daughter cells, the polo-like kinase 4 (PLK4) inhibitor centrinone was also included in the panel. The effect of crenolanib, recently described as a centrosome clustering inhibitor[102] was evaluated as well. At least in theory, aneuploid AML cells with centrosome amplification might be vulnerable to the latter two compounds[44].

Compound	Group	Rationale
8-Azaguanine	Purine analogue	Potentially aneuploidy-selective
17-AAG (17-Allylamino-geldanamycin)	Geldanamycin analogue	- Potentially aneuploidy-selective - HSP90 inhibitor
AICAR (5-Aminoimidazole-4-carboxamide ribonucleotide)	AMP analogue	- Potentially aneuploidy-selective - Stimulates AMPK and mimics energy stress
ASA (Acetylsalicylic acid)	Salicylate	- Potentially aneuploidy-selective - Stimulates AMPK
Centrinone	PLK4 inhibitor	Mitotic spindle interference
Chloroquine	Chinine analogue	- Potentially aneuploidy-selective - Inhibits autophagy
Cisplatin	Platin	- Cytostatic drug - Alkylating agent
Cytarabine (Cytosine arabinoside, Ara-C)	Arabinosyl nucleoside	- AML standard cytostatic drug - Antimetabolite

Crenolanib	FLT3 inhibitor	Centrosome clustering inhibitor
Daunorubicin	Anthracycline	- AML standard cytostatic drug - Topoisomerase II inhibitor
Metformin	Biguanide	- Potentially aneuploidy-selective - Activates AMPK and induces energy stress
Resveratrol	Phytoalexine	- Potentially aneuploidy-selective - Stimulates AMPK
Taxol	Taxane	- Cytostatic drug - Mitotic spindle interference
Vincristine	Vinca alkaloid	- Cytostatic drug - Mitotic spindle interference

Table 27 | Compounds screened in AML primary samples

4.1.2 8-Azaguanine selectivity against aneuploid primary AML samples

Primary AML samples with a euploid karyotype and with an aneuploid karyotype were treated for 72 hours with the above mentioned compounds at increasing concentrations (Fig. 4; Fig. S1). It is worth noting that all the samples included in the study were characterized by the presence of at least 80% of blasts. Euploid samples harbored a normal karyotype with the exception of three of them, which harbored few structural aberrations (Tab. S1); those with an aneuploid karyotype, harbored numerical aneuploidies and, with the exception of one, a complex karyotype (Tab. S2). Samples with aberrations which are considered to lead to a favorable prognosis were excluded from the analysis. Among all drugs tested, only 8-azaguanine was identified as more effective against aneuploid AML samples (Fig. 4A). Primary samples harboring three or more numerical aneuploidies (chromosome rearrangements were not considered in the analysis) were most responsive to the compound at high concentrations (Fig. 4B). This result suggests that the efficacy of 8-azaguanine may be influenced by the degree of aneuploidy, independent of the preponderance of chromosome gains or losses.

8-Azaguanine is a purine analogue. As other nucleoside analogues, it becomes active after phosphorylation to its triphosphate derivative and competes with endogenous nucleosides. Besides being incorporated into nucleic acids and thus affecting their structural integrity, nucleoside analogues can also interact with different enzymes, such as those involved in nucleotide metabolism, interfering with their active sites. Although nucleoside analogues share common structural features and traits of their mechanisms of action, they also display unique aspects. 8-Azaguanine has been described to be incorporated in both DNA and RNA, thereby inhibiting cell growth. It has been additionally demonstrated that its toxicity is mainly due to its incorporation into RNA[103]. The

compound has been shown to hinder the protein synthesis machinery and interfere with the initiation of translation in mouse chronic lymphocytic leukemia cells[104]. 8-Azaguanine has potential antineoplastic activity. Indeed, its efficacy against transplanted mouse adenocarcinomas, spontaneous tumors in mice and human high-ploidy breast cancer cells in vitro has already been demonstrated[105,77]. On the other hand, a subset of mouse and rat tumors such as sarcomas and carcinomas did not respond to the compound[105]. Moreover, an early clinical study reported a positive response of three AML patients treated with the drug[106].

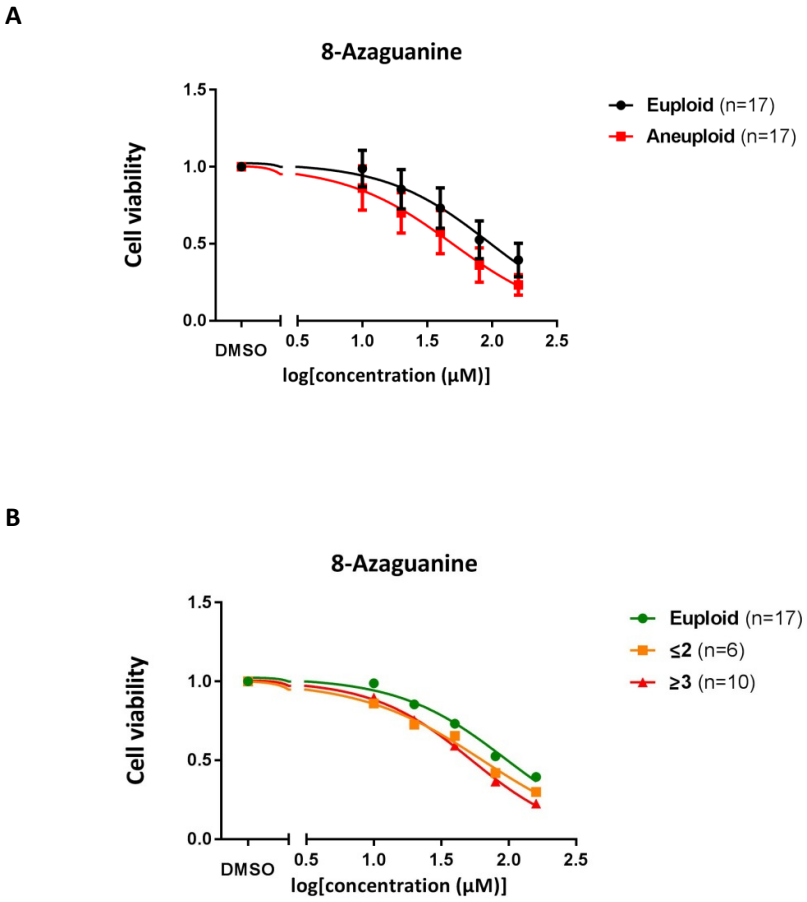

Figure 4 | 8-Azaguanine is selectively active against aneuploid primary AML samples

(A) Cell viability after 72 hours of treatment with 8-azaguanine. The graph shows means ± 95% CI. Statistical significances of the differences between euploid versus aneuploid AML samples treated with 8-azaguanine for AUC (area under the curve) and IC50 (inhibitory concentration 50%) are p=0.02 and p=0.008, respectively. **(B)** The aneuploid group was divided in two subgroups according to the number of numerical chromosome changes (≤2, ≥3), including both whole chromosome gains and losses.

4.2 Generation of EEB-derived cell lines differing in ploidy

The comparison between otherwise isogenic euploid and aneuploid AML cells is hampered by the lack of euploid AML cell lines. Leukemia cell lines are difficult to establish as AML primary cells are normally hard to grow in culture. To our knowledge, only three AML cell lines have been described as euploid in the literature[107,108,109]. Among them, the EEB cell line[108], which was established from a patient with early erythoblastic leukemia with 80% of blast carrying a normal karyotype, was the one which was efficiently growing in our hands. To reduce the variability among different cell lines, an isogenic AML cell model was established. We generated isogenic aneuploid clones which derive from the euploid AML cell line EEB and share a common genetic background but display aneuploidy to different degrees.

4.2.1 EEB cell line single seeding

Analysis of the EEB cell karyotype revealed a low level of aneuploidy. After single cell seeding three different clones were isolated: a clone with a normal diploid karyotype (46, XY) (relative frequency within the parental EEB cell line: 81%) (Fig. 5A-a), a subclone with loss of chromosome Y (45, X, -Y) (relative frequency within the parental EEB cell line: 17%) (Fig. 5A-b), and a subclone with a near-tetraploid karyotype with loss of both Y chromosomes (90, XX, -Y, -Y) (relative frequency within the parental EEB cell line: 2%) (Fig. 5A-c). The karyotypes of these clones were verified by M-FISH (Fig. 5A).

4.2.2 Generation of *de novo* aneuploidies

With the aim of expanding the model and obtaining additional clones we induced *de novo* aneuploidies by treating parental EEB cells with a combination of a CENP-E and a MPS1 inhibitor (NMS-P715 and GSK923295, respectively) for 24 hours, after 24 hours of thymidine G_1/S synchronization.

Centromere-associated protein-E (CENP-E) is a 312 kDa kinesin-like motor protein which contributes in generation and maintenance of chromosome-microtubule interactions and is involved in chromosome alignment by moving chromosomes from the spindle poles to the metaphase plate[110,111]. It accumulates in late G_2 and is degraded at the end of mitosis[112]. Multipolar spindle-1 (MPS1) is a protein kinase and core element of the SAC[31]. With CENP-E and MPS1 inhibition chromosomes are retained at the spindle poles and the SAC is inactivated. It has previously been shown that combining a CENP-E inhibitor (CENP-Ei) and low doses of a MPS1 inhibitor (MPS1i) results in chromosome missegregation without inducing any mitotic delay[113].

After treatment with the inhibitors and subsequent single cell seeding, three additional clones with trisomy 7 and 21 (47, X, -Y, +7, +21), trisomy 12 (47, XY, +12) and trisomy 22 (47, XY, +22), respectively, were isolated. The karyotypes of these clones were also verified by M-FISH (Fig. 5B). Clones with *de novo* aneuploidies were generated in collaboration with Ilka Jansen.

A

a

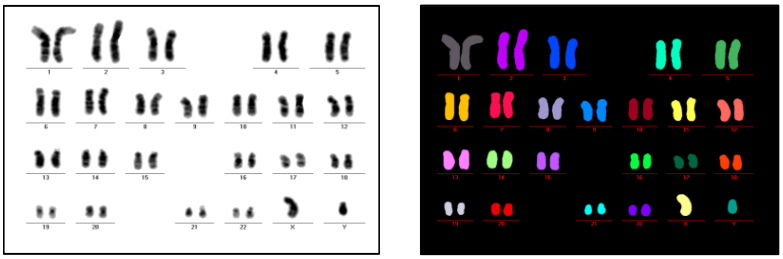

b

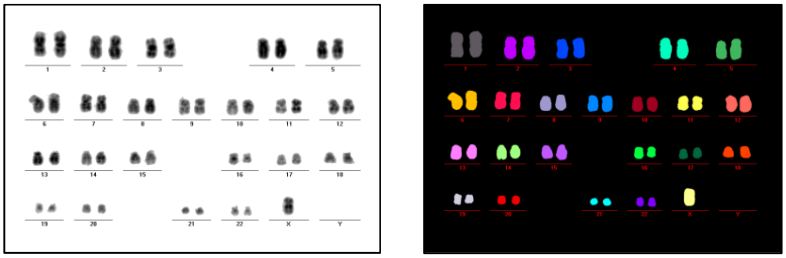

c

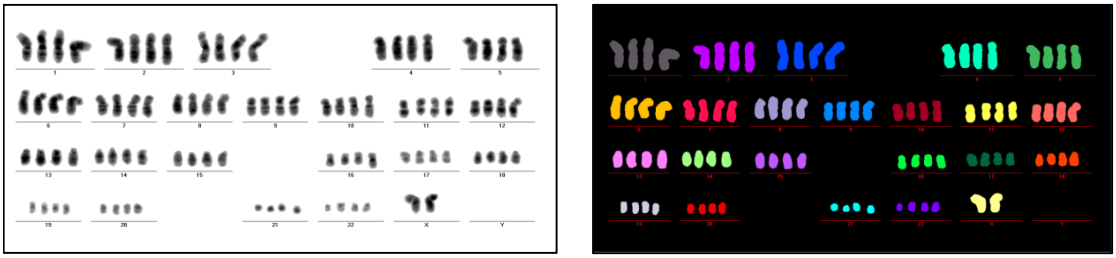

B

a

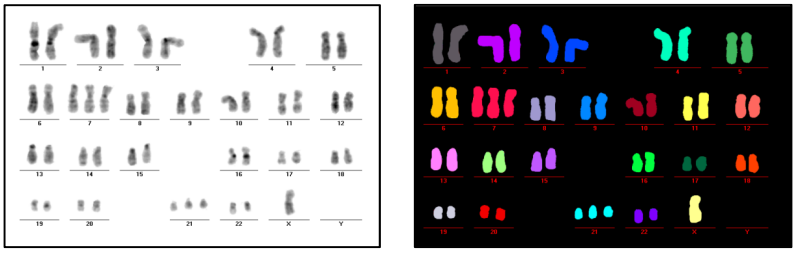

b

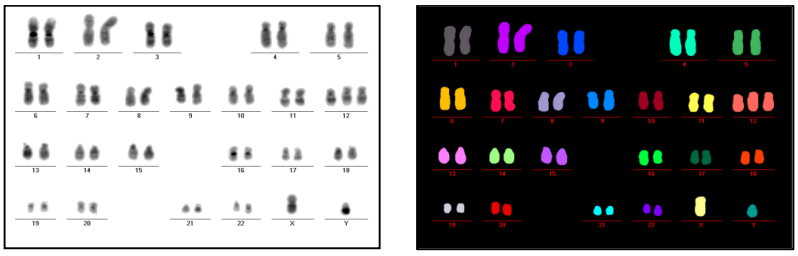

c

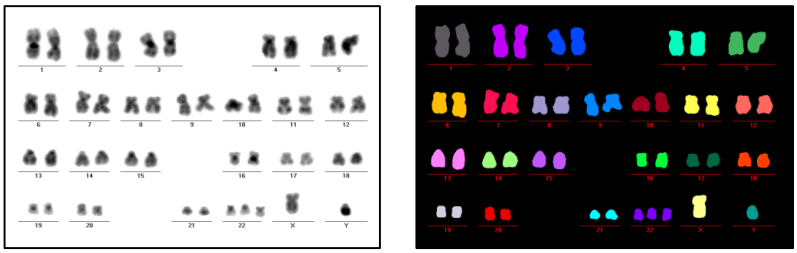

Figure 5 | Clones derived from the AML EEB cell line

(A) Karyotypes of euploid (46, XY) **(a)**, hypodiploid (45, X, -Y) **(b)** and near-tetraploid (90, XX, -Y, -Y) **(c)** EEB cells isolated after EEB single cell seeding, as determined by M-FISH analysis. **(B)** Karyotypes of double-trisomic (47, X, -Y, +7, +21) **(a)** and two trisomic (47, XY, +12) **(b)** (47, XY, +22) **(c)** clones generated after treatment with MPS1 and CENP-E inhibitors, as determined by M-FISH analysis.

4.2.3 Generation of p53 knock-out clones

Aneuploidy has been described to trigger p53 activation, limiting cell growth. However, the mechanisms which link chromosome aberrations to p53 activation remain not completely understood. It is still uncertain whether p53 is activated by mere aneuploidy or whether its activity is triggered by other conditions associated with chromosome missegregation. Thompson and Compton proposed that chromosome missegregation *per se* can activate p53 through p38 activation, without evidence of DNA damage[68]. On the other hand, another group observed that chromosome segregation errors cause at first DNA damage and subsequently the activation of ataxia-telangectasia mutated (ATM) and p53[65]. Along the same lines, a study reported elevated levels of reactive oxygen species (ROS) after chromosome missegregation, which subsequently induce oxidative DNA damage, ATM and p53 activation[69]. More recent work has demonstrated that aneuploid cells with complex aberrations show replication stress, DNA damage and p53 activation, followed by innate immune response[114].

Since p53 might therefore hamper the generation of aneuploid EEB clones by limiting aneuploid cell proliferation, we performed a CRISPR/CAS9-mediated *TP53* knock-out in order to generate additional aneuploid EEB clones and to eventually evaluate drug response in a p53 knock-out setting. Three independent p53 knock-out EEB-derived cell lines were generated from the euploid clone (Fig. 6). p53 knock-out cell lines were established in collaboration with Christin Schlegel.

The karyotypes of the p53 knock-out cell lines were also verified by M-FISH. Besides differing from the previously generated clones with regard to their p53 status, they presented widespread karyotypic heterogeneity, with cells harboring both numerical and structural abnormalities (Fig. 7). Within the cell line 10-1 no predominant aberrant clone could be detected. Line 9-5 showed two main aberrant clones (relative frequencies within 20 metaphases: both 30%) with other additional abnormalities in the remaining metaphases. The clone 8-1 mainly consisted of near-tetraploid cells, with the exception of one metaphase which was near triploid, both harboring several additional aberrations that lead to a complex clonal heterogeneity.

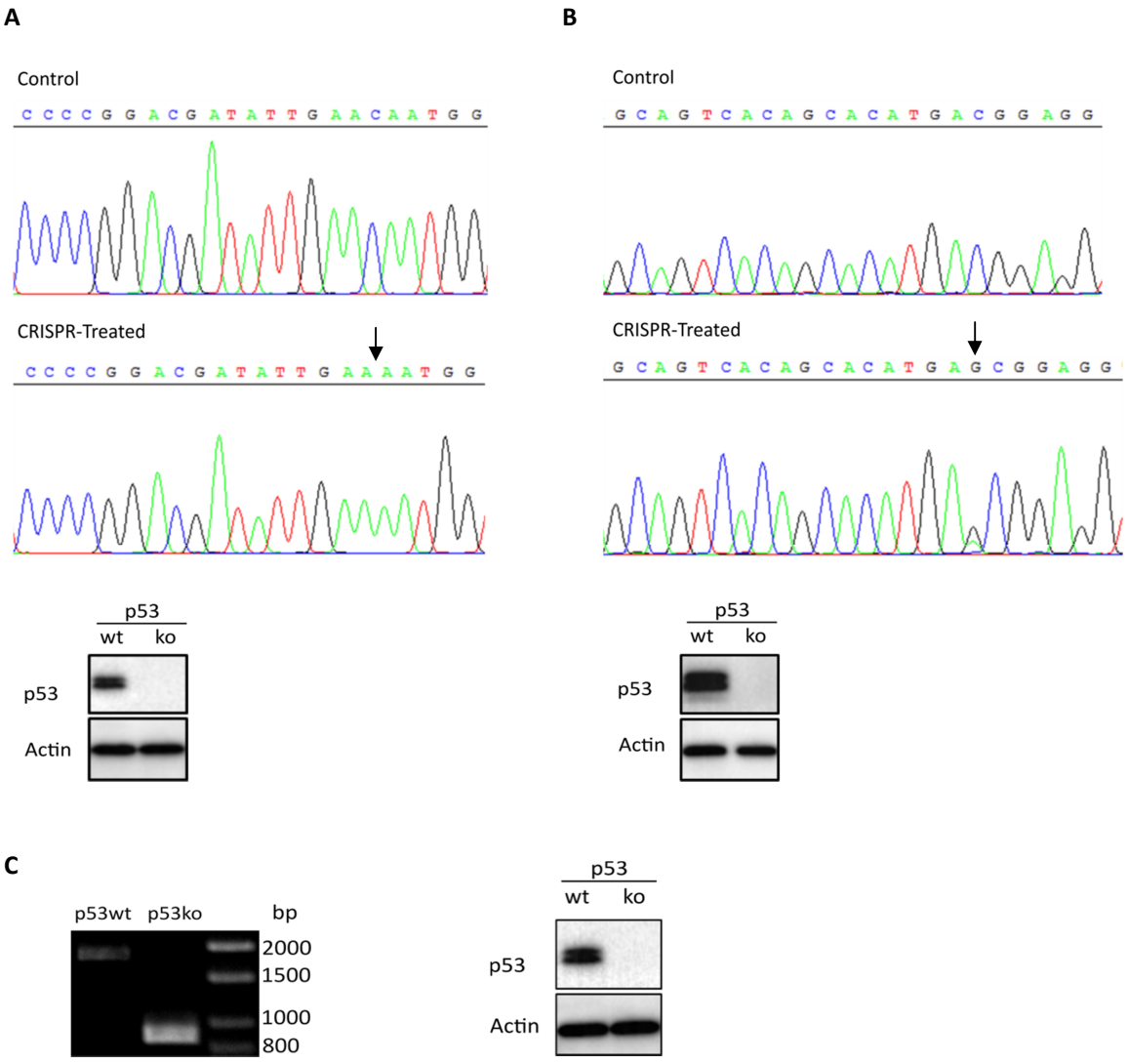

Figure 6 | Sanger sequencing and Western blot confirming CRISPR-induced p53 knock-out

(A) Confirmation of p53 mutation (arrow – deletion C) and knock-out (cell line 10-1). **(B)** Confirmation of p53 mutation (arrow – insertion G/A) and knock-out (cell line 9-5). **(B)** Confirmation of p53 mutation (deletion of 940 base pairs) and knock-out (cell line 8-1). wt: wild-type; ko: knock-out.

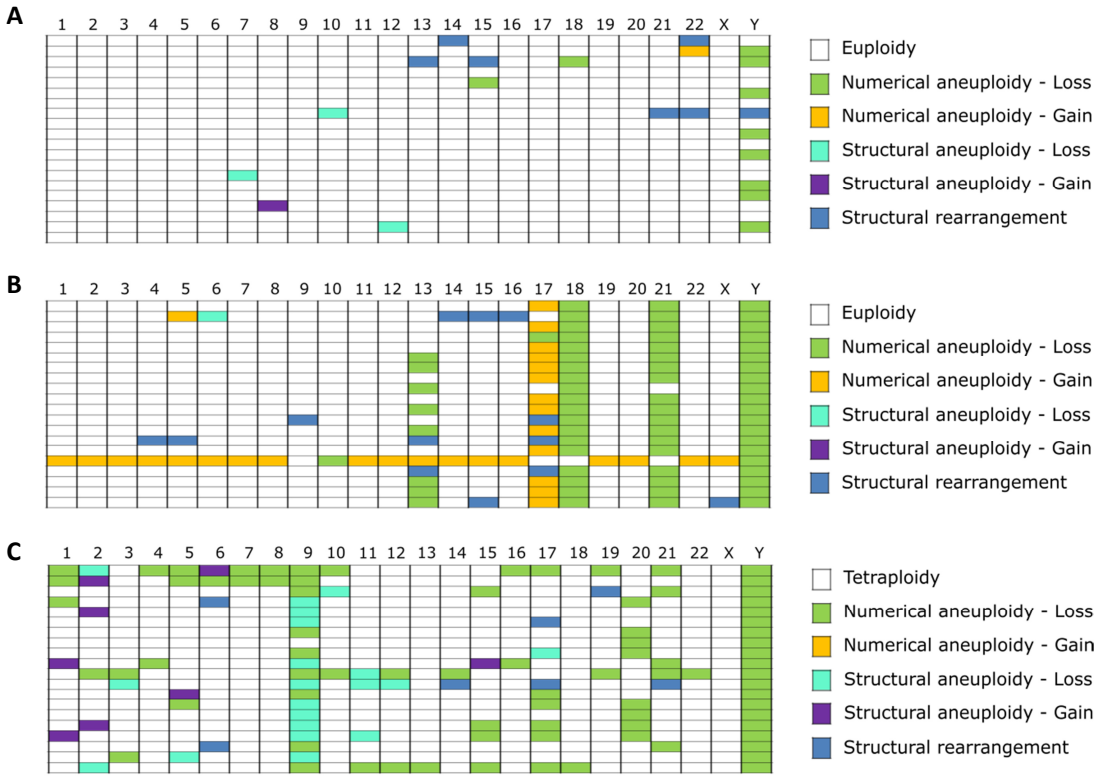

Figure 7 | Karyotypic heterogeneity of the p53 knock-out EEB-derived cell lines

(A) Cell line 10-1. **(B)** Cell line 9-5. **(C)** Cell line 8-1. Each row represents a metaphase. In addition to the depicted aneuploidies, some cells also harbored structural rearrangements (alteration of chromosome structure (Fig. 8)).

4.2.3.1 p53 deficiency allows for extensive karyotypic heterogeneity and propagation of structural aneuploidies and rearrangements in AML EEB cells

The link between p53 activation/deficiency and aneuploidy propagation is still a matter of discussion. It has been described that p53 deficiency alone is not sufficient to cause aneuploidy and CIN, but additional stimuli that trigger chromosome segregation errors need to occur[115,68]. It is still unclear whether aneuploidy *per se* can be sensed by p53. Untransformed RPE-1 p53 wild-type cells have been described to still actively proliferate in presence of numerical aneuploidies[113,114] and aneuploid MEFs do not show elevated p53 levels[61]. On the contrary, it has been reported that chromosome missegregation induces p53-dependent cell cycle arrest in HCT116 and RPE-1 cells[68].

The p53 knock-out cells we generated harbored several non-clonal chromosomal abnormalities. Thus, with the two purposes of investigating whether p53 disruption alone causes aneuploidy/CIN and further evaluating which type of chromosomal abnormalities, if any, can be propagated in p53-proficient versus p53-deficient cells, we single seeded p53 wild-type and p53 knock-out cells (cell line 10-1 (Fig.7A)). For each condition, we evaluated karyotypes from 20 cells of 6 subclones by M-FISH,

for a total of 120 cells for each setting. M-FISH analysis showed that a subset of untreated p53 wild-type EEB cells harbored a loss of chromosome Y, which we considered as a spontaneous characteristic event of the cell line. For this reason we did not score the loss of chromosome Y in our analysis. For the purpose of this study, with numerical aneuploidy we refer to gains or losses of entire chromosomes and with structural aneuploidy to gains or losses of sub-chromosomal regions. The term structural rearrangement instead refers to alterations of chromosome structure including telomere associations, Robertsonian translocations, isochromosomes, ring chromosomes, translocations and derivative chromosomes (Fig. 8). Since M-FISH was performed for the evaluation of chromosome aneuploidies and this technique allows for the evaluation of chromosome structural rearrangements, I decided to additionally include this category in our analysis.

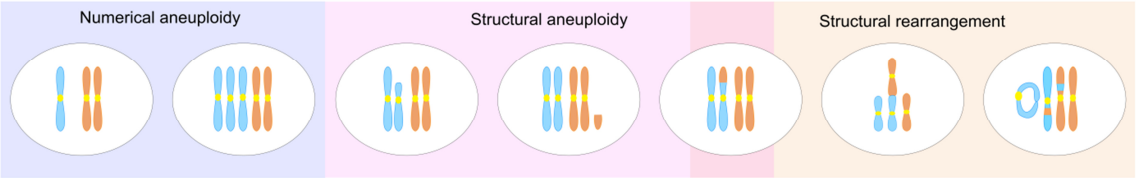

Figure 8 | Numerical aneuploidy, structural aneuploidy and structural rearrangement
Numerical aneuploidy: chromosome loss (left), chromosome gain (right). Structural aneuploidy: sub-chromosomal region loss (left), sub-chromosomal region gain (center and right). Structural rearrangement: unbalanced translocation (left), telomere association (center), chromosome ring and balanced translocation (right).

M-FISH analysis revealed that p53 knock-out led to a significantly higher number of cells with numerical aneuploidies in comparison to p53 wild-type cells (17% and 4%, respectively; p=0.02), and that a fraction of p53 knock-out cells harbored structural aneuploidies (10%), whereas p53 wild-type cells did not (p=0.06)(Fig. 9A-B). These data demonstrate that p53-deficient compared to p53-proficent cells can spontaneously acquire and propagate numerical aneuploidies and structural aneuploidies, even if this last difference failed to achieve statistical significance probably because of the small sample size.

We then treated both p53-proficient and p53-deficient cells with CENP-E and MPS1 inhibitors with the purpose to trigger *de novo* chromosome missegregation. We single seeded the treated cells and evaluated for each condition the karyotype from 20 cells of 6 subclones, for a total of 120 cells for each setting. In the case of p53 wild-type clones, the number of cells with numerical aneuploidy increased significantly in comparison to the respective untreated clones (18% vs 4%), but only few structural aneuploidies developed (3%). On the other hand, p53 knock-out clones treated with the inhibitors not only acquired a significantly higher amount of cells harboring numerical aneuploidies

compared to untreated clones (43% vs 17%), but also a large fraction with structural aneuploidies (27%) (Fig. 9A-B). The comparison between treated p53-proficient and p53-deficient cells showed a significant difference in the level of numerical aneuploidy (p=0.01) and the difference in the level of structural aneuploidy almost reached statistical significance (p=0.069). Once more these data suggest that p53 deficiency allows tolerance for at least numerical aneuploidies.

Considering structural rearrangements, they were not found in untreated p53-proficient cells and only few (6% of cells) appeared after the induction of chromosome missegregation by CENP-Ei and MPS1i. On the contrary, 9% of p53-deficient cells already spontaneously harbored structural rearrangements (p=0.02), which increased to 45% after the induction of chromosome missegregation (treated p53-proficient vs treated p53-deficient cells p=0.004) (Fig. 9C).

These results suggest that numerical aneuploidies are well tolerated by p53 wild-type AML EEB cells, whereas the presence of p53 limits the propagation of structural aneuploidies and structural rearrangements almost completely. While DNA damage could not be detected in p53-proficient cells, p53-deficient cells showed Western blot positivity for ɣ-H2AX, a marker of damaged DNA. This suggests that DNA damage occurring during the generation of structural aneuploidies and structural rearrangements may cause a p53-mediated cell cycle arrest and cell death, thus limiting the propagation of structural abnormalities to p53 knock-out cells (Fig. 9D).

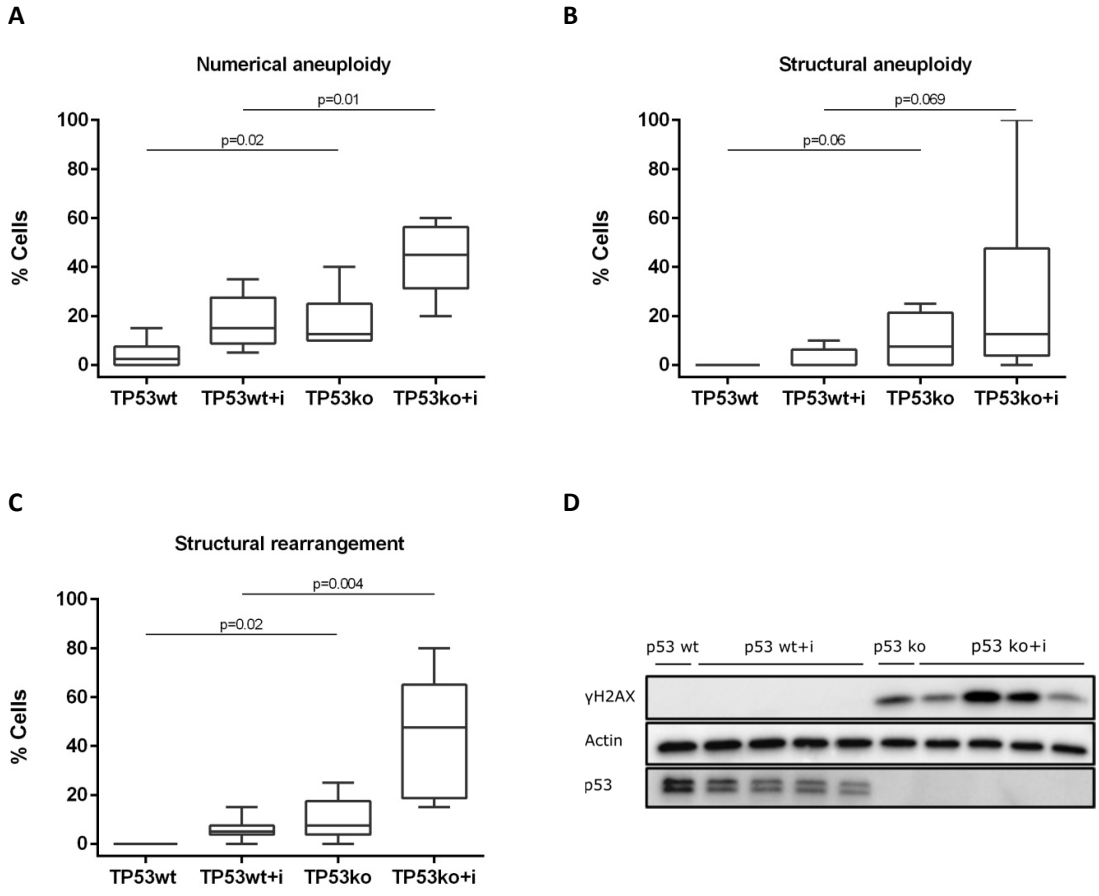

Figure 9 | p53 limits the propagation of structural aneuploidies and rearrangements

(A) Percentage of cells either expressing p53 or not, harboring numerical aneuploidies before and after the induction of segregation errors with CENP-E and MPS1 inhibitors (+i). **(B)** Percentage of cells either expressing p53 or not, harboring structural aneuploidies before and after the induction of segregation errors with CENP-E and MPS1 inhibitors (+i). **(C)** Percentage of cells either expressing p53 or not, harboring structural rearrangements before and after the induction of segregation errors with CENP-E and MPS1 inhibitors (+i). **(D)** DNA damage in p53 knock-out cells as detected by immunoblotting with an antibody to ɣ-H2AX. Actin served as a loading control. wt: wild-type; ko: knock-out.

In order to gain insight into the level of CIN of p53-proficient and p53-deficient AML EEB cells before and after the induction of segregation errors, we evaluated the CIN-index of every chromosome in 20 cells of 6 subclones for each setting (p53 wild-type, p53 wild-type + CENP-Ei/MPS1i, p53 knock-out, p53 knock-out + CENP-Ei/MPS1i), considering both numerical and structural aneuploidies[116,117]. The numerical CIN-index was defined as follows: for each chromosome the number of cells that deviated from the modal chromosome number of 2 was counted and then divided by the number of cells analyzed. The structural CIN-index was defined considering for each chromosome the number of cells that harbored a structural aneuploidy, then dividing this count by the number of cells analyzed. The average numerical CIN-index was obtained excluding chromosome Y, whereas the average structural CIN-index was calculated considering all chromosomes, including chromosome Y. While p53-proficient cells spontaneously did almost not display any deviation from the modal chromosome number and normal structure (max numerical CIN-index 5%; structural CIN-index 0%), p53-proficient cells after the induction of chromosome missegregation and p53-deficient cells both with and without addition of missegregation stimuli deviated from the modal chromosome number and normal structure (max numerical CIN-index: 10%, 20%, 35%, respectively; max structural CIN-index: 5%, 10%, 100%, respectively). The average numerical CIN-index for p53 wild-type cells before and after induction of chromosome missegregation was 0.3% and 1.7%, respectively; their average structural CIN-index before and after treatment with CENP-Ei and MPS1i was 0% and 0.3%, respectively (Fig. 10). The average numerical CIN-index for p53 knock-out cells before and after induction of chromosome segregation errors was 4.4% and 5.4%, respectively; their average structural CIN-index before and after treatment with CENP-Ei and MPS1i was 0.5% and 5.2%, respectively (Fig. 10).

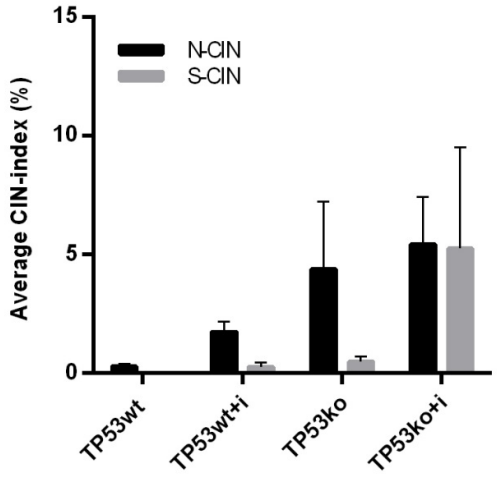

Figure 10 | p53 knock-out allows for chromosomal instability

Average numerical CIN (N-CIN) and average structural CIN (S-CIN) indices in p53-proficient and p53-deficient cells before and after induction of chromosome missegregation with CENP-E and MPS1 inhibitors (+i). Error bars show SEM. wt: wild-type; ko: knock-out.

Importantly, chromosome alterations (numerical and structural aneuploidies and structural rearrangements) obtained after p53 knock-out and also after the induction of chromosome missegregation were not clonal and varied largely from cell to cell (Fig. 11, Fig. S2). Only some cells harbored common chromosome alterations suggesting that they evolved from the same ancestor, but had acquired additional alterations on their own, which made them to differ from each other.

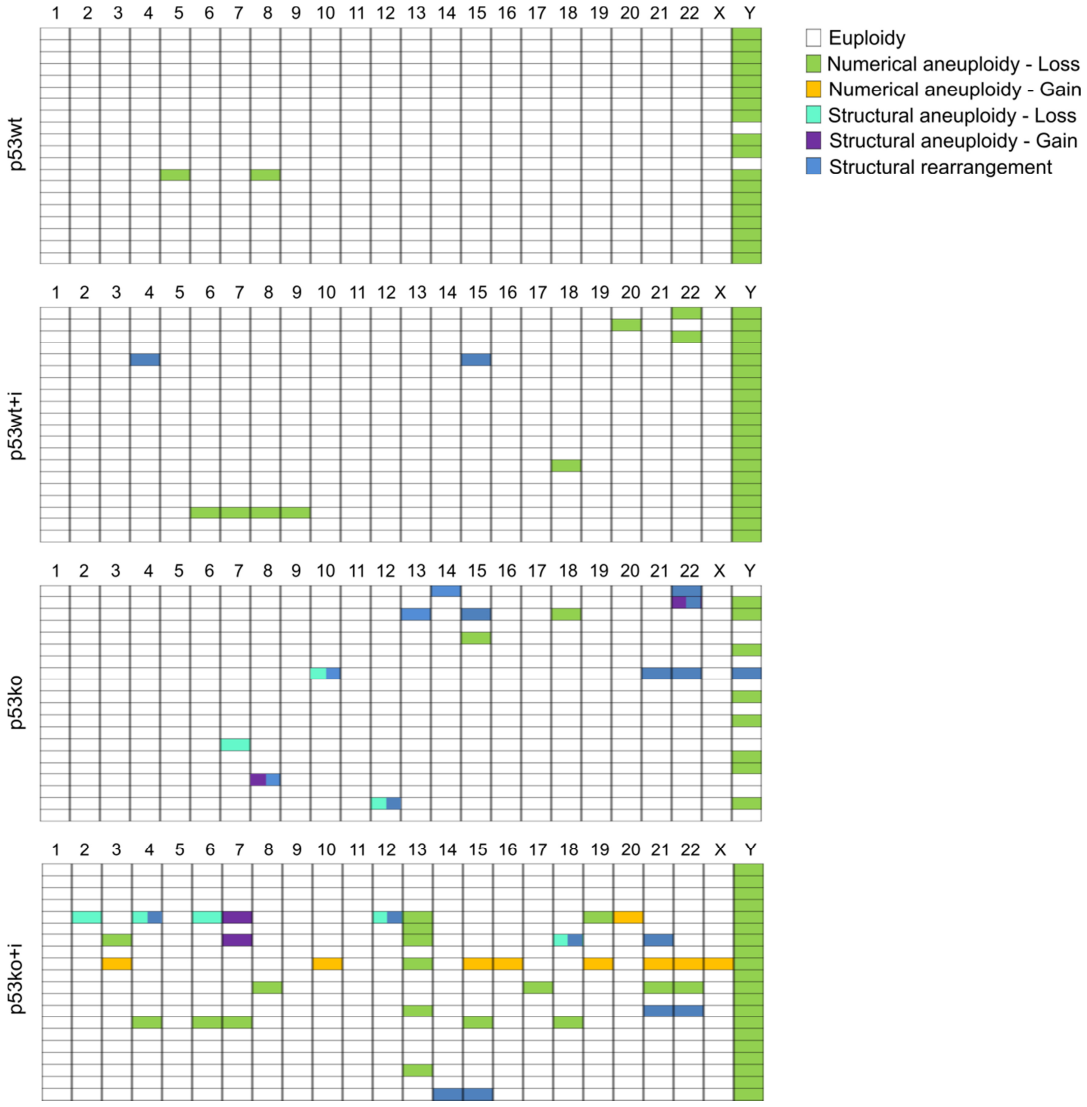

Figure 11 | p53 deficiency allows for karyotypic heterogeneity

Schematic representation of karyotypes considering 20 metaphases of one representative clone for each category (from top to bottom: p53 wild-type (wt), p53 wild-type treated with CENP-Ei and MPS1i (wt+i), p53 knock-out (ko) and p53 knock-out treated with CENP-Ei and MPS1i (ko+i)). Each row represents a metaphase. The presence of at least one chromosome with structural rearrangement in addition to aneuploidy is depicted with double color.

4.3 Evaluation of the influence of aneuploidy on cellular fitness

Aneuploidy has been described to limit cell proliferation under normal growth conditions. In our model the euploid and the hypo-/hyperdiploid p53 wild-type clones showed similar growth rates. This probably reflects the low level of chromosome abnormalities of these clones. Indeed, only the near-tetraploid clone showed a slower rate of proliferation (Fig. 12).

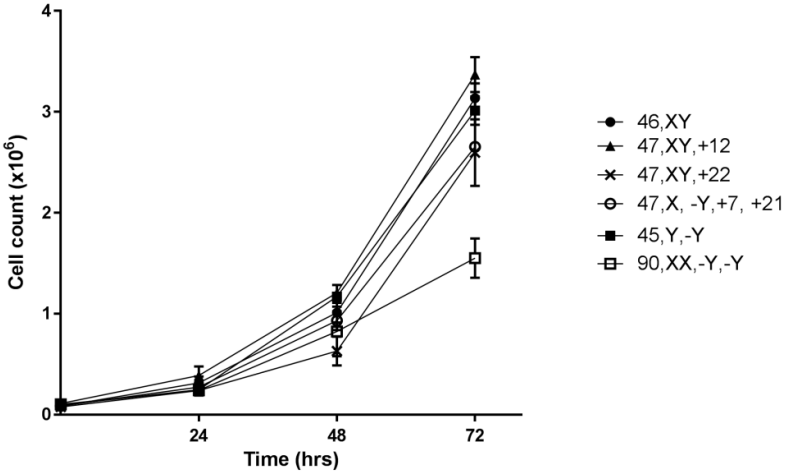

Figure 12 | Low levels of aneuploidy do not impair cell growth in p53-wild-type AML EEB cells
Growth curves of euploid and aneuploid p53-wild-type clones.

4.4 8-Azaguanine selectivity against aneuploid AML EEB clones

In order to confirm the observations made in primary AML samples, AML EEB-derived p53 wild-type clones, including the euploid clone (46, XY), the double-trisomic (47, X, -Y, +7,+21), the two trisomic clones (47, XY, +12; 47, X, Y, +22), the hypodiploid clone (45, X, -Y) and the near-tetraploid clone (90, XX, -Y, -Y) were exposed to increasing concentrations of 8-azaguanine.

As shown by the viability assay, three aneuploid clones (the hypodiploid (45, X, -Y), the double-trisomic (47, X, -Y, +7, +21) and the near-tetraploid (90, XX, -Y, -Y)), when compared to the euploid clone, responded better to the compound after 48 hours of treatment at concentrations of 1.25 and 2.5 µM (Fig. 13A). From here on these three aneuploid clones will be addressed as “responder aneuploid clones”. On the other hand, the two trisomic clones (47, XY, +12 and 47, XY, +22) showed lower responsiveness to the drug (“non-responder aneuploid clones”). These results were confirmed by an apoptosis assay after treatment with 1.25 µM 8-azaguanine for 48 and 72 hours. Indeed, at the 48 hour time point, while only 23.3 ± 10.4% of the euploid cells were undergoing apoptosis, 37.5 ± 5.2% of the hypodiploid ($p=0.029$), 42.6 ± 5.5% of the double-trisomic ($p<0.001$) and 58.6 ± 6.5% of the near-tetraploid ($p<0.001$) cells were apoptotic (Fig. 13B).

8-Azaguanine was also tested in the p53 knock-out cell lines. The percentage of apoptotic cells was significantly higher in two out of three of the p53 knock-out cell lines compared to the euploid p53 wild type clone (Fig. 13C). The p53 knock-out cell line 10-1, which does not efficiently respond to 8-azaguanine treatment, harbors low CIN levels as compared to the other two p53 knock-out cell lines (Fig. 7A)

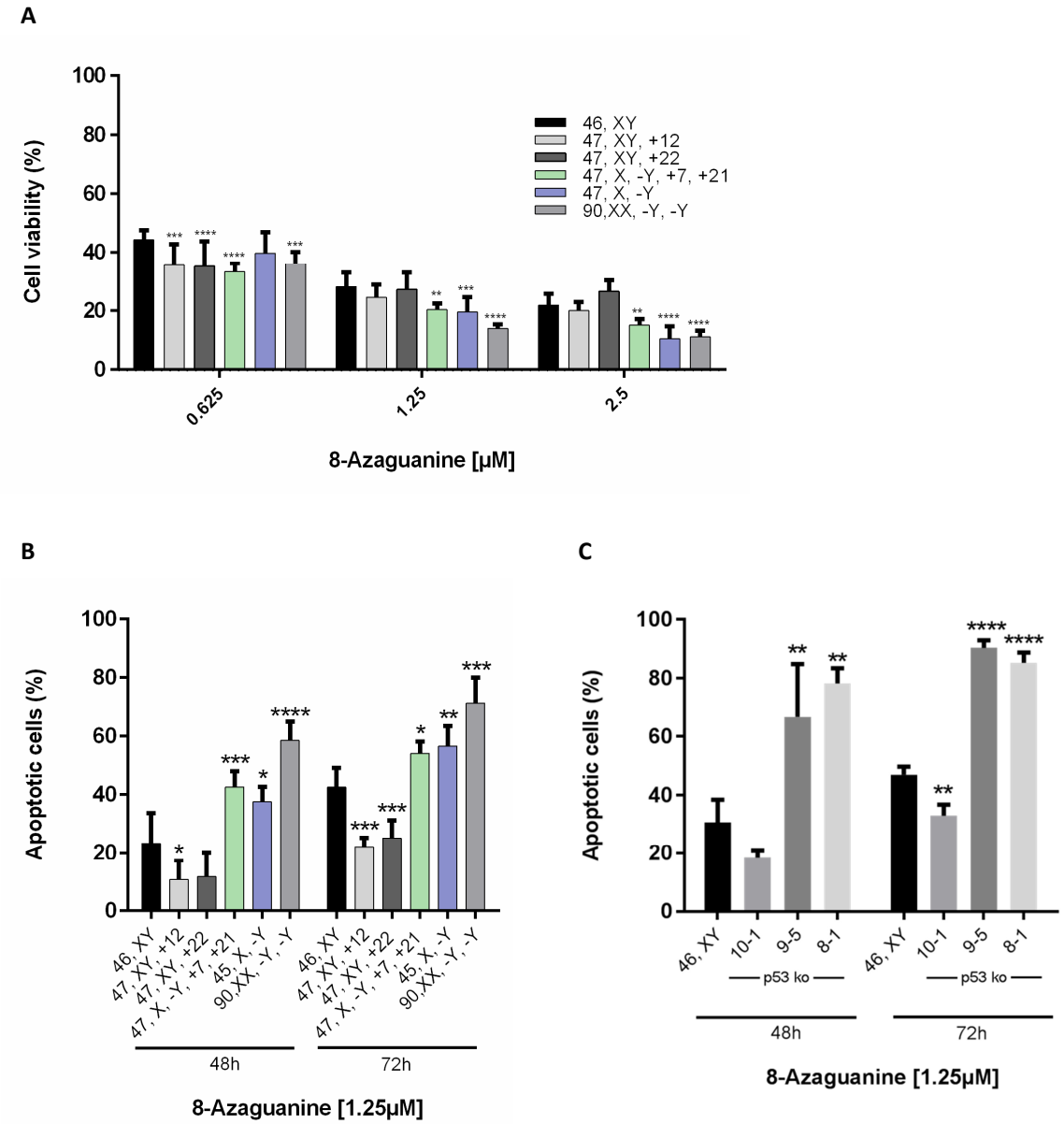

Figure 13 | 8-Azaguanine causes cell death more efficiently in most of the aneuploid AML clones
(A) Cell viability after 48 hours of treatment. **(B)** Apoptosis assay after 48 and 72 hours of treatment. **(C)** Apoptosis assay after 48 and 72 hours of treatment in p53 knock-out (ko) cells. The graphs show mean ± SD (*, 0.05>p≥0.01; **, 0.01>p≥0.001; ***, p<0.001).

4.5 Evaluation of 8-azaguanine mechanisms of action

4.5.1 8-Azaguanine induces ER stress

Bulk RNA sequencing (RNA-seq) was performed on the p53 wild-type EEB-derived clones. Distance matrix analysis of the Spearman rank correlation of all untreated p53 wild-type EEB clones showed high similarity among the transcriptomes of euploid and hypodiploid cells and among the transcriptomes of the non-responder aneuploid clones (Fig. 14A). These similarities were still consistent after drug treatment (Fig. 14B). Principal component analysis and unsupervised clustering separated samples, both untreated and treated, according to the responsiveness to 8-azaguanine (Fig. 15).

Ingenuity® Pathway Analysis (IPA®) of untreated aneuploid versus the euploid clone revealed that all of the aneuploid clones, with the exception of the hypodiploid one, exhibit upregulation of the NF-κB signaling pathway and downregulation of the NRF2-mediated oxidative-stress response pathway (Tab. S4).
Upstream regulator analysis of the non-responder aneuploid clones by IPA® predicted *ATF4*, thapsigargin, hydrogen peroxide, lipopolysaccaride (LPS) and cisplatin as inactivated upstream regulators (Tab. S5).

Among the 50 most differentially expressed genes between each of the 8-azaguanine treated samples and the respective untreated control, RNA-seq revealed remarkable similarities among all clones and identified a significant deregulation of genes involved in ER stress and cell differentiation. The top 30 most significantly deregulated genes in treated versus untreated clones included, among the overexpressed, mainly genes related to ER stress (*ATF3, HSPA13, INHBE, TRIB3, XBP1, DDIT3, ERN1, FAM129, MAP1LC3B, TNFRSF10B, ASNS, HERPUD1, CHAC1*), but also genes involved in apoptosis (*IL6ST*, *PMAIP1, MXD1*) and response to stress (*GDF15, SESN2*) (Fig. 16A; Tab. S3). Moreover, CHOP, encoded by the *DDIT3* gene, one of the most upregulated genes in the presence of ER stress[118,119], was activated in all clones after 24 hours of 8-azaguanine treatment (Fig. 16B). Treatment, predominantly in the responder clones, also led to the activation of JNK, which is involved in IRE1-mediated apoptosis induction[120] (Fig. 16B). Among the downregulated genes no main category could be identified. ER stress and oxidative stress were also shown as active processes within all clones treated with 8-azaguanine according to the IPA® analysis of the upstream regulators (activated: *ATF4, DDIT3, EIF2AK3*, thapsigargin, tunicamycin, LPS; inactivated: N-acetyl-L-cysteine (NAC)) (Tab. S7).

Furthermore, Gene Set Enrichment Analysis (GSEA), a computational technique used in the analysis of gene expression data, revealed significantly altered pathways. Kyoto Encyclopedia of Genes and Genomes (KEGG) was used as annotation database source of gene sets for the GSEA. Pathways involved in DNA replication, purine and pyrimidine metabolism, drug metabolism and ribosomal function were significantly downregulated in treated clones compared to the untreated ones (Fig. 16C). Nucleotide metabolism downregulation was also identified by IPA® pathway analysis (Tab. S6). Among the deregulated pathways after treatment, mitogen-activated protein kinase (MAPK) signaling was upregulated (Fig. 15C; Tab. S6). p38 MAPK is described to be involved in CHOP activation via phosphorylation of its transactivation domain[121].

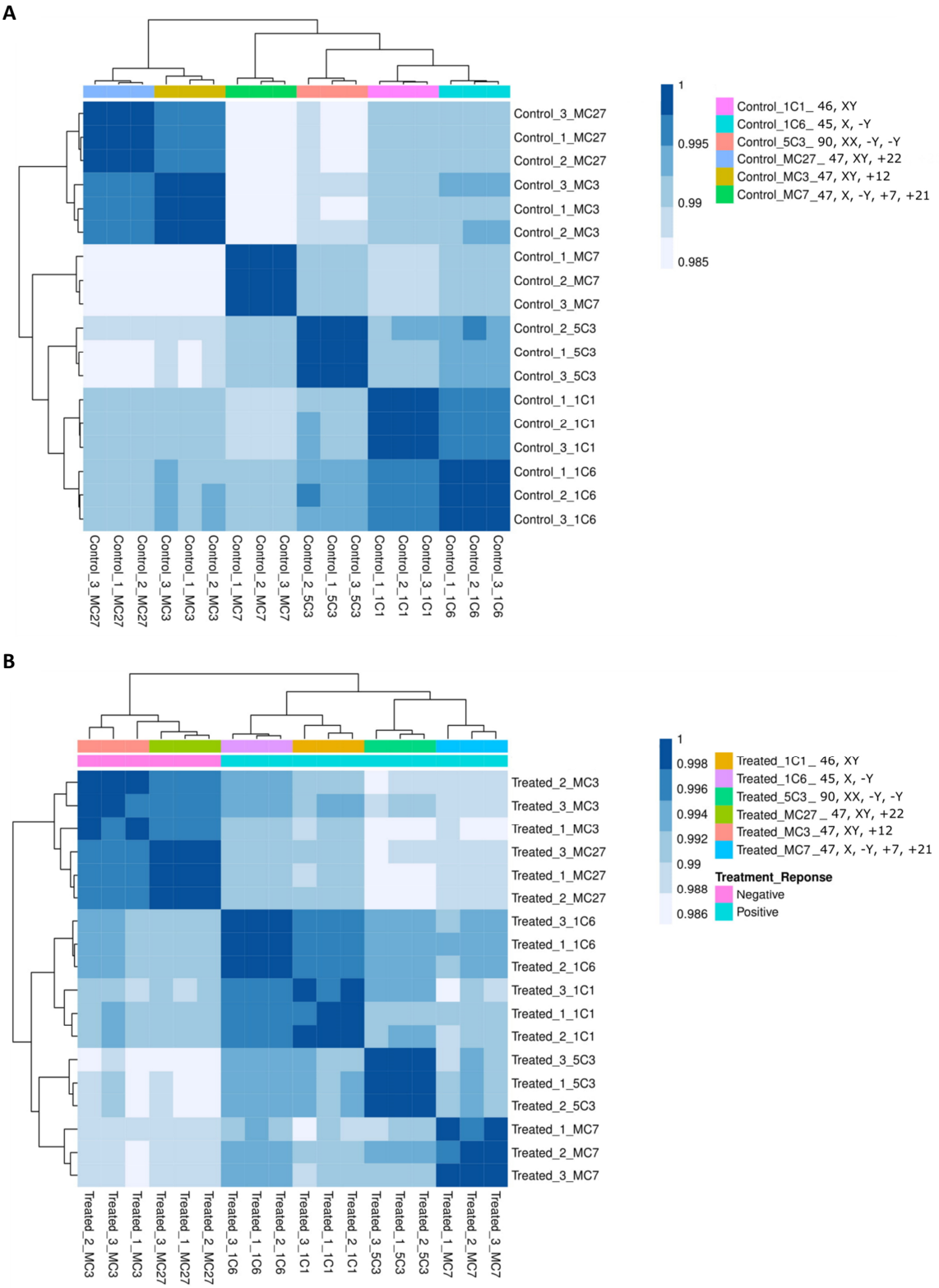

Figure 14 | Transcriptome similarities between responder and non-responder clones

Distance matrix of the Spearman rank correlation of all **(A)** untreated and **(B)** treated EEB-derived clones**.**

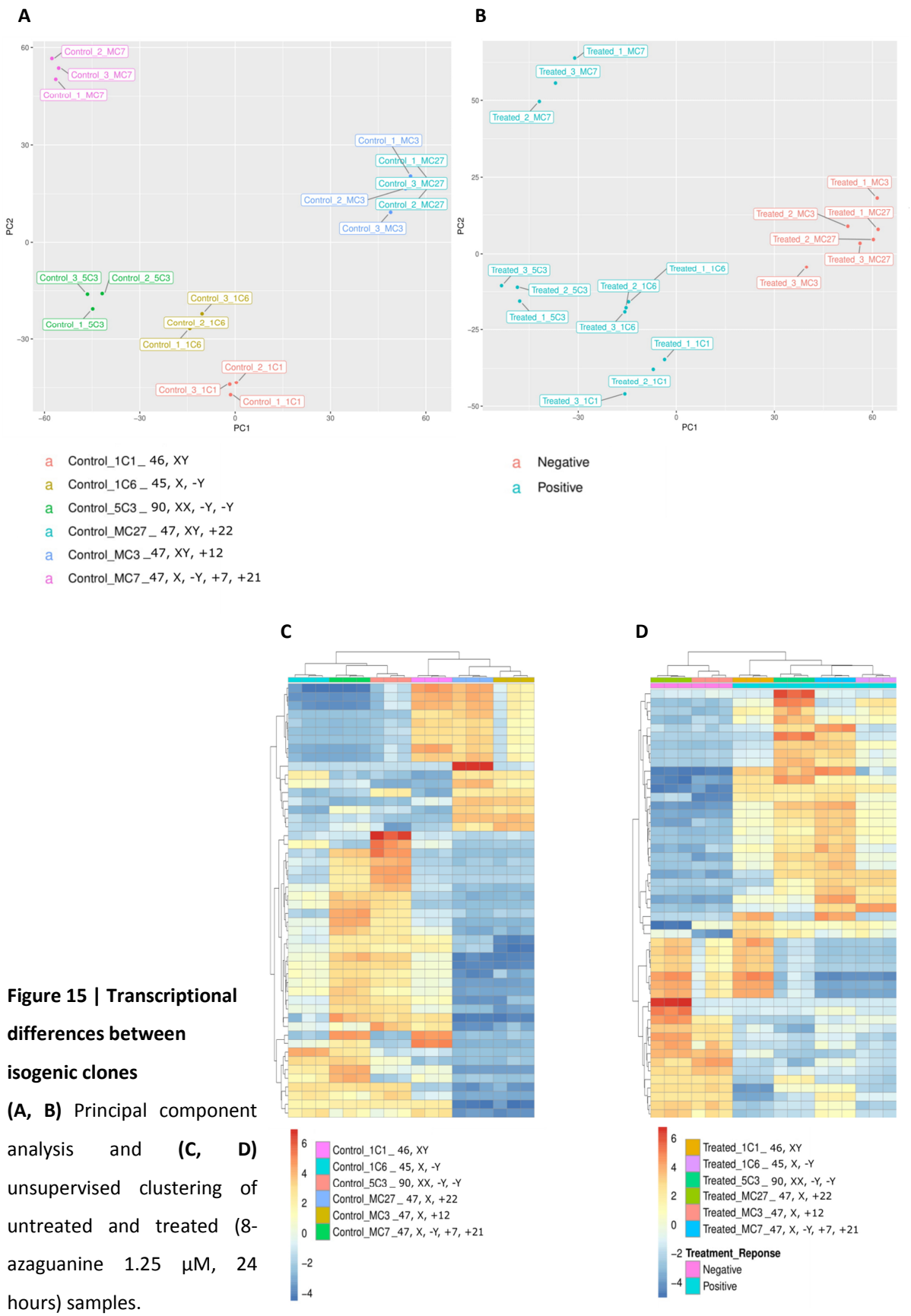

Figure 15 | Transcriptional differences between isogenic clones

(A, B) Principal component analysis and **(C, D)** unsupervised clustering of untreated and treated (8-azaguanine 1.25 µM, 24 hours) samples.

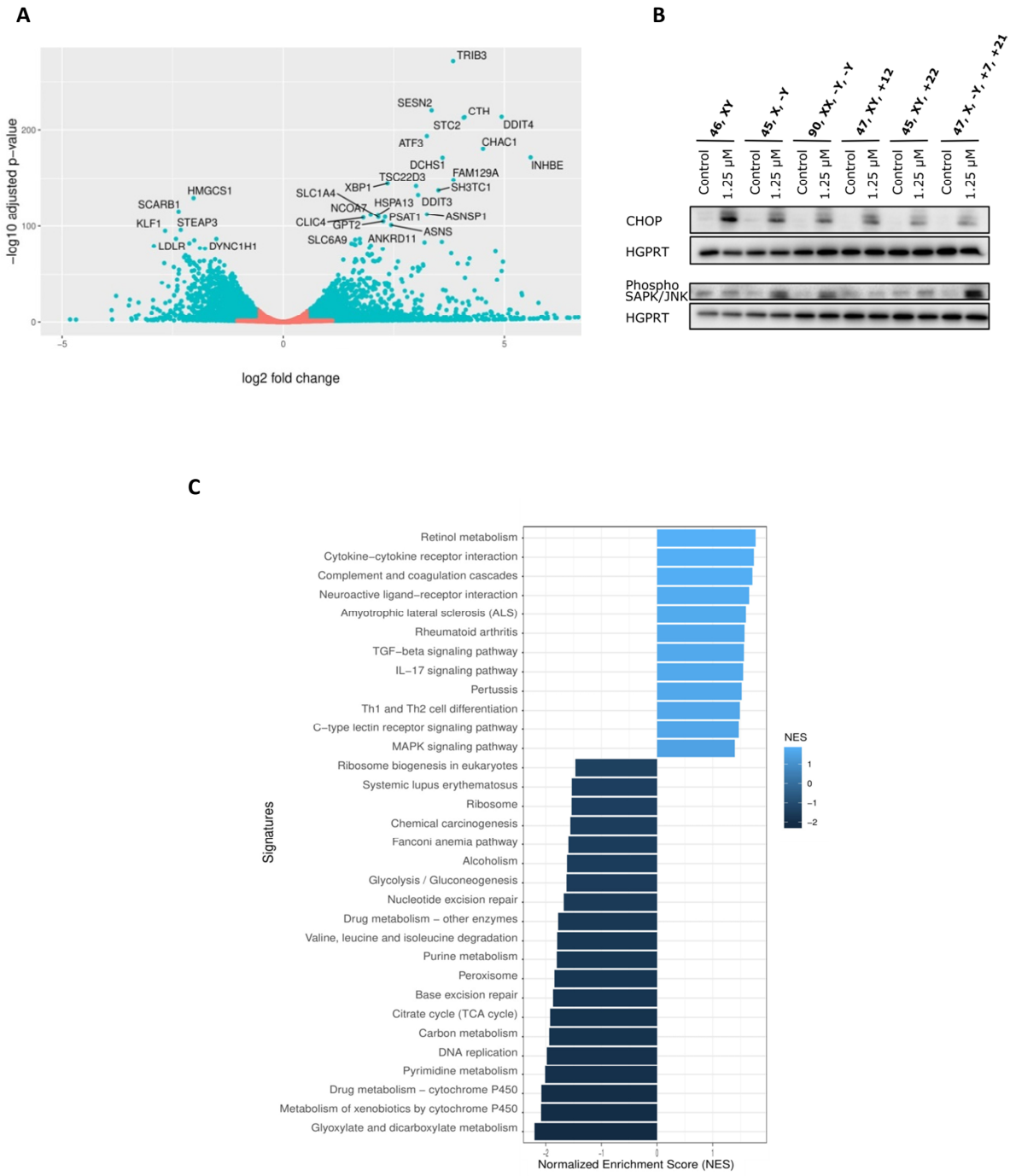

Figure 16 | 8-Azaguanine induces ER stress and deregulation of pathways related to MAPK signaling, DNA replication, nucleosides metabolism, drug metabolism and ribosomal function

(A) Volcano plot showing the top 30 most significant deregulated genes. **(B)** 8-Azaguanine triggers CHOP and JNK activation as shown by Western blot analysis of cell lysates after 24 hours of treatment with 8-azaguanine. **(C)** Most significantly deregulated KEGG pathways in all treated clones in comparison to untreated samples, as shown by GSEA.

4.5.2 8-Azaguanine triggers apoptosis

In order to confirm the observations made with the apoptosis assay, the activation of the apoptosis pathway was investigated at the Western blot level. Caspase 3, the executioner caspase, was cleaved and thus activated after treatment with 8-azaguanine (Fig. 17B). Active caspase 3 is responsible for the cleavage of PARP (Fig. 17B). The executioner caspase is activated by the action of the initiator caspases, caspase 8 and caspase 9. These two proteins initiate the apoptotic pathway in response to extrinsic and intrinsic stimuli, respectively. In our model system, 8-azaguanine induced apoptosis through the activation of the intrinsic pathway. Indeed, caspase 9 was cleaved, whereas caspase 8 was not activated (Fig. 17A). Caspase 2, which is mostly considered as an initiator caspase, was activated as well (Fig. 17B). The activation of the analyzed caspases was more pronounced in the three responder aneuploid clones as compared to the euploid and the two non-responder aneuploid clones (Fig. 17A-B).

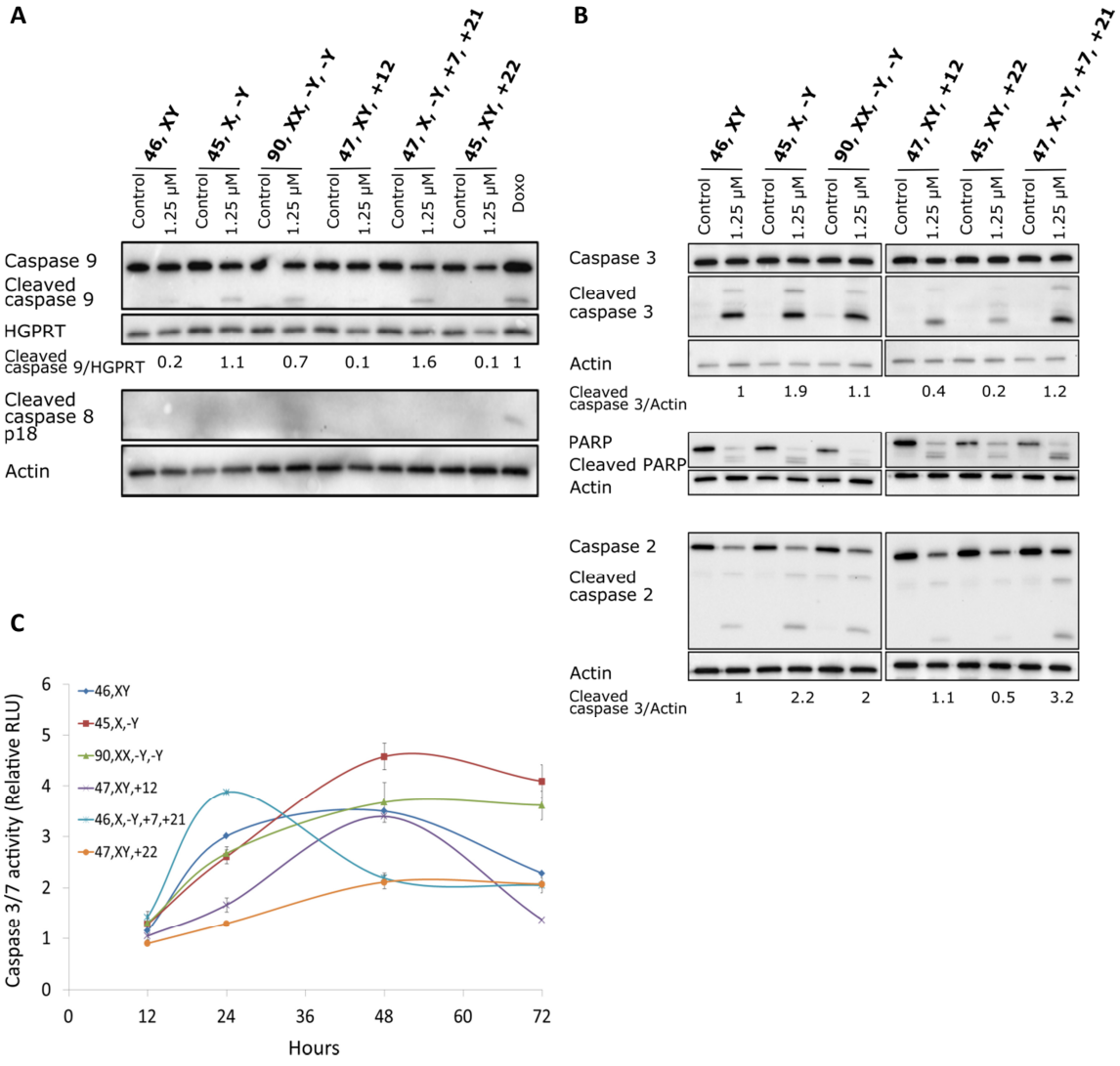

Figure 17 | Apoptosis is triggered after 8-azaguanine treatment

(A) Caspase 9 activation and **(B)** caspase 3, PARP and caspase 2 cleavage, as shown by Western blot analysis of cell lysates after 48 hours of treatment with 8-azaguanine. A doxorubicin treated sample (Doxo) was used as a positive control. **(C)** Time course evaluation of caspase 3/7 activity after treatment with 1.25 µM 8-azaguanine.

Caspase 3/7 activity was also measured by Caspase-Glo® assay. The three responder aneuploid clones reached a higher peak of caspase 3/7 activation in comparison to the euploid and the two non-responder aneuploid clones. Moreover, considering the responder aneuploid clones, the caspase activity peaked at 24 hours for the clone with trisomy 7 and 21, whereas for the hypodiploid and the near-tetraploid clones it peaked at 48 hours and remained at high levels even at 72 hours (Fig. 17C).

4.5.3 8-Azaguanine causes DNA damage

To determine whether 8-azaguanine treatment leads to DNA damage the phosphorylation of histone H2AX on Ser139 (ɣ-H2AX) was evaluated by immunoblotting. H2AX phosphorylation occurs early after DNA damage, and is particularly induced by DNA double strands breaks (DSBs), in order to recruit DNA repair proteins[122]. We also determined the occurrence of ɣ-H2AX and tumor suppressor p53 binding protein 1 (53BP1)-containing nuclear bodies by immunofluorescence microscopy. 53BP1 foci have been described to mark unrepaired DNA lesions that persist during mitosis and co-localize with ɣ-H2AX[123]. Treatment with 8-azaguanine caused a significant increase of ɣ-H2AX in all of the clones, as shown by Western blotting, as well as an increase of ɣ-H2AX/53BP1 foci, as shown by immunofluorescence microscopy (Fig. 18A-B). Moreover, the intensity of ɣ-H2AX was higher in the three responder aneuploid clones in comparison to the euploid clone (Fig. 18A). The near-tetraploid clone showed a basal, treatment-independent level of DSBs, possibly due to an increased amount of spontaneous DNA damage in comparison to near-diploid cells, and to either a possible saturation or less efficient DNA damage-repair mechanisms.

A

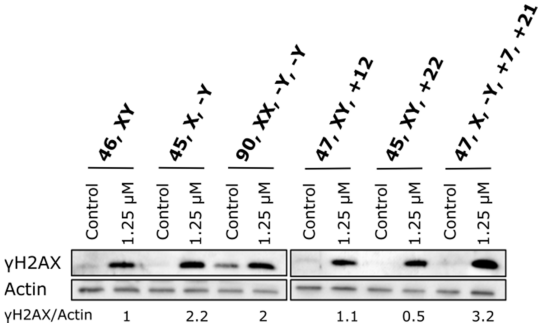

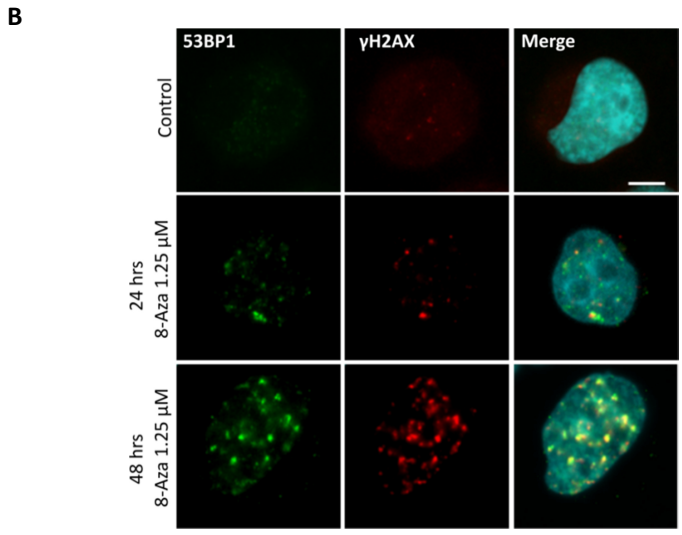

Figure 18 | DNA damage after 8-azaguanine treatment

(A) Phosphorylation of H2AX, as shown by Western blot analysis of cell lysates after 48 hours of 8-azaguanine treatment. **(B)** Representative immunofluorescence microscopy image of the euploid clone (46, XY) showing increased amounts of 53BP1 and ɣ-H2AX foci at increasing 8-azaguanine concentrations (scale bar, 10 µM).

4.5.4 8-Azaguanine causes cell cycle arrest

48 hours after 8-azaguanine treatment cell cycle progression was evaluated by FACS analysis. The addition of the compound induced cell cycle arrest in G_2/M (Fig. 19A). Inhibition of cell cycle progression was not dependent on p53 activation. Indeed, p53 knock-out cells were arrested as well after treatment with the drug (Fig. 19B).

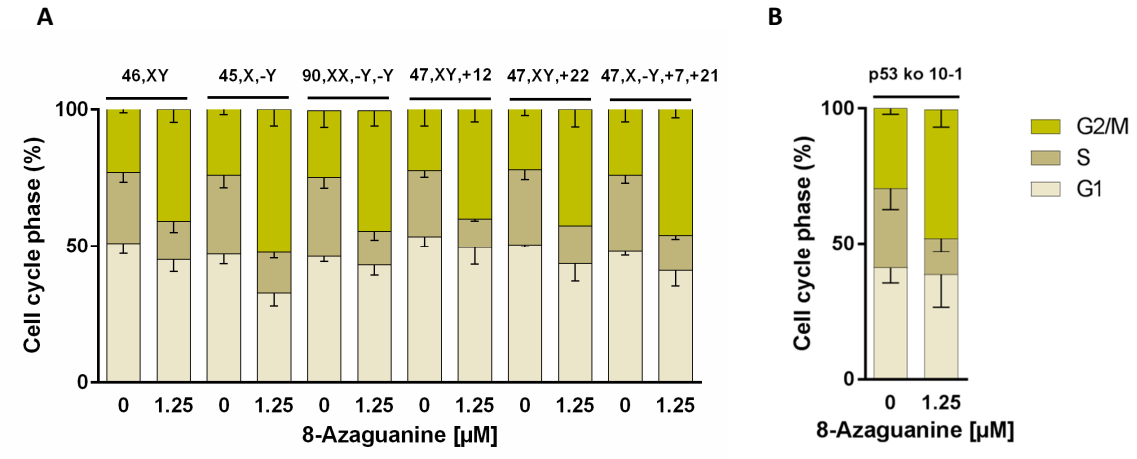

Figure 19 | 8-Azaguanine treatment causes cell cycle arrest

Accumulation of cells in G_2/M phase after 48 hours of treatment with 8-azaguanine in both **(A)** p53 wild-type and **(B)** p53 knock-out (ko) cells, as shown by FACS analysis.

4.5.5 Cell cycle arrest induced by 8-azaguanine treatment is mediated by phospho-ERK1/2

To further evaluate the mechanisms of 8-azaguanine activity we tested one MAPK key protein to investigate whether the MAPK pathway is involved in the cellular response to 8-azaguanine. Treatment with 1.25 µM of the compound for 48 hours led to increased levels of extracellular signal-regulated kinase 1/2 (ERK1/2) phosphorylation (Fig. 20A). This suggests that 8-azaguanine induces at least one branch of the MAPK signaling pathway.

Since phospho-ERK1/2 has already been described by others as a mediator of G_2/M cell cycle arrest and p21 induction[124], we hypothesized a possible role of phospho-ERK1/2 in 8-azaguanine induced cell cycle arrest as well. To further analyse this hypothesis, we next inhibited mitogen-activated protein kinase (MEK) kinase by U0126 to prevent the subsequent ERK1/2 phosphorylation. As expected, cells treated with 8-azaguanine alone were arrested in G_2/M phase. The addition of U0126 together with 8-azaguanine prevented this cell cycle arrest. This effect could already be detected with 1 µM of the inhibitor, but was enhanced at 2.5 µM. The inhibitor alone, in control cells, at both 1 and 2.5 µM, did not show any effect on cell cycle progression (Fig. 20B). At the Western blot level it was possible to detect a decrease of phospho-ERK1/2 and p21 with the addition of 2.5 µM of U0126 in comparison to 8-azaguanine treatment alone (Fig. 20C).

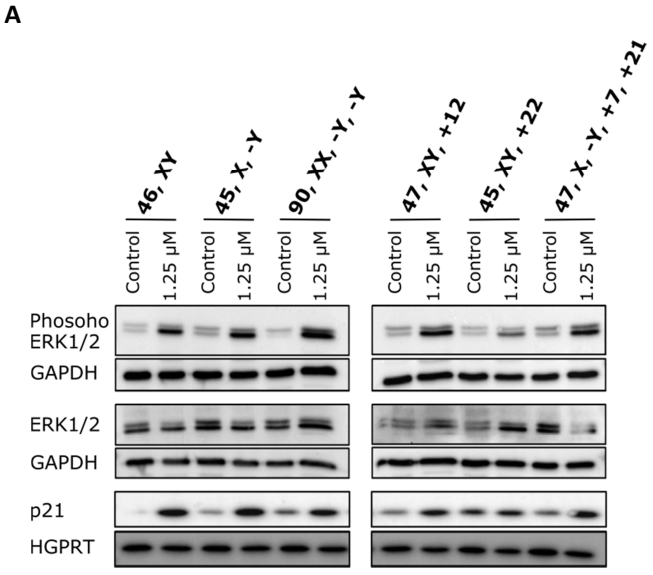

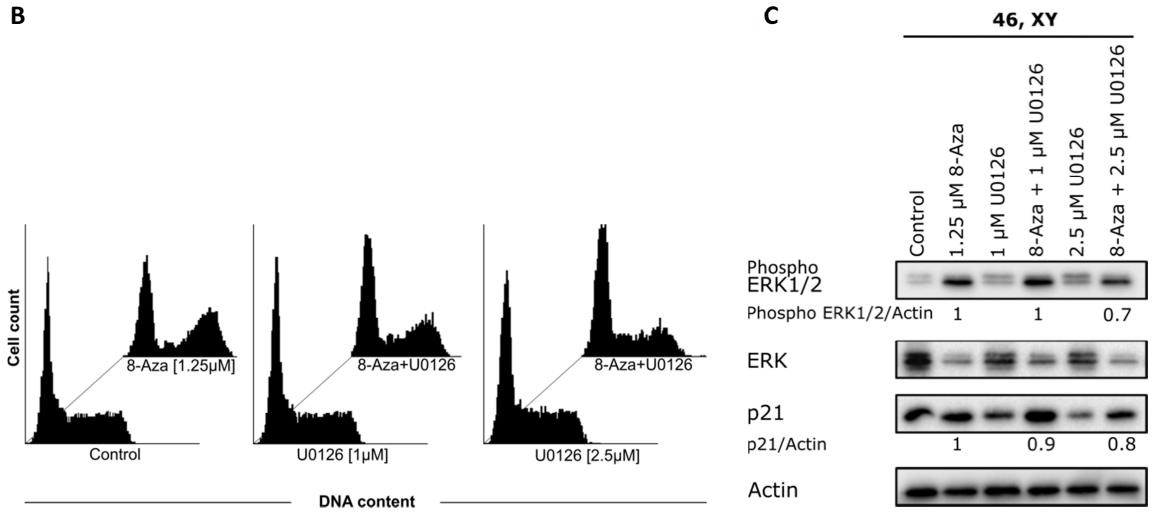

Figure 20 | Phospho-ERK1/2 mediates 8-azaguanine-induced G_2/M cell cycle arrest

(A) Increase of phospho-ERK1/2 and p21 overexpression, as shown by Western blot analysis of cell lysates after 48 hours of treatment with 8-azaguanine. **(B)** Cell cycle arrest in G_2/M phase induced by 8-azaguanine treatment and U0126-dependent cell cycle arrest rescue, as shown by FACS analysis.**(C)** Decrease of ERK1/2 phosporylation and p21 upregulation after combined treatment with 8-azaguanine and 2.5 μM U0126, as shown by Western blot analysis of cell lysates after 48 hours of treatment.

4.5.6 8-Azaguanine causes cell differentiation

Cell surface markers (CD13, CD16, CD117, HLA-DR, CD10, CD11b, CD35, CD64, CD14, CD300, CD36, CD105, CD71, CD33, CD56, CD19, CD7, CD15, NG2, CD38, CD22) were evaluated by flow cytometry before and after 24 hours of 8-azaguanine treatment. Among all the markers tested, only CD117, also known as C-KIT, decreased after treatment in the three responder aneuploid clones and in the euploid clone. On the other hand, the two non-responder clones already showed low levels of CD117 before treatment. According to the RNA-seq analysis of untreated cells, *C-KIT* was one of the most significantly downregulated genes in these two clones (padj= 1,85E-43).

CD117 (% ± SD)	Control	8-Aza
46, XY	73.1 ± 6.1	26.9 ± 8
45, X, -Y	74.45 ± 1.05	33.45 ± 2.05
90, XX, -Y, -Y	80.9 ± 2.3	47.85 ± 17.05
47, XY, +12	18.3 ± 5	5.45 ± 1.75
47, XY, +22	17.3 ± 1.9	7.5 ± 3.6
47, X, -Y, +7, +21	66.9 ± 3	23.65 ± 1.65

Table 28 | CD117 expression decreases after 8-azaguanine treatment

5 Discussion

Pathway deregulation, hampered proliferation, increased energy and metabolic requests, proteotoxic stress and genomic instability are typical features of aneuploid cells. Given the detrimental consequences of aneuploidy, it is evident why its prevalence in somatic cells is low[7].

Although the dismal effects of aneuploidy are well described, karyotype imbalances may confer proliferative advantages and promote tumorigenesis. Indeed, under specific circumstances, chromosome aberrations can have a tumor suppressor role, but once aneuploid cells overcome certain limitations, aneuploidy itself becomes beneficial for cancer development. Aneuploidy is in fact a common characteristic of 85% of both solid and hematological tumors and of 60% of AML at first diagnosis[15,91]. Moreover, many cancer cells not only harbor aneuploidy, but also chromosomal instability with high rates of chromosome missegregation at each cell division, eventually favoring cancer evolution by generating intra-tumor genetic diversity.

Recent studies have started to investigate whether aneuploidy can constitute a potential therapeutical target in cancer treatment. These studies were performed using aneuploid MEFs, HCT116, RPE-1 and other cell lines[60,61,74]. The effectiveness of the identified aneuploidy-selective antiproliferative compounds was mainly attributable to increased levels of stress induced by chromosome copy number changes.

So far, no study evaluating potential aneuploidy-selective antiproliferative compounds in AML has been reported. Patients with AML that harbor complex karyotypes have poor prognosis after treatment with the conventional chemotherapy, consisting in the combination of the nucleoside analog cytarabine and the anthracycline daunorubicin. Since the effectiveness of compounds specifically targeting aneuploidy has been demonstrated in other cancer types in vitro, the identification of drugs with selective efficacy against aneuploid karyotypes for the treatment of AML appears as a reasonable and competitive approach.

8-Azaguanine is a drug with selective activity against aneuploid AML primary samples and cell lines

Since aneuploid cells derived from different organisms and different cell lines share common characteristics that can be exploited as targets for cancer therapy, aneuploidy-selective antiproliferative compounds already described in the literature might be effective against aneuploid AML cells as well. Therefore 8-azaguanine, 17-AAG, AICAR, ASA, chloroquine, metformin and resveratrol were tested on primary AML samples. Centrinone, cisplatin, crenolanib, taxol and

vincristine were tested as well. In addition, cytarabine and daunorubicin, which are used in daily practice for AML treatment, were also included in the analysis.
8-Azaguanine was the only compound with selective activity against complex karyotype AML primary samples as compared to normal karyotype AML. Moreover, our results suggest that the efficacy of 8-azaguanine towards primary samples may be influenced by the degree of aneuploidy, independent of the preponderance of chromosome gains or losses.

The comparison between euploid and aneuploid AML cells in vitro is hampered by the lack of suitable AML cell line models. Additionally, the comparison of cell lines with different genetic backgrounds shows many limitations. Therefore, we established an isogenic AML cell model. For this purpose, a euploid clone and spontaneously arising aneuploid cells were isolated from the EEB AML cell line and additionally, with the induction of chromosome retention at spindle poles and the inactivation of the mitotic checkpoint via CENP-E and MPS1 inhibition, three more aneuploid clones were generated.

In our EEB AML cell line model, 8-azaguanine was more effective against three out of five p53 wild-type aneuploid clones versus the euploid clone, partially confirming the results obtained with primary AML samples. We hypothesize that the unresponsiveness of two aneuploid cell lines might be due, at least in part, to their differentiation status. The EEB cell line belongs to the erythroid lineage and expresses CD117/C-KIT. With the increasing differentiation, erythroid precursors progressively loose the expression of CD117. C-KIT is a tyrosine-protein kinase that acts as cell-surface receptor for the cytokine KITLG/SCF. In response to KITLG/SCF binding, C-KIT can activate several signaling pathways and plays a crucial role in the regulation of hematopoiesis, cell survival and proliferation. We could demonstrate that all responder clones including the euploid one expressed high levels of CD117 which were reduced after drug treatment, suggesting an impact of 8-azaguanine on cell differentiation. On the other hand, CD117 was almost completely absent from the non-responder clones, indicating more advanced differentiation.

The near-tetraploid clone responded best to the drug, suggesting that the extent of aneuploidy might influence the response to 8-azaguanine – similar to the situation in primary AML cells – as well. Based on this observation we argue that 8-azaguanine has a stronger effect on cells with a high burden of chromosomal aberrations. Tetraploid or near tetraploid AML is rare, occurring in only 0.7-1.2% of patients[125]. Although known to have a dismal prognosis, it is not well characterized. Given our results, 8-azaguanine could represent an interesting option for the treatment of patients whose AML blasts harbor a high number of chromosomal aberrations.

We further generated isogenic EEB cells lacking p53, which harbored heterogeneous karyotypes with many different numerical and structural aberrations, and demonstrated that 8-azaguanine can be effective against chromosomally unstable p53 knock-out EEB AML cells as well.

8-Azaguanine selectivity against aneuploid cells might be due to an increased burden on the ER

As demonstrated by gene expression analysis and confirmed by Western blotting, 8-azaguanine triggers the activation of ER stress pathways. Proteotoxic stress is a well known consequence of aneuploidy itself[50,55,57,59,60,61]. Indeed, enhanced protein production in karyotypically abnormal cells induces a saturation of the protein folding pathways, which in turn leads to increased amounts of misfolded proteins. Once cells sense the insufficiency of the ER protein folding capacity, the unfolded protein response (UPR) is triggered and the ER stress sensors ATF6, IRE1 and PERK cause a reduction of the protein load to the ER. Furthermore, misfolded proteins that are retained in the ER are transported to the cytosol and degraded in a process called ER-associated degradation (ERAD). If the stress cannot be solved and homeostasis is not reestablished, cells enter apoptosis. Since proteotoxic stress has already been described as a typical consequence of aneuploidy, we argue that in such a situation the addition of an ER stress inducing agent as 8-azaguanine pushes cells into apoptosis, thereby explaining the aneuploidy-selective antiproliferative effect of the drug. This is indeed sustained by our RNA-seq data, which revealed that the untreated aneuploid clones already exhibited an upregulation of the NF-κB signaling pathway. NF-κB activation, together with the release of Ca^{2+} from the ER and the production of reactive oxygen species, is involved in the ER overload response (EOR) which is triggered by the accumulation of membrane proteins in the ER[126]. Furthermore, the unresponsiveness to 8-azaguanine of the two non-responder clones could be due to their reduced susceptibility to ER stress and higher tolerance to oxidative stress, as suggested by the upstream regulator analysis in IPA®.

Moreover, in our model, 8-azaguanine triggered the activation of the intrinsic apoptosis pathway as well as stronger and prolonged activation of the executioner caspase 3 in the responder aneuploid clones in comparison to the euploid and the non-responder clones. We therefore suggest that apoptosis is caused by massive ER stress and triggered by a downstream effector of the ER stress pathway, CHOP, whose expression promotes cell death in the presence of prolonged stress[118,119], and by the activation of IRE1-mediated JNK signaling, which is involved in the inhibition and activation of Bcl-2 and Bim, respectively[120,127,128].

In all the clones analyzed 8-azaguanine caused cell cycle arrest in G_2/M phase through p53-independent mechanisms, as G_2/M arrest was found in p53-deficient clones after drug treatment as well. This cell cycle arrest is likely a consequence of extensive DNA damage, which seemed also to be

more enhanced in the aneuploid responder cells in comparison to the euploid clone, even if we cannot exclude a possible causative role of ER stress as well.

p53 deficiency leads to extensive karyotypic heterogeneity and to the propagation of structural aberrations

Aneuploidy, due to its detrimental consequences, which have been already shown at both cellular and organismal levels, can lead to p53 activation and inhibition of proliferation. Nevertheless, the aspects which determine p53 activation after chromosome missegregation have still to be determined. It has been proposed that aneuploidy *per se* can activate p53 via p38, even without any evidence of DNA damage, as described by Thompson and Compton. In this case, p53 activation has been suggested to be caused by transcript imbalances of genes located on supernumerary chromosomes[68]. On the other hand, others reported that p53 is not directly activated by aneuploidy, but via related conditions. Janssen and colleagues observed that chromosome missegregation causes DNA damage and, only subsequently, ATM and p53 activation[65]. Li and colleagues reported that after chromosome segregation errors elevated levels of ROS were produced, inducing oxidative DNA damage, and subsequent ATM and p53 activation[69]. More recent studies showed that p53-mediated cell cycle arrest occurs in more severely aneuploid cells with structural abnormalities, as a consequence of DNA replication stress[113,114]. These inconsistencies might be due to different experimental settings, prolonged mitotic timing that causes a subsequent p53-dependent G_1 arrest, and undetected DNA damage [70]. A clear definition of the mechanisms which link aneuploidy to p53 activation will help to better define how abnormal karyotypes arise and to understand the acquired tolerance of tumor cells to aberrant karyotypes. Another still controversial issue is whether p53 deficiency itself leads to aneuploidy. Bunz and colleagues have initially investigated this hypothesis in HCT116 cells with inactivated p53 and showed that p53 deficiency does not lead to aneuploidy development in this system[115]. On the contrary, we demonstrated that AML EEB p53-deficient cells can spontaneously acquire and propagate chromosome abnormalities, including numerical aneuploidies, structural aneuploidies and structural rearrangements, without the addition of missegregation stimuli. We showed that p53 deficiency is sufficient to allow the propagation of chromosomal instability at higher rates compared to those obtained after the induction of chromosome missegregation in p53 wild-type cells, arguing for the important role of p53 in the maintenance of genomic stability. Loss of p53 leads to non-clonal abnormalities and thus allows for extensive karyotypic heterogeneity. Taken together our results are consistent with epidemiological data. Indeed *TP53* alterations are the most frequently described aberrations in patients with complex karyotype AML (*TP53* mutations and *TP53* losses are found in 60%-80% and 40% of AML patients with complex karyotype, respectively[129,130]). Furthermore, in complex karyotype AML, cases

harboring *TP53* alterations are characterized by an increased total number of chromosomal aberrations in comparison to complex karyotype AML cells with wild-type *TP53*[129].

In our AML model we demonstrated that numerical aneuploidy can be propagated in p53-proficient EEB cells, indicating that aneuploidy does not always lead to p53-mediated cell cycle arrest and cell death. On the other hand the presence of p53 limits the propagation of structural aneuploidies and structural rearrangements almost completely. These results are in agreement with reports by Soto and Santaguida on untransformed RPE-1 cells[113,114]. In our model chromosome missegregation was likely triggered to the same extent in both p53-proficient and p53-deficient cells. Since segmental aneuploidies and structural rearrangements as well as DNA damage were only detected in the absence of p53, our data suggest that chromosome missegregation events resulting in structural chromosome abnormalities cause DNA damage with consequential p53-mediated permanent cell cycle arrest and/or cell death.

6 Outlook

The present work has led to the identification of 8-azaguanine as a potential AML aneuploidy-selective anti-cancer drug, as demonstrated in primary AML samples and an isogenic AML cell line model. The 8-azaguanine effect seems to be more pronounced in cells harboring a more extensive level of aneuploidy, suggesting a potential clinical application in patients with complex karyotype or tetraploid AML. Studies evaluating the efficacy of this compound in animal models of complex karyotype or tetraploid versus euploid AML are thus required to confirm our *in vitro* findings.

8-Azaguanine causes activation of the ER stress response and subsequent cell death possibly by exaggerating the basal ER stress level of aneuploid cells, as shown in our cell line model and suggested by RNA-seq results. However, additional analyses have to be performed to prove at the molecular level the presence of basal ER stress in aneuploid cells. It would be interesting to demonstrate a similar pattern also in primary AML samples.

Additionally, we demonstrated that 8-azaguanine, as a purine analogue, causes DNA damage as a consequence of replication impairment, but the characteristics of the compound leading to the generation of ER stress remains unclear. 8-Azaguanine mechanisms of action need therefore to be investigated in more depth.

7 Index

7.1 Lists of abbreviations

Abbreviations	Name
17-AAG	17-Allylamino-geldanamycin
AICAR	5-Aminoimidazole-4-carboxamide ribonucleotide
abn	Abnormal
AML	Acute Myeloid Leukemia
AMPK	AMP-Activated Protein Kinase
APC/C	Anaphase Promoting Complex
APS	Aneuploidy-Associated Protein Signature
APS	Ammonium Persulfate
ASA	Acetylsalicylic Acid
ATF6	Activating Transcription Factor 6
AUC	Area Under The Curve
8-Aza	8-Azaguanine
BM	Bone Marrow
BMNCs	Bone Marrow Mononuclear Cells
53BP1	Tumor Suppressor p53 Binding Protein 1
BSA	Bovine Serum Albumin
CDC20	Cell-Division Cycle Protein 20
CDK1	Cyclin-Dependent Kinase 1
CENP-E	Centromere-Associated Protein-E
CHOP	C/EPB homologous protein
CI	Confidence Interval
CIN	Chromosomal Instability
CLL	Chronic Lymphocytic Leukemia
ddH_2O	Double Distilled Water
DPBQ	2,3-Diphenylbenzo[g]quinoxaline-5,10-dione
D-PBS	Dulbecco's Phosphate Buffered Saline
DMSO	Dimethylsulfoxide
DNA	Deoxyribonucleic Acid
ELN	European Leukemianet
ER	Endoplasmic Reticulum
FAB	French-American-British
FBS	Fetal Bovine Serum
FISH	Fluorescence In Situ Hybridization
GSEA	Gene Set Enrichment Analysis
HSF1	Heat Shock Factor 1
HSP90	Heat Shock Protein 90
HSP72	Heat Shock Protein 72
IC50	Inhibitory Concentration 50%
IF	Immunofluorescence
inv	Inversion
IPA	Ingenuity Pathway Analysis
IRE1	Inositol-Requiring Enzyme 1
JNK	cJun NH_2-Terminal Kinase
KEGG	Kyoto Encyclopedia of Genes and Genomes

ko	Knock-out
LB	Lysogeny Broth
LC3	Autophagy Marker Light Chain 3
LPS	Lipopolysaccharide
MAD2	Mitotic Arrest Deficient 2
MCM	Mononuclear Cell Medium
MEFs	Mouse Embryonic Fibroblasts
M-FISH	Multiplex Fluorescence In Situ Hybridization
MOPS	3-(N-morpholino)propanesulfonic acid
MPS1	Multipolar Spindle-1
MVA	Mosaic Variegated Aneuploidy
NAC	N-acetyl-L-cysteine
p53	Tumor protein p53
p	P Value
padj	P Value Adjusted
PERK	Protein Kinase RNA-Like Endoplasmic Reticulum Kinase
PB	Peripheral Blood
PBMCs	Peripheral blood mononuclear cells
PBS	Phosphate Buffered Saline
PLK4	Polo-Like Kinase 4
PNK	T4 Polynucleotide Kinase
RIN	RNA Integrity Number
RNA	Ribonucleic acid
RNA-seq	RNA Sequencing
ROS	Reactive Oxygen Species
SAC	Spindle Assembly Checkpoint
SAP	Shrimp Alkaline Phosphatase
SD	Standard Deviation
sgRNA	Single guide RNA
SOB	Super Optimal Broth
SOC	Super Optimal Broth With Catabolite Repression
SQSTM1	P62/Sequestosome-1
t	Translocation
TAE	Tris-Acetate-EDTA
TBS-T	Tris Buffered Saline with Tween 20
TEMED	Tetramethylethylendiamin
UPR	Unfolded Protein Response
UV	Ultraviolet
WHO	World Health Organization
wt	Wild-type

Abbreviations of units	Unit
bp	Base Pairs
°C	Degree Celsius
Da	Dalton
k	kilo
m	milli
µ	micro
M	molar
n	nano
rcf	Relative centrifugal force
rpm	Rounds per minute
V	Voltage

7.2 List of figures

7.3 List of tables

8 Supplementary material

	Euploid samples
1	46, XY [29]
2	46, XX [4]
3	46, XX [27]
4	46, XY [28]
5	46, XX [25]
6	46, XY [25]
7	46,XY [25]
8	46, XY [25]
9	46, XX [25]
10	46, XY [25]
11	46, XY [25]
12	46, XX [25]
13	46, XY [25]
14	46, XX [25]
15	46, XX, del(5)(q21q34), del(6)(q13q25), del(12)(q21q24) [19] / 46, XX [2]
16	46, XX, r(10)(p12q11), der(11)t(10;11)(q11;q13), ish r(10)(5'MLL+), der(11)t(10;11)(5'MLL+,3'MLL-) [18] / 46, XX [2]
17	46, XY, der(5)del(5)(q31)t(4;5)(?;3).ish der(5)(EGR1-), ish t(11;?)(5'MLL) [2] / 46, XY, der(5)del(5)(q31)t(4;5)(?;q31).ish der(5)(EGR1)

Table S1 |Karyotype of euploid AML primary samples

	Aneuploid samples
1	47, XY, +21 [12] / 47, XY, +21, del(4)(q?) [3] / 47, XY, +21 del(13)(q?) [5] / 47, XY, +21, del(4)(q?), del(13)(q?) [1]
2	47, XX, t(6;11)(q27;q23), +der(6)t(6;11)(q27;q23) [10] / 48, XX, t(6;11)(q27;q23), +der(6)t(6;11)(q27;q23), +19 [9]
3	45-47, XY, t(4;?)(q13;?), del(8)(p11.2), -13, -16, +2mar [cp17]
4	47, XY, +8, t(11;16)(q23;p13)[22] / 48, XY, +8, t(11;16)(q23;p13), +?22, ?inc [cp4] / 46, XY, ?inc [3]
5	44, XY, -3, dic(7;17)(q11.2;p11.2), der(11), der(17)t(3;17)(?q26.2q12;?q21) [16]
6	45, XX, add(8)(p11.2), -11, -14, -16, +21, +mar [6] / 46, sl, +add(8)(p11.1) [18] / 46,XX [1]
7	45, add(X)(p22.3)Y, add(3)(p13), del(5)(q31q35), add(6)(p21), +der(6)t(6;17)(p21;q?11.2), del(9)(q22), del(13)(q12), -17, -21, -21, +mar, inc [17] / 46,XY [6]
8	46-50, XX, der(4)add(4)(p16)ins(4;?(q?21;??), del(5)(q13q33), l(8)(q10), +l(8)(q10)x1, -2, -15, -16, add(17)(q2?3), -18, del(20)(q11), +mar1x1-2, +mar2
9	47, XX, +11 / 48, XX, add(6p), +8, +8, +10, der(15;17)(q10;q10) / 48, ml, add(11q) / 48, XX, +9, +8, +10, -17, add(19q)
10	38-45, XY, del(1)(?q21), ins(1;4)(q?21;?), der(3)(3qter->3p21::?17q11.2->?17q21::?6->?6), t(5;17)(p10;q10), del(6)t(6;12)(p21;?), der(6)t(6;17)(p21;?),
	del(7)t(7;17)(p13;?)t(?3;7)(p21;q?22), +8, i(8)(q10), +1, -2, -16, -17 [cp14] / 46,XY [1]
11	47, XX, der(4)del(4)(q?11)t(4;?11)(q?11;q23q23), der(7)(del(7)(q?11)t(7;?10)(q?11;p12), +8, der(10;11)(10qter-->10p12::11q23-->11q23:
12	45, X, -Y, -4, del(5)(q?12q33), -16, -17, -21, +4mar [4]
13	46-50, XY, +3, +8, t(9;11)(p22;q23), +der(9)t(9;11)(p22;q23), -13, +14 [cp22]
14	44, XY, +del(1)(q12), der(1)dup(1)(q32q21)t(1;20)(p12,p11.1), del(4)(q21q33), del(5)(q15q33), -7, +8, add(12)(p13), add(13)(p11,2), add(14)(p11.2), -16, -17, -20 [25]
15	45-47, -X [12], del(5)(q15q33) [27], add(9)(p13) [27], i(11)(q10) [27] / -16 [27], add(16)(p11.1) [27] / del(17)(p11.2) [27], add(18)(p11.2) [27],
	add(21)(p11.1) [2], -22 [27], +1~5mar [27] [cp27]
16	Highly complex karyotype without MLL rearrangement, without monosomy 7
17	46, XX, t(8;16)(p11.1-2;p13.3) [24] / 45, sl, -22 [3]

Table S2 |Karyotype of aneuploid AML primary samples

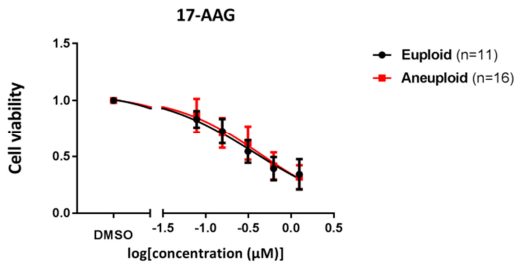
17-AAG
Cell viability
1.5
1.0
0.5
0.0
DMSO
-1.5
-1.0
-0.5
0.0
0.5
log[concentration (µM)]
Euploid (n=11)
Aneuploid (n=16)

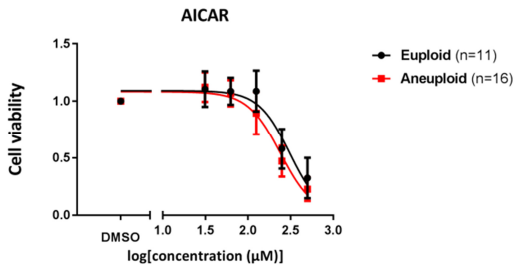
AICAR
Cell viability
1.5
1.0
0.5
0.0
DMSO
1.0
1.5
2.0
2.5
3.0
log[concentration (µM)]
Euploid (n=11)
Aneuploid (n=16)

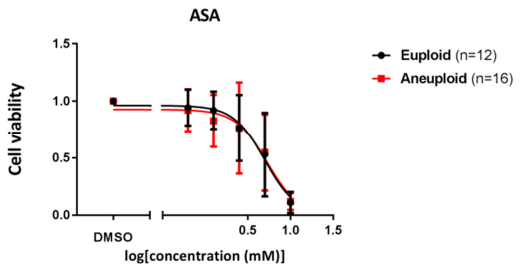
ASA
Cell viability
1.5
1.0
0.5
0.0
DMSO
0.5
1.0
1.5
log[concentration (mM)]
Euploid (n=12)
Aneuploid (n=16)

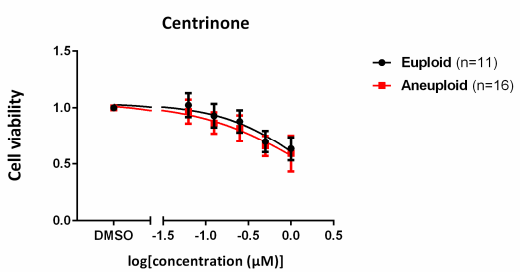
Centrinone
Cell viability
1.5
1.0
0.5
0.0
DMSO
-1.5
-1.0
-0.5
0.0
0.5
log[concentration (µM)]
Euploid (n=11)
Aneuploid (n=16)

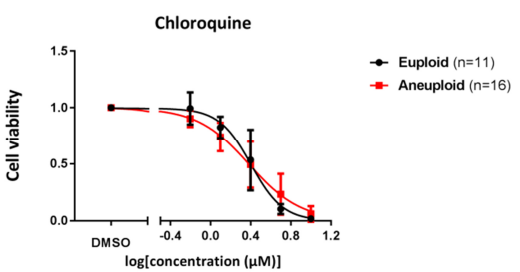
Chloroquine
Cell viability
1.5
1.0
0.5
0.0
DMSO
-0.4
0.0
0.4
0.8
1.2
log[concentration (µM)]
Euploid (n=11)
Aneuploid (n=16)

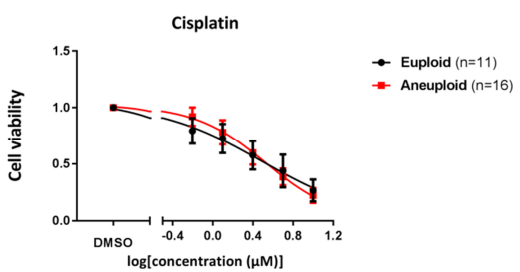
Cisplatin
Cell viability
1.5
1.0
0.5
0.0
DMSO
-0.4
0.0
0.4
0.8
1.2
log[concentration (µM)]
Euploid (n=11)
Aneuploid (n=16)

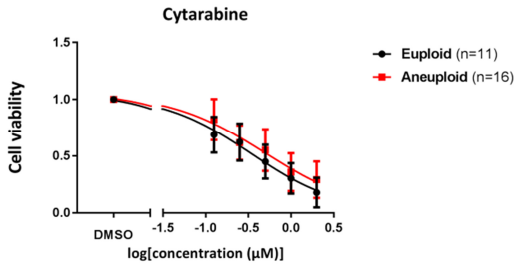
Cytarabine
Cell viability
1.5
1.0
0.5
0.0
DMSO
-1.5
-1.0
-0.5
0.0
0.5
log[concentration (µM)]
Euploid (n=11)
Aneuploid (n=16)

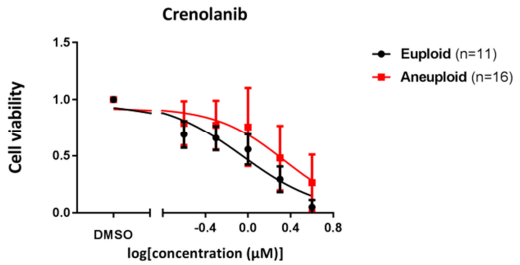
Crenolanib
Cell viability
1.5
1.0
0.5
0.0
DMSO
-0.4
0.0
0.4
0.8
log[concentration (µM)]
Euploid (n=11)
Aneuploid (n=16)

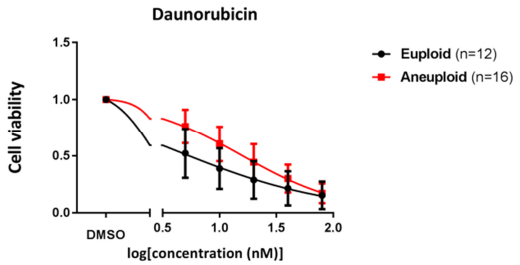
Daunorubicin
Cell viability
1.5
1.0
0.5
0.0
DMSO
0.5
1.0
1.5
2.0
log[concentration (nM)]
Euploid (n=12)
Aneuploid (n=16)

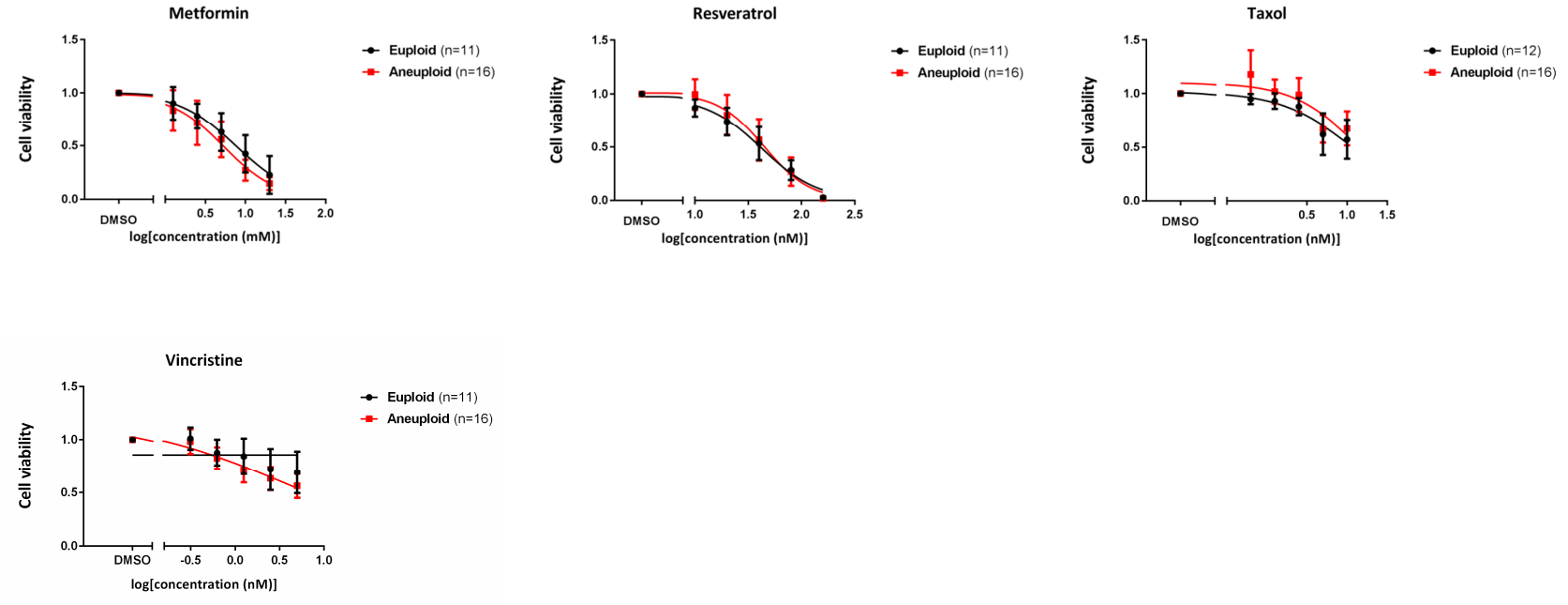

Figure S1 | Drug response curves

Cell viability after 72 hours of treatment with the mentioned compounds. The graphs show means ± 95% CI.

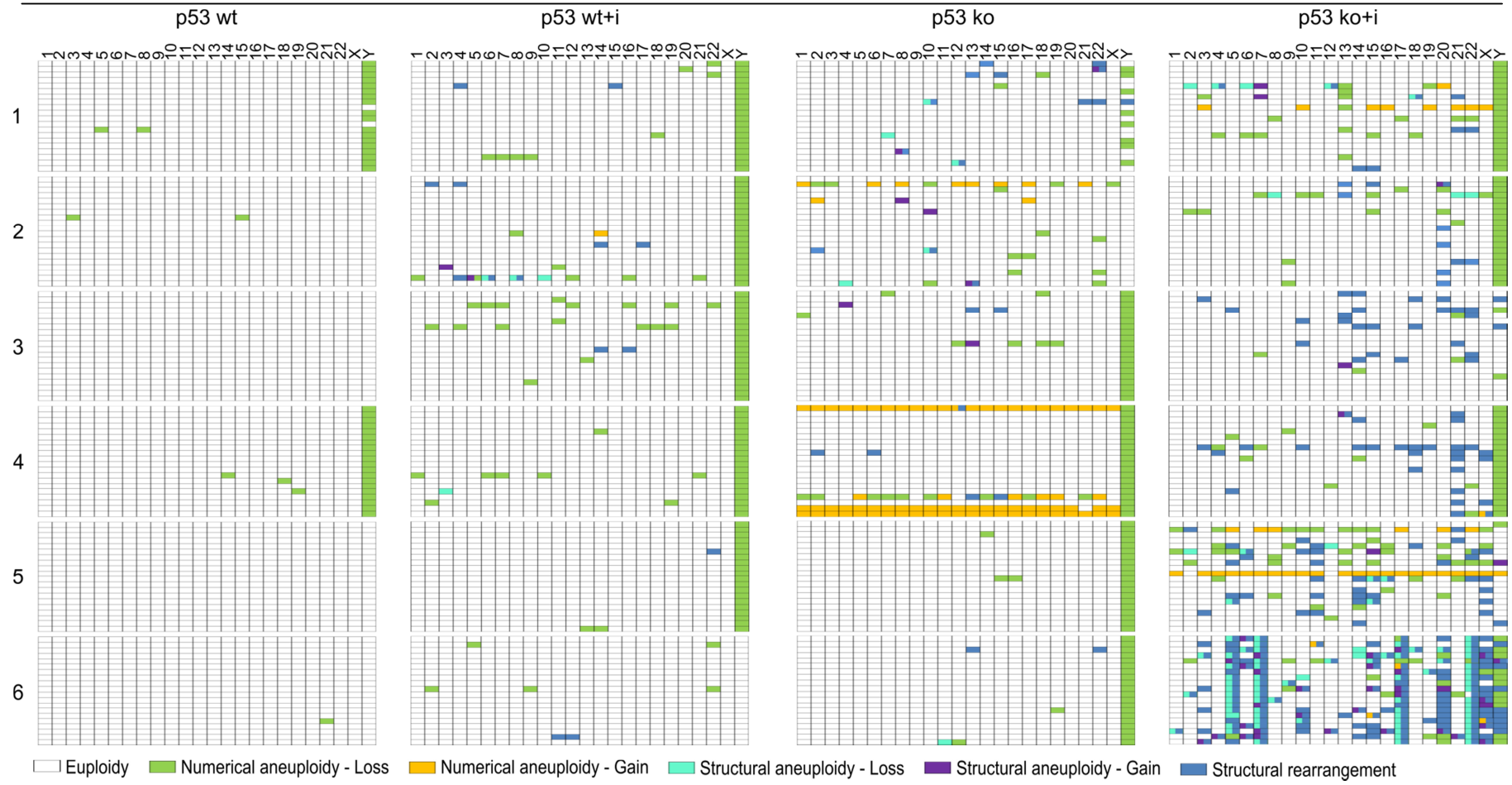

Figure S2 | Representations of all karyotypes analyzed

Each row represents a metaphase. The presence of at least one chromosome with structural rearrangement in addition to aneuploidy is depicted with double color. wt: wild-type; ko: knock-out.

46, XY			45, X, -Y			90, XX, -Y, -Y			47, XY, +12			47, X, -Y, +7, +21			47, XY, +22		
gene	log2FoldChange	padj	gene	log2FoldChange	padj	gene	log2FoldChange	padj	gene	log2FoldChange	padj	gene	log2FoldChange	padj	gene	log2FoldChange	padj
ASNSP1	2,531616385	1,01E-70	*APLNR*	-4,600480137	1,17E-82	*ALPK3*	4,323523049	4,29E-72	*AC137932.1*	2,683185605	3,32E-23	*ADM2*	2,721544308	1,83E-37	*ANKRD11*	1,7310145	2,58E-87
ATF3	3,049436334	7,3E-107	*ATF3*	3,250718985	3E-110	*ARC*	4,857138765	1,81E-66	*ADM2*	4,503069467	3,79E-27	*AQP2*	2,860274954	1,34E-31	*ASNS*	2,44030285	1,3E-101
C12orf39	4,33035767	5,98E-46	*C11orf24*	2,080990747	5,1E-174	*ATF3*	2,608566531	8,89E-67	*ASNS*	2,438882268	9,47E-23	*AREG*	4,113655166	7,93E-32	*ASNSP1*	3,248419664	5,6E-113
C1orf95	-4,795741365	9,5E-65	*C19orf26*	2,94720746	2,28E-98	*AVIL*	3,279535939	9,16E-65	*ASNSP1*	2,973311644	5,67E-24	*ASNSP1*	2,205606262	2,36E-29	*ATF3*	3,247598426	1,9E-194
DCAF4L1	4,574118624	1,22E-47	*DCAF4L1*	3,848218172	2,7E-102	*C1orf233*	-3,769174177	1,1E-106	*ATF3*	2,964146479	1,43E-38	*ATF3*	3,444978404	6,43E-61	*CHAC1*	4,516391688	1,2E-180
DCHS1	5,540665201	1,9E-128	*DCHS1*	4,533130197	2E-165	*C1orf95*	-5,580461768	2,2E-124	*CHAC1*	4,506825421	4,83E-81	*C19orf26*	2,634899066	2,67E-36	*CLIC4*	1,810380849	1,5E-109
DDIT4	3,163941581	1,18E-55	*DDIT3*	3,078408004	5,1E-131	*DCHS1*	4,325873783	3,7E-125	*DCAF4L1*	3,047935244	3E-27	*CTH*	3,022617139	4,77E-64	*CTH*	4,0998694	7,3E-214
FAM69A	5,209383872	3,1E-59	*DDN*	-2,281451285	1,11E-90	*DDIT3*	3,375431748	1,64E-69	*DCHS1*	3,77071077	5,97E-47	*DCAF4L1*	4,000048016	7,73E-52	*DCHS1*	3,601710168	1,5E-171
GPBAR1	5,961947717	2,03E-52	*DDR2*	3,186790787	2,91E-95	*DDR2*	3,173443748	1,85E-61	*DDIT3*	2,850379527	1,85E-28	*DCHS1*	4,495643217	3,17E-84	*DDIT3*	3,049185496	3,5E-133
HSPA13	1,844606133	2,03E-47	*DIRAS1*	-2,093062788	3,54E-94	*FAM129A*	2,203588193	1,81E-66	*DDIT4*	4,273896908	1,21E-48	*DDIT3*	3,481351496	3,41E-69	*DDIT4*	4,937632664	3,5E-214
IL6ST	2,603478875	6,08E-49	*ERN1*	2,22586902	6,2E-100	*GADD45B*	3,380359191	2,98E-63	*FAM69A*	4,830234688	3,05E-45	*DLX2*	2,446383241	9,26E-29	*DYNC1H1*	-1,512742303	2,24E-87
INHBE	4,65399528	2,51E-86	*FAM129A*	3,096273082	5,2E-173	*HSD3BP5*	4,426346389	7,74E-69	*FGF18*	4,756474248	4,53E-29	*FGF18*	5,558382345	2,23E-35	*FAM129A*	3,849308494	4,4E-149
LRIT3	4,402359191	3,04E-55	*GOT1*	1,511171101	1,14E-86	*INHBE*	4,381179804	1E-103	*GPBAR1*	4,584830648	3,45E-32	*GDF15*	2,359684573	8,31E-35	*GPT2*	2,261337183	1,5E-105
LRTM2	-2,929778	5,26E-63	*MAP1LC3B*	2,010343663	2,16E-98	*LINC00176*	3,23211159	1,78E-65	*GPT2*	2,232811351	2,27E-24	*GPBAR1*	4,513001516	2,88E-37	*HMGCS1*	-2,027277492	6E-130
MARVELD1	-3,128546509	2,37E-62	*MARVELD1*	-2,708742744	6E-118	*MARVELD1*	-3,074138399	8,4E-102	*HERPUD1*	1,684184761	2,45E-21	*HAVCR2*	4,882028782	3,35E-34	*HSPA13*	2,147441739	1,6E-112
MYLK2	3,042393982	6,41E-52	*OVGP1*	4,173577343	5,44E-87	*MCF2*	-3,460027012	7,53E-67	*INHBE*	6,079411027	4,54E-84	*HSD3BP5*	4,123117189	3,55E-38	*INHBE*	5,592976101	5E-172
NCOA7	2,16539197	2,13E-49	*P2RY11*	1,967689791	4,07E-87	*MXD1*	2,210885306	2,6E-61	*LRIT3*	4,607818154	3E-30	*HSPA13*	2,112493779	3,22E-44	*KLF1*	-2,670348091	1,14E-95
NFIL3	1,934927275	1,4E-44	*PMAIP1*	1,981239617	5,2E-102	*PDE4DIP*	2,550103547	1,2E-60	*OVGP1*	3,573785513	9,01E-28	*IER3*	2,193400467	6,95E-36	*LDLR*	-2,426172187	1,78E-87
OVGP1	3,843733961	1,04E-54	*PNPLA1*	3,418337076	2,7E-175	*PYGM*	4,578605742	1,01E-66	*PHKG1*	2,457199051	3,59E-21	*INHBE*	4,854834698	2,6E-67	*NCOA7*	1,976982229	2,2E-112
PHKG1	3,338958379	4,1E-44	*RAB27A*	2,077138558	7,6E-102	*SDPR*	-3,481152137	6,82E-76	*PSAT1*	2,18021867	2,91E-22	*KDM6B*	2,311428766	1,45E-39	*PSAT1*	2,301050254	3,4E-110
PLCB3	-2,147153266	1,52E-46	*RGS16*	3,283267498	1,3E-187	*SERTAD1*	2,962276677	1,42E-74	*RRH*	4,900167872	1,04E-30	*LRIT3*	5,378068018	9,75E-30	*SCARB1*	-2,366449699	5,3E-116
PMAIP1	1,946989971	1,15E-47	*RNF207*	-3,134806895	4,9E-100	*SESN2*	2,886825215	1,3E-89	*SESN2*	3,453216228	3,15E-54	*MYLK2*	3,25328575	3,41E-48	*SESN2*	3,355075445	1,1E-221
RGS16	2,76964525	4,47E-62	*SKIL*	2,23652276	1,9E-143	*SKIL*	2,469431392	4,3E-69	*SLC1A4*	1,961960974	6,53E-24	*PHKG1*	2,970134393	2,76E-38	*SH3TC1*	3,507544793	4,5E-138
RNF207	-2,842811489	6,99E-49	*SLC40A1*	-2,674423197	2E-104	*STMN3*	-2,755558188	1,85E-61	*SLC7A11*	2,401715148	7,16E-23	*PNPLA1*	2,90742204	1,01E-45	*SLC1A4*	2,151497733	4E-110
SESN2	2,624102377	1,78E-56	*TNFRSF10B*	1,935351637	1,84E-86	*TRIB3*	3,683021385	4E-144	*SP6*	2,406483042	1,09E-22	*RGS16*	2,58805679	9,46E-31	*SLC6A9*	1,62582381	1,44E-86
SLC40A1	-2,628360499	1,5E-65	*TRIB3*	3,910069998	5,6E-226	*TSC22D3*	2,928638537	3E-65	*TRIB3*	3,553907402	6,96E-40	*SESN2*	3,275645552	3,17E-61	*STC2*	4,080017857	2,9E-213
STC2	2,552403729	1,55E-52	*TSC22D3*	3,068893238	5,4E-110	*UNC13D*	-2,710611588	1,27E-59	*TSC22D3*	3,246003061	1,48E-44	*TRIB3*	4,021625945	3,9E-107	*STEAP3*	-2,318636466	1,11E-96
TRIB3	3,419024856	3,71E-73	*XBP1*	2,378522413	1,29E-87	*WNK4*	4,522553027	1,6E-73	*ULBP1*	3,676242863	1,68E-25	*TSC22D3*	2,861638532	1,06E-38	*TRIB3*	3,840354992	1,8E-272
TSC22D3	2,513972964	3,74E-61	*ZFAND3*	2,098168982	1,48E-91	*XBP1*	2,239566656	9,21E-72	*XBP1*	2,191940865	2E-24	*ULBP1*	2,742244071	1,07E-33	*TSC22D3*	3,002693156	1,5E-142
XBP1	2,369071973	9,29E-94	*ZNF512B*	-2,220424072	5,8E-159							*XBP1*	2,435796277	1,26E-49	*XBP1*	2,359566297	2,8E-145

Table S3 | Top 30 most significant deregulated genes for each treated clone

Canonical pathway	45, X, -Y		90, XX, -Y, -Y		47, XY, +12		47, X, -Y, +7, +21		47, XY, +22	
	z-score	p value	z-score	p value	z-score	p value	z-score	p value	z-score	p value
NF-κB signaling pathway	ND	ND	1.664	6.81E-05	3.153	3.63E-05	1.131	5.76E-03	1.236	2.73E-02
NRF2-mediated oxidative-stress response	ND	ND	-2.353	2.24E-04	-2.137	2.17E-04	-3.212	1.48E05	-1.543	5.78E-06

Table S4 | Canonical pathways of untreated aneuploid clones compared with untreated euploid clone

Upstream regulators	47, XY, +12		47, XY, +22	
	z-score	p value	z-score	p value
ATF4	-5.012	4.55E-05	-5.082	1.92E-06
Thapsigargin	-2.828	1.57E-03	-2.191	3.5E-03
LPS	-1.468	3.3E-03	-1.341	7.12E-04
Hydrogen Peroxide	-2.971	1.52E-04	-2.766	1.22E-04
Cisplatin	-3.322	1.42E-09	-3.899	1.07E-06

Table S5| Upstream regulators of untreated non-responder clones in comparison to untreated euploid clone

Canonical pathway	46, XY		45, X, -Y		90, XX, -Y, -Y		47, XY, +12		47, X, -Y, +7, +21		47, XY, +22	
	z-score	p value	z-score	p value	z-score	p value	z-score	p value	z-score	p value	z-score	p value
Salvage pathways of pyrimidine ribonucleotides	-2.649	1.28E-04	-3.042	7.58E-04	-2.414	1.68E-02	ND	ND	-2.058	3.13E-02	-2.058	1.42E03
Purine nucleotides *de novo* biosynthesis II	-3.00	1.62E-04	-2.530	8.43E-06	-2.530	1.11E-06	-2.333	5.15E-06	-3.00	1.79E-04	-2.333	3.44E-05
Pyrimidine deoxyribonucleotides *de novo* biosynyhesis I	-2.887	6.02E-03	-2.887	4.82E-03	-2.887	7.15E-04	-2.121	3.41E-02	ND	ND	-2.309	1.16E-03
Pyrimidine ribonucleotides *de novo* byosinthesis	-4.243	3.2E-02	ND	ND	ND	ND	-3.606	4.49E-02	ND	ND	-3.500	2.6E-02
p38 MAPK signaling	1.067	6.89E-04	1.234	2.69E-03	2.722	2.42E04	2.785	1.9E-02	1.342	4.67E-04	1.521	1.54E-02

Table S6 | Canonical pathways of 8-azaguanine treated clones

Upstream regulators	46, XY		45, X, -Y		90, XX, -Y, -Y		47, XY, +12		47, X, -Y, +7, +21		47, XY, +22	
	z-score	p value	z-score	p value	z-score	p value	z-score	p value	z-score	p value	z-score	p value
ATF4	5.062	9.20E-07	5.422	1.91E-06	4.616	3.87E-07	5.620	1.59E-13	5.498	7.77E-09	5.888	4.11E-13
DDIT3	3.980	7.54E-03	3.866	1.15E-02	3.397	1.67E-03	2.901	4.54E-05	3.181	9.07E-03	3.520	1.9E-04
EIF2AK3	3.242	5.43E-04	3.189	6.51E-04	2.551	6.22E-05	3.420	2.94E-09	3.752	3.81E-09	3.097	9.08E-08
Thapsigargin	3.657	4.6E-03	3.730	5.14E-04	2.792	9.69E-05	3.989	7.51E-04	3.959	8.22E-05	4.076	6.19E-06
Tunicamycin	4.276	1.82E-02	4.414	2.19E-04	3.034	1.22E-04	3.839	9.66E-07	5.136	1.48E-06	4.328	2.76E-06
LPS	3.648	1.64E-02	4.379	3.96E-03	3.851	2.61E-05	4.146	7.66E-02	5.542	7.56E-04	4.117	2.33E-02
NAC	-	NS	-3.109	2.25E-02	-2.616	1.41E-03	-2.697	9.41E-03	-3.037	8.15E-03	-3.488	1.78E-03

Table S7 | Upstream regulators of 8-azaguanine treated clones

9 References

1. Täckholm, G. Zytologische Studien überdie Gattung Rosa. *Acta horti Bergiani* **7,** 97–381 (1922).

2. Rehen, S. K. *et al.* Chromosomal variation in neurons of the developing and adult mammalian nervous system. *Proc. Natl. Acad. Sci.* **98,** 13361–13366 (2001).

3. Rehen, S. K. *et al.* Constitutional Aneuploidy in the Normal Human Brain. *J. Neurosci.* **25,** 2176–2180 (2005).

4. Pack, S. D. *et al.* Individual adult human neurons display aneuploidy: Detection by fluorescence in situ hybridization and single neuron PCR. *Cell Cycle* **4,** 1758–1760 (2005).

5. Duncan, A. W. *et al.* The ploidy conveyor of mature hepatocytes as a source of genetic variation. *Nature* **467,** 707–710 (2010).

6. Duncan, A. W. *et al.* Frequent Aneuploidy Among Normal Human Hepatocytes. *Gastroenterology* **86,** 573–579 (2007).

7. Knouse, K. A. *et al*. Single cell sequencing reveals low levels of aneuploidy across mammalian tissues. *Proc. Natl. Acad. Sci.* **111,** 13409–13414 (2014).

8. Plaja, A. *et al.* Variegated aneuploidy related to premature centromere division (PCD) is expressed in vivo and is a cancer-prone disease. *Am. J. Med. Genet.* **98,** 216–223 (2001).

9. Hanks, S. *et al.* Constitutional aneuploidy and cancer predisposition caused by biallelic mutations in BUB1B. *Nat. Genet.* **36,** 1159–1161 (2004).

10. Andriani, G. A. *et al*. Mechanisms and consequences of aneuploidy and chromosome instability in the aging brain. *Mech Ageing Dev.* **161,** 19–36 (2017).

11. Jacobs, K. B., *et al*. Detectable clonal mosaicism and its relationship to aging and cancer. *Nat. Genet.* **44,** 651–658 (2012).

12. Laurie, C. C. *et al.* Articles Detectable clonal mosaicism from birth to old age and its relationship to cancer. *Nat. Genet.* **44,** 642–650 (2012).

13. Forsberg, L. A. *et al.* Age-Related Somatic Structural Changes in the Nuclear Genome of Human Blood Cells. *Am. J. Hum. Genet.* **90,** 217–228 (2012).

14. Thompson, S. L. & Compton, D. A. Examining the link between chromosomal instability and aneuploidy in human cells. *J. Cell Biol.* **180,** 665–672 (2008).

15. Weaver, B. A. & Cleveland, D. W. Does aneuploidy cause cancer? *Curr. Opin. Cell Biol.* **18,** 658–667 (2006).

16. Lengauer, C. *et al*. Genetic instability in colorectal cancers. *Nature* **10,** 623–7 (1997).

17. Heilig, C. E. *et al.* Chromosomal instability correlates with poor outcome in patients with myelodysplastic syndromes irrespectively of the cytogenetic risk group. *J. Cell. Mol. Med.* **14,** 895–902 (2010).

18. von Hansemann, D. Ueber asymmetrische zelltheilung in epithelkrebsen und deren biologische bedeutung. *Virschows Arch Pathol Anat.* **119,** 299–326 (1890).

19. Boveri, T. Zur Frage der Entstehung maligner Tumoren. *Fischer, Jena.* (1914).

20. Zimonjic, D. *et al*. Derivation of human tumor cells in vitro without widespread genomic instability. *Cancer Res.* **61,** 8838–8844 (2001).

21. Paulsson, K. & Johansson, B. Trisomy 8 as the sole chromosomal aberration in acute myeloid leukemia and myelodysplastic syndromes. *Pathol. Biol.* **55,** 37–48 (2007).

22. Sotillo, R. *et al.* Mad2 Overexpression Promotes Aneuploidy and Tumorigenesis in Mice. *Cancer Cell* **11,** 9–23 (2007).

23. Weaver, B. A. A. *et al*. Aneuploidy Acts Both Oncogenically and as a Tumor Suppressor. *Cancer Cell* **11,** 25–36 (2007).

24. Silk, A. D. *et al.* Chromosome missegregation rate predicts whether aneuploidy will promote or suppress tumors. *Proc. Natl. Acad. Sci.* **110,** E4134–E4141 (2013).

25. Michel, L. S. *et al.* MAD2 haplo-insufficiency causes premature anaphase and chromosome instability in mammalian cells. *Nature* **409,** 355–359 (2001).

26. Dai, W. *et al.* Slippage of Mitotic Arrest and Enhanced Tumor Development in Mice with BubR1 Haploinsufficiency. *Cancer Res.* **64,** 440–445 (2004).

27. Iwanaga, Y. *et al.* Heterozygous deletion of mitotic arrest-deficient protein 1 (MAD1) increases the incidence of tumors in mice. *Cancer Res.* **67,** 160–166 (2007).

28. Sato, M. *et al.* Infrequent mutation of the hBUB1 and hBUBR1 genes in human lung cancer. *Japanese J. Cancer Res.* **91,** 504–509 (2000).

29. Tighe, A. *et al*. Aneuploid colon cancer cells have a robust spindle checkpoint. *EMBO Rep.* **2,** 609–614 (2001).

30. Gascoigne, K. E. & Taylor, S. S. Cancer Cells Display Profound Intra- and Interline Variation following Prolonged Exposure to Antimitotic Drugs. *Cancer Cell* **14,** 111–122 (2008).

31. Musacchio, A. & Salmon, E. D. The spindle-assembly checkpoint in space and time. *Nat. Rev. Mol. Cell Biol.* **8,** 379–393 (2007).

32. Pinsky, B. A. & Biggins, S. The spindle checkpoint: Tension versus attachment. *Trends Cell Biol.* **15,** 486–493 (2005).

33. Gregan, J. *et al.* Merotelic kinetochore attachment: Causes and effects. *Trends Cell Biol.* **21,** 374–381 (2011).

34. Cimini, D. *et al.* Merotelic kinetochore orientation is a major mechanism of aneuploidy in mitotic mammalian tissue cells. *J. Cell Biol.* **152,** 517–527 (2001).

35. Cimini, D. *et al*. Merotelic kinetochore orientation occurs frequently during early mitosis in mammalian tissue cells and error correction is achieved by two different mechanisms. *J. Cell Sci.* **116,** 4213–4225 (2003).

36. Solomon, D. a *et al.* Causes Aneuploidy in Human Cancer. *Science* **333,** 1039–1043 (2011).

37. Guo, G. *et al.* Whole-genome and whole-exome sequencing of bladder cancer identifies frequent alterations in genes involved in sister chromatid cohesion and segregation. *Nat. Genet.* **45,** 1459–1463 (2013).

38. Kon, A. *et al.* Recurrent mutations in multiple components of the cohesin complex in myeloid neoplasms. *Nat. Genet.* **45,** 1232–1237 (2013).

39. Welch, J. S. *et al.* The origin and evolution of mutations in acute myeloid leukemia. *Cell* **150,** 264–278 (2012).

40. Balbás-Martínez, C. *et al.* Recurrent inactivation of STAG2 in bladder cancer is not associated with aneuploidy. *Nat. Genet.* **45,** 1464–1469 (2013).

41. Vitre, B. D. & Cleveland, D. W. Centrosomes, chomosome instability (CIN) and aneuploidy. *Curr Opin Cell Biol.* **24,** 809–815 (2012).

42. Pihan, G. a *et al.* Centrosome Defects and Genetic Instability in Malignant Tumors. *Cancer Res.* **58,** 3974–3985 (1998).

43. Lingle, W. L. & Salisbury, J. L. Altered centrosome structure is associated with abnormal mitoses in human breast tumors. *Am. J. Pathol.* **155,** 1941–1951 (1999).

44. Neben, K. *et al*. Centrosome aberrations in acute myeloid leukemia are correlated with cytogenetic risk profile. *Blood* **101,** 289–291 (2003).

45. Giehl, M. *et al.* Centrosome aberrations in chronic myeloid leukemia correlate with stage of disease and chromosomal instability. *Leukemia* **19,** 1192–1197 (2005).

46. Nigg, E. A. Centrosome aberrations: cause or consequence of cancer? *Nat Rev Cancer* **2,** 815–25 (2002).

47. Ganem, N. J. *et al*. A mechanism linking extra centrosomes to chromosomal instability. *Nature* **460,** 278–282 (2009).

48. Cosenza, M. R. *et al.* Asymmetric Centriole Numbers at Spindle Poles Cause Chromosome Missegregation in Cancer Article Asymmetric Centriole Numbers at Spindle Poles Cause Chromosome Missegregation in Cancer. *Cell Rep.* **20,** 1906–1920 (2017).

49. Segal, D. J. & Mccoy, A. E. E. Studies on Down's syndrome in tissue culture. I. Growth rates protein contents of fibroblast cultures. *J. CELL. PHYSIOL*. 142–144 (1974).

50. Torres, E. M. et al. Effects of Aneuploidy on Cellular Physiology and Cell Division in Haploid Yeast. *Science* **317,** 916–923 (2007).

51. Stingele, S. *et al*. Global analysis of genome, transcriptome and proteome reveals the response to aneuploidy in human cells. *Mol. Syst. Biol.* **8,** 1–12 (2012).

52. Williams, B. R. *et al.* Aneuploidy affects proliferation and spontaneous immortalization in mammalian cells. *Science* **322,** 703–709 (2008).

53. Dürrbaum, M. *et al.* Unique features of the transcriptional response to model aneuploidy in

human cells. *BMC Genomics* **15,** 1–14 (2014).

54. Upender, M. B. *et al.* Chromosome Transfer Induced Aneuploidy Results in Complex Dysregulation of the Cellular Transcriptome in Immortalized and Cancer Cells. *Cancer Res.* **64,** 6941–6949 (2004).

55. Dephoure, N. *et al.* Quantitative proteomic analysis reveals posttranslational responses to aneuploidy in yeast. *eLife Sci.* 1–27 (2014). doi:10.7554/eLife.03023

56. Viganó, C. *et al.* Quantitative proteomic and phospho-proteomic comparison of human colon cancer DLD-1 cells differing in ploidy and chromosome stability. *Mol. Biol. Cell* **29,** 1031–1047 (2018).

57. Torres, E. M. *et al.* Identification of Aneuploidy-tolerating Mutations. *Cell* **143,** 71–83 (2010).

58. Sheltzer, J. M. *et al*. Transcriptional consequences of aneuploidy. *Proc. Natl. Acad. Sci.* **109,** 12644–12649 (2012).

59. Oromendia, A. B. *et al*. Aneuploidy causes proteotoxic stress in yeast. *GENES Dev.* **26,** 2696–2708 (2012).

60. Donnelly, N. *et al*. HSF1 deficiency and impaired HSP90-dependent protein folding are hallmarks of aneuploid human cells. *EMBO J.* **33,** 2374–2387 (2014).

61. Tang, Y.-C. *et al*. Identification of aneuploidy-selective antiproliferation compounds. *Cell* **144,** 499–512 (2011).

62. Santaguida, S. *et al*. Aneuploidy-induced cellular stresses limit autophagic degradation. *GENES Dev.* **29,** 2010–2021 (2015).

63. Sheltzer, J. M. *et al.* Aneuploidy drives genomic instability in yeast. *Science* **333,** 1026–1030 (2011).

64. Passerini, V. *et al.* The presence of extra chromosomes leads to genomic instability. *Nat. Commun.* **7,** 1-12 (2016).

65. Janssen, A. *et al*. Chromosome Segregation Errors as a Cause of DNA Damage and Structural Chromosome Aberrations. *Science* **333,** 1895–1898 (2011).

66. Crasta, K. *et al.* DNA breaks and chromosome pulverization from errors in mitosis. *Nature* **482,** 53–58 (2012).

67. Stephens, P. J. *et al.* Massive genomic rearrangement acquired in a single catastrophic event during cancer development. *Cell* **144,** 27–40 (2011).

68. Thompson, S. L. & Compton, D. A. Proliferation of aneuploid human cells is limited by a p53-dependent mechanism. *J. Cell Biol.* **188,** 369–381 (2010).

69. Li, M. *et al.* The ATM-p53 pathway suppresses aneuploidy-induced tumorigenesis. *Proc. Natl. Acad. Sci. U. S. A.* **107,** 14188–93 (2010).

70. Santaguida, S. & Amon, A. Short- and long-term effects of chromosome mis-segregation and aneuploidy. *Nat. Rev. Mol. Cell Biol.* **16,** 473–485 (2015).

71. Chen, G. *et al*. Hsp90 stress potentiates rapid cellular adaptation through induction of aneuploidy. *Nature* **482,** 246–250 (2012).

72. Laughney, A. M. *et al.* Dynamics of Tumor Heterogeneity Derived from Article Dynamics of Tumor Heterogeneity Derived from Clonal Karyotypic Evolution. *Cell Rep.* **12,** 809–820 (2015).

73. Ozery-Flato, M. *et al*. Large-scale analysis of chromosomal aberrations in cancer karyotypes reveals two distinct paths to aneuploidy. *Genome Biol.* **12,** R61 (2011).

74. Lissa, D. *et al.* Resveratrol and aspirin eliminate tetraploid cells for anticancer chemoprevention. *Proc. Natl. Acad. Sci.* **111,** 3020–3025 (2014).

75. Storchova, Z. & Kuffer, C. The consequences of tetraploidy and aneuploidy. *J. Cell Sci.* **121,** 3859–3866 (2008).

76. Vitale, I. *et al.* Illicit survival of cancer cells during polyploidization and depolyploidization. *Cell Death Differ.* **18,** 1403–1413 (2011).

77. Choudhary, A. *et al.* Identification of selective lead compounds for treatment of high-ploidy breast cancer. *Mol Cancer Ther.* **15,** 48–59 (2016).

78. http://seer.cancer.gov/statfacts/html/amyl.html.

79. Mauritzson, N. *et al.* Pooled analysis of clinical and cytogenetic features in treatment-related and de novo adult acute myeloid leukemia and myelodysplastic syndromes based on a consecutive series of 761 patients analyzed 1976-1993 and on 5098 unselected cases reported in the literature 1974-2001. *Leukemia* **16,** 2366–2378 (2002).

80. Godley, L. A. & Larson, R. A. Therapy-related Myeloid Leukemia. *Semin. Oncol.* **35,** 418–429 (2008).

81. Döhner, H. *et al*. Acute Myeloid Leukemia. *N. Engl. J. Med.* **373,** 1136–1152 (2015).

82. Dohner, H. *et al.* Diagnosis and management of AML in adults: 2017 ELN recommendations from an international expert panel. *Blood* **129,** 424–448 (2017).

83. Bennett, J. *et al.* Proposed revised criteria for the classification of acute myeloid leukemia. A report of the French-American-British Cooperative Group. *Ann Intern Med.* **103,** 620–5 (1985).

84. Jaffe, E. S. *et al*. World Health Organization classification of neoplastic diseases of the hematopoietic and lymphoid tissues. A progress report. *Am. J. Clin. Pathol.* **111,** S8–S12 (1999).

85. Vardiman, J. W. *et al*. The World Health Organization (WHO) classification of the myeloid neoplasms. *Blood* **100,** 2292–2302 (2002).

86. Vardiman JW, Thiele J, A. D. E. A. The 2008 revision of the WHO classification of myeloid neoplasms and acute leukemia: rationale and important changes. *Blood* **114,** 937–952 (2008).

87. Shen, Y. *et al.* Gene mutation patterns and their prognostic impact in a cohort of 1185 patients with acute myeloid leukemia. *Blood* **118,** 5593–5603 (2011).

88. Döhner, H. *et al.* Diagnosis and management of acute myeloid leukemia in adults:

recommendations from an international expert panel, on behalf of the European LeukemiaNet. *Blood* **115,** 453–74 (2010).

89. Preudhomme, C. *et al.* Favorable prognostic significance of CEBPA mutations in patients with de novo acute myeloid leukemia : a study from the Acute Leukemia French Association (ALFA). *Blood* **100,** 2717–2723 (2002).

90. Döhner, K. *et al.* Mutant nucleophosmin (NPM1) predicts favorable prognosis in younger adults with acute myeloid leukemia and normal cytogenetics: Interaction with other gene mutations. *Blood* **106,** 3740–3746 (2005).

91. Grimwade, D. & Hills, R. K. Independent prognostic factors for AML outcome. *Hematol. Am Soc Hematol Educ Program.* 385–95 (2009). doi:10.1182/asheducation-2009.1.385

92. Grimwade, D. *et al.* Refinement of cytogenetic classification in acute myeloid leukaemia: Determination of prognostic significance of rarer recurring chromosomal abnormalities amongst 5,876 younger adult patients treated in the UK Medical Research Council trials. *Blood* **116,** 354–365 (2010).

93. Bochtler, T. *et al.* Marker chromosomes can arise from chromothripsis and predict adverse prognosis in acute myeloid leukemia. *Blood* **129,** 1333–1342 (2017).

94. Rosenbaum, M. W. *et al*. Ring chromosome in myeloid neoplasms is associated with complex karyotype and disease progression. *Hum. Pathol.* **68,** 40–46 (2017).

95. Huh, Y. O. *et al.* Double minute chromosomes in acute myeloid leukemia, myelodysplastic syndromes, and chronic myelomonocytic leukemia are associated with micronuclei, MYC or MLL amplification, and complex karyotype. *Cancer Genet.* **209,** 313–320 (2016).

96. Schoch, C. *et al.* Loss of genetic material is more common than gain in acute myeloid leukemia with complex aberrant karyotype: a detailed analysis of 125 cases using conventional chromosome analysis and fluorescence in situ hybridization including 24-color FISH. *Genes Chromosom. Cancer.* **35(1),** 20–9. (2002).

97. Mrózek, K. Cytogenetic, Molecular Genetic, and Clinical Characteristics of Acute Myeloid Leukemia With a Complex Karyotype. *Semin. Oncol.* **35,** 365–377 (2008).

98. Stölzel, F. *et al.* Karyotype complexity and prognosis in acute myeloid leukemia. *Blood Cancer J.* **6,** 1–7 (2016).

99. Lichtman, M. A. A historical perspective on the development of the cytarabine (7days) and daunorubicin (3days) treatment regimen for acute myelogenous leukemia: 2013 the 40th anniversary of 7+3. *Blood Cells, Mol. Dis.* **50,** 119–130 (2013).

100. Dombre, H. & Gardin, C. An update of current treatments for adult acute myeloid leukemia. *Blood* **127,** 53–62 (2016).

101. Thomas, J. & Kornbergt, R. D. An octamer of histones in chromatin and free in solution. *Proc. Natl. Acad. Sci.* **72,** 2626–2630 (1975).

102. Konotop, G. *et al.* Pharmacological inhibition of centrosome clustering by slingshot-mediated cofilin activation and actin cortex destabilization. *Cancer Res.* **76,** 6690–6700 (2016).

103. Nelson, J. *et al*. Mechanisms of action of 6-thioguanine, 6-mercaptopurine, and 8-azaguanine. *Cancer Res.* **35,** 2872–2873 (1975).

104. Rivest, R. S. *et al*. Inhibition of initiation of translation in L1210 Cells by 8-azaguanine. *Biochem. Pharmacol.* **31,** 2505–2511 (1982).

105. Sugiura, K. *et al*. The Effect of 8-Azaguanine on the Growth of Carcinoma, Sarcoma, Osteogenic Sarcoma, Lymphosarcoma and Melanoma in Animals. *Cancer Res.* **10,** 178–185 (1950).

106. Colsky, J. *et al*. Response of patients with leukemia to 8-azaguanine. *Blood* **10,** 482–492 (1954).

107. https://www.dsmz.de/catalogues/details/culture/ACC-726.html.

108. Kawano-Yamamoto, C. *et al.* Establishment and characterization of a new erythroblastic leukemia cell line, EEB: Phosphatidylglucoside-mediated erythroid differentiation and apoptosis. *Leuk. Res.* **30,** 829–839 (2006).

109. Munker, R. *et al.* Characterization of a new myeloid leukemia cell line with normal cytogenetics (CG-SH). *Leuk. Res.* **33,** 1405–1408 (2009).

110. Wood, K. W. *et al*. CENP-E is a plus end-directed kinetochore motor required for metaphase chromosome alignment. *Cell* **91,** 357–366 (1997).

111. Thorne, K. S. *et al.* Chromosomes Can Congress to the Metaphase Plate Before Biorientation. *Science.* **311,** 388–391 (2006).

112. Brown, K. D. *et al*. Cyclin-like Accumulation and Loss of the Putative Kinetochore Motor CENP-E Results from Coupling Continuous Synthesis with Specific Degradation at the End of Mitosis. **125,** 1303–1312 (1994).

113. Soto, M. *et al.* p53 Prohibits Propagation of Chromosome Segregation Errors that Produce Structural Aneuploidies. *Cell Rep.* **19,** 2423–2431 (2017).

114. Santaguida, S. *et al.* Chromosome Mis-segregation Generates Cell- Cycle-Arrested Cells with Complex Karyotypes that Are Eliminated by the Immune System. *Dev. Cell* **41,** 638–651 (2017).

115. Bunz, F. *et al.* Targeted Inactivation of p53 in Human Cells Does Not Result in Aneuploidy. *Cancer Res*. **62,** 1129–1133 (2002).

116. Lengauer, C. *et al*. Genetic instability in colorectal cancers. *Nature* **386,** 623–627 (1997).

117. Bayani, J. *et al.* Distinct Patterns of Structural and Numerical Chromosomal Instability Characterize Sporadic Ovarian Cancer. *Neoplasia* **10,** 1057–1065 (2008).

118. Matsumoto, M. *et al*. Ectopic expression of CHOP (GADD153) induces apoptosis in M1 myeloblastic leukemia cells. *FEBS Lett.* **395,** 143–147 (1996).

119. Oyadomari, S. & Mori, M. Roles of CHOP/GADD153 in endoplasmic reticulum stress. *Cell Death Differ.* **11,** 381–389 (2004).

120. Urano, F. *et al.* Coupling of Stress in the ER to Activation of JNK Protein Kinases by

Transmembrane Protein Kinase IRE1. *Science* **287,** 664–667 (2000).

121. Wang, X. & Ron, D. Stress-induced Phosphorylation and Activation of the Transcription Factor CHOP (GADD153) by p38 MAP Kinase. *Science* **272,** 1994–1997 (1996).

122. Kuo, L. J. & Yang, L.-X. γ-H2AX – A Novel Biomarker for DNA Double-strand Breaks. *In Vivo* **22,** 305–309 (2008).

123. Rappold, I. *et al*. Tumor Suppressor p53 Binding Protein 1 (53BP1) Is Involved in DNA Damage – signaling Pathways. *JCB* **153,** 613–620 (2001).

124. Dangi, S. *et al*. Activation of extracellular signal-regulated kinase (ERK) in G2 phase delays mitotic entry through p21 Cip1. *Cell Prolif.* **39,** 261–279 (2006).

125. Huang, L. *et al.* Tetraploidy/near-tetraploidy acute myeloid leukemia. *Leuk. Res.* **53,** 20–27 (2017).

126. Pahl, H. L. & Baeuerle, P. A. The ER-overload response: activation of NF-kB. *Trends Biochem. Sci.* **22,** 63–67 (1997).

127. Deng, X. *et al.* Novel Role for JNK as a Stress-activated Bcl2 Kinase. *J. Biol. Chem.* **276,** 23681–23688 (2001).

128. Lei, K. & Davis, R. J. JNK phosphorylation of Bim-related members of the Bcl2 family induces Bax-dependent apoptosis. *Proc. Natl. Acad. Sci.* **100,** 2432–2437 (2003).

129. Ru, F. G. *et al.* TP53 alterations in acute myeloid leukemia with complex karyotype correlate with specific copy number alterations , monosomal karyotype , and dismal outcome. *Blood* **119,** 2114–2122 (2012).

130. Estrov, Z. *et al.* TP53 mutations in newly diagnosed Acute Myeloid Leukemia: Clinico-molecular characteristics, response to therapy, and outcomes. *Cancer* **122,** 3484–3491 (2016).